Geosci. Model Dev. Discuss., 8, 7063–7187, 2015
www.geosci-model-dev-discuss.net/8/7063/2015/
doi:10.5194/gmdd-8-7063-2015

Geoscientific Model Development Discussions
Open Access

ERSEM 15.06: a generic model for marine biogeochemistry and the ecosystem dynamics of the lower trophic levels

M. Butenschön[1], J. Clark[1], J. N. Aldridge[2], J. I. Allen[1,3], Y. Artioli[1], J. Blackford[1], J. Bruggeman[1], P. Cazenave[1], S. Ciavatta[1,3], S. Kay[1], G. Lessin[1], S. van Leeuwen[2], J. van der Molen[2], L. de Mora[1], L. Polimene[1], S. Sailley[1], N. Stephens[1], and R. Torres[1]

[1]Plymouth Marine Laboratory, Prospect Place, The Hoe, Plymouth, PL1 3DH, UK
[2]Centre for Environment, Fisheries, and Aquaculture Science, Lowestoft, UK
[3]National Centre for Earth Observation, Plymouth, UK

Received: 6 July 2015 – Accepted: 25 July 2015 – Published: 26 August 2015

Correspondence to: M. Butenschön (momm@pml.ac.uk)

Published by Copernicus Publications on behalf of the European Geosciences Union.

Abstract

The ERSEM model is one of the most established ecosystem models for the lower trophic levels of the marine food-web in the scientific literature. Since its original development in the early nineties it has evolved significantly from a coastal ecosystem model for the North-Sea to a generic tool for ecosystem simulations from shelf seas to the global ocean. The current model release contains all essential elements for the pelagic and benthic part of the marine ecosystem, including the microbial food-web, the carbonate system and calcification. Its distribution is accompanied by a testing framework enabling the analysis of individual parts of the model. Here we provide a detailed mathematical description of all ERSEM components along with case-studies of mesocosm type simulations, water column implementations and a brief example of a full-scale application for the North-West European shelf. Validation against in situ data demonstrates the capability of the model to represent the marine ecosystem in contrasting environments.

1 Introduction

Over the last two decades a number of marine ecosystem models describing ocean biogeochemistry and the lower trophic levels of the food-web have emerged in a variety of contexts ranging from simulations of batch cultures or mesocosms over estuarine and coastal systems to the global ocean (e.g. Fasham et al., 1990; Flynn, 2010; Geider et al., 1997; Wild-Allen et al., 2010; Zavatarelli and Pinardi, 2003; Aumont et al., 2003; Follows et al., 2007; Yool et al., 2013; Stock et al., 2014). Some of them have matured with the years into sound scientific tools in operational forecasting systems and are used to inform policy and management decisions regarding essential issues of modern human society, such as climate change, ecosystem health, food provision and other ecosystem goods and services (e.g. Lenhart et al., 2010; Glibert et al., 2014; van der Molen et al., 2014; Doney et al., 2012; Bopp et al., 2013; Chust et al., 2014; Barange

GMDD
8, 7063–7187, 2015

et al., 2014). Given the importance of these applications transparent descriptions of the scientific contents of these models are necessary in order to allow full knowledge and assessment of their strength and weaknesses, as well as maintenance and updating according to scientific insight and progress.

Here we provide a full description of one of these models, ERSEM (European Regional Seas Ecosystem Model), developed in the early nineties (Baretta et al., 1995; Baretta, 1997)[1] out of a European collaborative effort, building on previous developments (Radford and Joint, 1980; Baretta et al., 1988). Subsequent development of the model has occured in separate streams leading to individual versions of the model, the main ones being the ERSEM version described in Allen et al. (2001); Blackford and Burkill (2002); Blackford et al. (2004) and the version of Vichi et al. (2004, 2007); Leeuwen et al. (2012); van der Molen et al. (2014); http://www.nioz.nl/northsea_model, also referred to as the Biogeochemical Flux Model. The present release is based on the former development stream (Blackford et al., 2004). It has since the beginnings of ERSEM gradually evolved into what is now the principal model for shelf-seas applications within the UK and beyond. It is part of the operational suite of the UK Met Office, and the biogeochemical component for the North-West European shelf seas within the European Copernicus Marine Service.

While it was originally created as scientific tool for the North Sea ecosystem (hence the name), it has since evolved considerably in its scientific content, broadening the scope of the model to coastal systems across the globe as well as the open ocean. Allen et al. (2001) have adopted the model for simulations across the entire North-West European shelf sea, further extended in Holt et al. (2012); Artioli et al. (2012) to include the North East Atlantic. Blackford et al. (2004) have applied the model across six different ecosystem types across the globe, Barange et al. (2014) have used applications of the model in the major coastal upwelling zones of the planet and Kwiatkowski et al.

[1]The two given references are the introductions to two special issues published on the original model versions ERSEM I and II, representing the entire volumes. More specific reference to single papers within these volumes are given in the relevant process descriptions.

GMDD
8, 7063–7187, 2015

(2014) have assessed the skill of the model demonstrating its competitiveness with respect to other established global ocean models. The model has been subject to validation on various levels ranging from basic statistical metrics of point-to-point matches to observational data (Shutler et al., 2011; de Mora et al., 2013) to multi-variate analysis (Allen et al., 2007; Allen and Somerfield, 2009) and pattern recognition (Saux Picart et al., 2012).

The model has been applied in a wide number of contexts that include short-term forecasting (Edwards et al., 2012), ocean acidification (Blackford and Gilbert, 2007), climate-change (Holt et al., 2012), coupled climate-acidification projections (Artioli et al., 2013), process studies (Polimene et al., 2012, 2014), biogeochemical cycling (Wakelin et al., 2012), habitat (Villarino et al., 2015) and end-to-end modelling (Barange et al., 2014). The wide range of applications and uses of the model coupled with developments since earlier manuscripts documenting the model (Baretta-Bekker, 1995; Baretta, 1997; Blackford et al., 2004) make a thorough and integral publication of its scientific ingredients overdue.

Being an evolution of former models within the ERSEM family that emerged in parallel to other, separate development streams of the original model, the core elements of the current model version closely resemble earlier versions even if presented in much more detail compared to previous works. We present a model for ocean biogeochemistry, the planktonic and benthic parts of the marine ecosystem that includes explicitly the cycles of the major chemical elements of the ocean (carbon, nitrogen phosphorus, silicate and iron); it includes the microbial food-web, a sub-module for the carbonate system, calcification and a full benthic model.

The present paper provides a full description of all model components and simple case-studies illustrating the model capabilities in an idealised mesocosm type framework and in three vertical water-column implementations of opposing character supplemented by a brief illustration of a full scale three dimensional application. The next section gives an overview of the model and its philosophy while the two following sections contain the descriptions of the pelagic and benthic components, describe the

GMDD
8, 7063–7187, 2015

air–sea and seabed interfaces and detail some generic terms that are used throughout the model. The model description is complemented by two sections that present different implementations of the model and illustrate the testing framework. We complete the work with the technical specifications of the software package, license and instructions of where and how to access the model code.

2 The ERSEM model

ERSEM is, since its origins, an ecosystem model of intermediate complexity for marine biogeochemistry, pelagic plankton and benthic fauna. Its functional types (Baretta et al., 1995; Vichi et al., 2007) are based on their macroscopic role in the ecosystem rather than species or taxa and its state variables are the major chemical components of each type (carbon, chlorophyll *a*, nitrogen, phosphate, silicate and optionally iron). It is composed of a set of modules that compute the rates of change of its state variables given the environmental conditions of the surrounding water body, physiological processes and preditor–prey interactions. In the simplest case the environmental drivers can be provided offline, or through a simple 0-dimensional box model. However, for more realistic representations, including the important processes of horizontal and vertical mixing (or advection) and biogeochecmial feed-backs, a direct (or online) coupling to a physical driver, such as a 3-D hydrodynamic model, is required.

The organisms in the model are categorised along with the main classes of ecosystem function into primary producers, consumers and bacterial decomposers, particulate and dissolved organic matter (POM, DOM) in the pelagic and consumers, bacterial decomposers, particulate and dissolved organic matter in the benthos. Most of these classes are further subdivided into sub-types to allow for an enhanced plasticity of the system in adapting the ecosystem response to the environmental conditions in comparison to the classical NPZD type models. A particularity of ERSEM is the fully dynamic stoichiometry in essentially all its types (with the exception of mesozooplankton, benthic bacteria and zoobenthos which use fixed stoichiometric ratios). The model

GMDD
8, 7063–7187, 2015

dynamics of a living functional type are generally based on the assimilation of carbon into organic compounds by primary production or uptake, and the loss processes of respiration, excretion, exudation and mortality (see also Vichi et al., 2007 – "2. Towards a generic formalism for pelagic biogeochemistry"). These are accompanied by nutrient uptake in inorganic or organic form according to the external availability and actual requirement and uptake capacity of the relevant functional type balanced by nutrient loss according to the internal quota and storage capacity. This stoichiometric flexibility allows for a diverse response in between the functional types in adapting to the environmental conditions with respect to fixed quota models (e.g. through varying resistance against low nutrient conditions and luxury storages supporting a more realistic evolution of the community structure). Figure 1 illustrates the pathways of these fluxes within the food-web of the model.

ERSEM is not designed to directly model cell physiology. Its equations are a synthesis of physiological processes and their macroscopic consequences on larger water bodies in which the distributions of the plankton biomass, organic and inorganic material can be approximated as smooth continuous fields. This is important to keep in mind in small scale and high-resolution applications where this basic assumption of the continuum hypothesis may break down, in which case the system of partial differential balance equations no longer holds.

Mathematically, the set of prognostic equations describing the dynamics of marine biogeochemical states is generally given by:

$$\frac{\partial c_\mathrm{p}}{\partial t} + \boldsymbol{u}\cdot\frac{\partial c_\mathrm{p}}{\partial \boldsymbol{x}} + {}^{c_\mathrm{p}}w_\mathrm{sed}\frac{\partial c_\mathrm{p}}{\partial z} = \nu\frac{\partial^2 c_\mathrm{p}}{\partial \boldsymbol{x}^2} + \left.\frac{\partial c_\mathrm{p}}{\partial t}\right|_\mathrm{bgc} + \left.\frac{\partial c_\mathrm{p}}{\partial t}\right|_\mathrm{seabed} \tag{1}$$

$$\frac{\partial c_\mathrm{b}}{\partial t} = \left.\frac{\partial c_\mathrm{b}}{\partial t}\right|_\mathrm{bgc}, \tag{2}$$

where c_p are the pelagic concentrations (per volume) and c_b the benthic contents (per sediment surface area) of the organic or inorganic model components. ${}^{\mathrm{sed}}w_{c_\mathrm{p}}$ is the

GMDD
8, 7063–7187, 2015

velocity of gravitational sinking of particles in the water column. The set of equations is closed by the horizontal boundary conditions of the system generally given by the air–sea fluxes $\mathcal{F}|^{\text{air}}_{\text{sea}}$ and the fluxes across the seafloor $\mathcal{F}|^{\text{pel}}_{\text{ben}}$ and lateral boundary conditions if present in the given configuration.

ERSEM computes the biogeochemical rates of change in pelagic ($\frac{\partial c_{\text{p}}}{\partial t}\Big|_{\text{bgc}}$) and benthic ($\frac{\partial C_{\text{b}}}{\partial t}\Big|_{\text{bgc}}$) systems, the gas transfer across sea-surface ($\mathcal{F}|^{\text{air}}_{\text{sea}}$ for oxygen and carbon) and the fluxes across the seabed ($\mathcal{F}|^{\text{pel}}_{\text{ben}}$). The actual numerical integration of these rates along with the advection-diffusion processes that solves Eqs. (1) and (2) needs to be addressed appropriately through an external driver as e.g. discussed in (Butenschön et al., 2012).

2.1 Nomenclature and units

Pelagic state variables in ERSEM are concentrations and are referred to as c_{p}. When indicating a specific class or type, they are denoted by upper case letters (P: phytoplankton, Z: zooplankton, B: bacteria, R: organic matter, O: gases, N: nutrients), with the chemical component in the subscript in blackboard style ($\mathbb{C}$: carbon, $\mathbb{N}$: nitrogen, $\mathbb{P}$: phosphorus, $\mathbb{S}$: silicon, $\mathbb{F}$: iron with the exception of the chlorophyll a components which are distinguished by using C, as chlorophyll a is not a chemical element but a compound), and the specific type in the super-script, e.g. $\overset{\text{dia}}{P}_{\mathbb{C}}$ for diatom carbon. Correspondingly, benthic states use c_{b} for generic contents and the specific states (H: bacteria Y: zoobenthos, Q: organic matter, G: gases, K: nutrients, D: states of vertical distribution). Primes ($'$) mark available concentrations or contents to loss processes (see Sect. 2.3). Where equations are valid for more than one specific functional type χ, ψ, Ψ are used as place holders for functional types and the chemical components may be given as a comma separated list, implying that an equation is valid for all these components, e.g. $\overset{\chi}{P}_{\mathbb{C},\mathbb{N},\mathbb{P}}$ represents the carbon, phosphorus and nitrogen content of

GMDD
8, 7063–7187, 2015
ERSEM 15.06
M. Butenschön et al.

each phytoplankton type. The physical environment is given in roman letters, e.g. T for temperature.

Parameters are represented by lower case letters with r for specific rates, q for quotas or fractions, l for limitation or regulating factors, h for half-saturation constants and p for most others. Food preferences of predators on their prey are given as $f_{\mathrm{pr}}\big|_P^Z$ being the preference of predator Z on food P.

Fluxes between state variables are given as $\mathcal{F}\big|_A^B$ for the flux from A to B. Specific rates are notated using $\mathcal{S}$. Dynamic internal quotas of two components A and B are given by the notation $q_{A:B}$, e.g. $\overset{\mathrm{dia}}{q}_{\mathbb{N}:\mathbb{C}}$ being the internal nitrogen to carbon quota of diatoms $\frac{\overset{\mathrm{dia}}{P_{\mathbb{N}}}}{\overset{\mathrm{dia}}{P_{\mathbb{C}}}}$. Derived quotas or fractions are given by a caligraphic $\mathcal{Q}$.

The coordinate system used describes the horizontal coordinates in x and y, while the vertical coordinate is given by z, 0 at the sea surface increasing downwards. The corresponding velocity fields are given by u, v and w. We are referring to Cartesian coordinates in this publication for simplicity.

The sediment depth coordinate is given by ζ, which is 0 at the sediment surface increasing downwards.

All equtations are given as scalar equations for a single pixel of the model domain.

Rates of change of the biogeochemical state variables due to individual subprocesses or groupings of these are given as $\frac{\partial \phi}{\partial t}\Big|_{\mathrm{subprocess}}$, where the following abbreviations are used for the subprocesses: bgc = biogeochemical fluxes, bur = burying, calc = calcification, decomp = decomposition, denit = denitrification, dis = dissolution, excr = excretion, lys = lysis, mort = mortality, net = comprehensive net fluxes, nitr = nitrification, pred = predation, rel = release, remin = remineralisation, resp = respiration, scav = scavenging, sed = sedimenation, upt = uptake.

Units in the model for all organic and inorganic nutrient concentrations are in $\mathrm{mmol\,m^{-3}}$ with the excpetion of iron being in $\mathrm{\mu mol\,m^{-3}}$. All forms of organic carbon are in $\mathrm{mg\,m^{-3}}$ while all species of inorganic carbon are in $\mathrm{mmol\,m^{-3}}$ with the excep-

GMDD
8, 7063–7187, 2015
ERSEM 15.06
M. Butenschön et al.

tion of the internal computations of the carbonate system where they are converted to $\mu mol\,kg^{-3}$. Corresponding benthic contents are two-dimensional and consequently given in $mmol\,m^{-2}$, $mg\,m^{-2}$ and $\mu mol\,m^{-2}$. The penetration depth and depth horizons in the sediments are given in m. Temperatures are generally considered in °C, salinity in psu, sea-water density in $kg\,m^{-3}$ and pressure is given in Pa, with the exception of the internal calculations of the carbonate system where temperature is converted to absolute temperature in K and pressure to bar. Partial pressure of carbon dioxide is used in ppm.

2.2 Dependencies on the physical environment

Several processes in the model depend directly on the physical environment that the model states are exposed to:

- Metabolic processes depend on the sea-water temperature.
- Primary Production relies additionally on the photosynthetically active radiation (PAR) as energy input which is computed from shortwave radtion at the sea surface I_{surf}.
- Empirical regressions for alkalinity, saturation states and chemical equilibrium coefficient of the carbonate system reactions require temperature T, salinity S, pressure p and density ρ of the sea-water.
- Air–sea fluxes of carbon dioxide and oxygen depend on temperature T and the absolute wind speed $vecu_{wind}$ near the sea-surface.
- Deposition of organic matter on the sea floor and resuspension depend on the shear stress at the sea floor τ_{bed}.

GMDD
8, 7063–7187, 2015
ERSEM 15.06
M. Butenschön et al.

2.3 States and negativity control

In order to avoid the occurrence of negative concentrations or contents in the integration process and reduce the vulnerability to numerical noise all state variables include a lower buffer $\epsilon_{p,b}$, based on a carbon concentration of $0.01\,mg\,m^{-3}$ modified adequately for the various state varibales using reference stoichiometric quotas and unit conversions. This buffer is not accessible to the loss processes of the biogeochemical dynamics. Consequently all process that diminish the biomass of each state are based on the available concentrations or contents given by $c'_{p,b} = c_{p,b} - \epsilon_{p,b}$. These small resilient buffers additionally support the spawning of new biomass as soon as favourable conditions occur.

3 The pelagic system

In its current form the pelagic part of ERSEM comprises 4 functional types for primary producers, originally defined as diatoms, nanoflagellates, picophytoplankton and dinoflagellates. This classification was historically coined for the North Sea but has since been widened to a broader interpretation almost exclusively based on the single trait size (with the exception of the requirement of silicate by diatoms and an implicit calcification potential of nanoflagellates) leading to the classes of picophytoplankton, nanophytoplankon, microphytoplankton and diatoms. Similarly the zooplankton pool is divided into hetero nanoflagellates, microzooplankton and mesozooplankton. Particulate organic matter is treated in three size classes (small, medium and large) in relation to its origin. Dissolved organic matter is distinguished according to its decomposition time scales into a labile dissolved inorganic state, semi-labile and semi-refractory carbon (see Sect. 3.3.1).

The inorganic state variables of the pelagic model are dissolved oxidised nitrogen, ammonium, phosphate, silicid acids, dissolved inorganic iron, dissolved inorganic carbon, dissolved oxygen and calcite. In addition the model holds a state variable for al-

GMDD
8, 7063–7187, 2015
ERSEM 15.06
M. Butenschön et al.

kalinity subject to fluctuations generated from the modelled biogeochemical processes (see Sect. 3.8 and Artioli et al., 2012). The complete list of pelagic state variables is given in Tables 1 and 2.

The recently implemented iron cycle (following largely the implementation of Vichi et al., 2007) and the silicate cycle are abbreviated for simplicity, their pathways bypass the predator and decomposers by turning grazing of phytoplankton iron or silicate directly into detritus and remineralising iron implicitly from detritus into the dissovled inorganic form, while silicate is not remineralised in the water column. Chlorophyll *a* takes a special role in between the chemical components of the model: being a compound of other elements it is not strictly conserved by the model equations but rather derived from assimilation of carbon and subsequent decomposition of organic compounds. The addition of chlorophyll *a* states to the model allows for dynamic chlorophyll *a* to carbon relationships in the photosynthesis description and a more accurate comparsion to observations of biomass or chlorophyll *a*.

The growth dynamics in the model are generally based on mass-specific production and loss equations that are expressed in the currency of each chemical component, regulated and limited by the availability of the respective resources.

3.1 Primary producers

The phytoplankton dynamics are modelled for each phytoplankton type as net result of source and loss processes (Varela et al., 1995) given by gross primary production and the losses through excretion, respiration, lysis and predation of zooplankton for the carbon and chlorophyll *a* component, while the nutrient content is balanced by uptake,

GMDD
8, 7063–7187, 2015

lysis and predation:

$$\left.\frac{\partial \overset{\chi}{P}_{\mathbb{C},C}}{\partial t}\right|_{\text{bgc}} = \left.\frac{\partial \overset{\chi}{P}_{\mathbb{C},C}}{\partial t}\right|_{\text{gpp}} - \left.\frac{\partial \overset{\chi}{P}_{\mathbb{C},C}}{\partial t}\right|_{\text{excr}} - \left.\frac{\partial \overset{\chi}{P}_{\mathbb{C},C}}{\partial t}\right|_{\text{resp}} - \left.\frac{\partial \overset{\chi}{P}_{\mathbb{C},C}}{\partial t}\right|_{\text{lys}} - \left.\frac{\partial \overset{\chi}{P}_{\mathbb{C},C}}{\partial t}\right|_{\text{pred}}, \quad (3)$$

$$\left.\frac{\partial \overset{\chi}{P}_{\mathbb{N},\mathbb{P},\mathbb{F}(,\mathbb{S})}}{\partial t}\right|_{\text{bgc}} = \left.\frac{\partial \overset{\chi}{P}_{\mathbb{N},\mathbb{P},\mathbb{F}(,\mathbb{S})}}{\partial t}\right|_{\text{upt}} - \left.\frac{\partial \overset{\chi}{P}_{\mathbb{N},\mathbb{P},\mathbb{F}(,\mathbb{S})}}{\partial t}\right|_{\text{lys}} - \left.\frac{\partial \overset{\chi}{P}_{\mathbb{N},\mathbb{P},\mathbb{F}(,\mathbb{S})}}{\partial t}\right|_{\text{pred}}, \quad (4)$$

with χ in (pico, *nano*, micro, dia) and where only for diatoms the silicate component ($\mathbb{S}$) is active.

Specific gross primary production is computed as

$$\overset{\chi}{S}_{\text{gpp}} = \overset{\chi}{g}_{\max} \overset{\chi}{I}_{\mathbb{T}} \overset{\chi}{I}_{\mathbb{S}} \overset{\chi}{I}_{\mathbb{F}} \left(1 - e^{-\frac{\overset{\chi}{\alpha}_{\mathrm{PI}} E_{\mathrm{PAR}} \overset{\chi}{q}_{C:\mathbb{C}}}{\overset{\chi}{g}_{\max} \overset{\chi}{I}_{\mathbb{T}} \overset{\chi}{I}_{\mathbb{S}} \overset{\chi}{I}_{\mathbb{F}}}}\right) e^{-\frac{\overset{\chi}{\beta}_{\mathrm{PI}} E_{\mathrm{PAR}} \overset{\chi}{q}_{C:\mathbb{C}}}{\overset{\chi}{g}_{\max} \overset{\chi}{I}_{\mathbb{T}} \overset{\chi}{I}_{\mathbb{S}} \overset{\chi}{I}_{\mathbb{F}}}}}, \quad (5)$$

based on the formulation by Geider et al. (1997) modified for photoinhibition according to Blackford et al. (2004). The symbols in this equation represent the chlorophyll *a* to carbon quotae of each functional type $\overset{\chi}{q}_{C:\mathbb{C}} = \overset{\chi}{P}_C / \overset{\chi}{P}_{\mathbb{C}}$, the metabolic response to temperature $\overset{\chi}{I}_{\mathbb{T}}$ (see Eq. 231) and the silicate and iron limitation factors $\overset{\chi}{I}_{\mathbb{S},\mathbb{F}} \epsilon [0,1]$ (see Eqs. 235 and 236). The $\overset{\chi}{g}_{\max}$ are the maximum potential photosynthetic rate parameters in unlimited conditions at reference temperature. Note, that these are different to the maximum potential growth rates usually retrieved in physiological experiments (e.g. in the work of Geider et al., 1997) or measured at sea, in that they are exclusive upper bounds of the specific growth rate function. In fact, the products of the exponential

GMDD
8, 7063–7187, 2015
ERSEM 15.06
M. Butenschön et al.

terms in Eq. (5) have a maximum of $\left(1.0 - \frac{\overset{\chi}{\beta}_{\mathrm{PI}}}{\overset{\chi}{\alpha}_{\mathrm{PI}}+\overset{\chi}{\beta}_{\mathrm{PI}}}\right)\left(\frac{\overset{\chi}{\beta}_{\mathrm{PI}}}{\overset{\chi}{\alpha}_{\mathrm{PI}}+\overset{\chi}{\beta}_{\mathrm{PI}}}\right)^{\frac{\overset{\chi}{\beta}_{\mathrm{PI}}}{\overset{\chi}{\alpha}_{\mathrm{PI}}}} < 1$. In addition, we refer to gross primary production here as total carbon fixation, a fraction of which is directly excreted to the dissolved organic carbon pool. Other parameters are the initial slope $\overset{\chi}{\alpha}_{\mathrm{PI}}$ and the photoinhibition parameter $\overset{\chi}{\beta}_{\mathrm{PI}}$ of the light saturation curve (Platt et al., 1982).

A fraction of the specific gross production is directly excreted as a fixed fraction $\overset{\chi}{q}_{\mathrm{excr}}$ augmented according to the combined nitrogen and phosphorus limitation up to the total gross production:

$$\overset{\chi}{Q}_{\mathrm{excr}} = \left[1 - \left(\left(1 - \overset{\chi}{I}_{\langle \mathrm{INIP} \rangle}\right)\left(1 - \overset{\chi}{q}_{\mathrm{excr}}\right) + \overset{\chi}{q}_{\mathrm{excr}}\right)\right], \tag{6}$$

where $\overset{\chi}{I}_{\langle \mathrm{INIP} \rangle}$ is the combined nitrogen-phosphorus limitation factor defined in Eq. (234).

The second generic sink term is given by lysis which occurs proportional to the current biomass by the constant specific rate $\overset{\chi}{r}_{\mathrm{lys}}$ augmented by nutrient stress according to:

$$\overset{\chi}{S}_{\mathrm{lys}} = \frac{1}{\min\left(\overset{\chi}{I}_{\langle \mathrm{INIP} \rangle}, \overset{\chi}{I}_{\mathrm{S}}\right)} \overset{\chi}{r}_{\mathrm{lys}}. \tag{7}$$

The carbon and chlorophyll *a* dynamics of each phytoplankton type in Eq. (3) are then specified by the following terms:

Carbon is assimilated according to

$$\left.\frac{\partial \overset{\chi}{P}_{\mathrm{C}}}{\partial t}\right|_{\mathrm{gpp}} = \overset{\chi}{S}_{\mathrm{gpp}} \overset{\chi}{P}_{\mathrm{C}}. \tag{8}$$

GMDD
8, 7063–7187, 2015
ERSEM 15.06
M. Butenschön et al.

Chlorophyll *a* is synthesised at the acclimated quota

$$\overset{\chi}{\varphi} = \left(\overset{\chi}{q}_{\varphi\max} - q_{\min_{C:\mathbb{C}}}\right) \frac{\overset{\chi}{S}_{\text{gpp}}}{\overset{\chi}{\alpha}_{\text{PI}} E_{\text{PAR}} \overset{\chi}{q}_{C:\mathbb{C}}} + q_{\min_{C:\mathbb{C}}}, \tag{9}$$

where $\overset{\chi}{q}_{\varphi\max}$ are the maximum achievable chlorophyll *a* to carbon quota for each type, $q_{\min_{C:\mathbb{C}}}$ is the minimum chlorophyll *a* to carbon quota.

This formulation differs from the original formulation of Geider et al. (1997) in its asymptotic limit of the carbon to chlorophyll *a* synthesis at high PAR, which in the original formulation is unbound, while in this formulation it is bound by the inverse minimum chlorophyll *a* to carbon ratio $q_{\min_{C:\mathbb{C}}}$ in order to avoid excessive quotas not observed in nature.

The synthesis rate of chlorophyll *a* is then given by:

$$\left.\frac{\partial \overset{\chi}{P}_{C}}{\partial t}\right|_{\text{gpp}} = \overset{\chi}{I}_{\langle \mathbb{N}\mathbb{P} \rangle} \overset{\chi}{\varphi} \overset{\chi}{S}_{\text{gpp}} \overset{\chi}{P}_{\mathbb{C}}. \tag{10}$$

As opposed to the previous formulation of Blackford et al. (2004), the relative synthesis of chlorophyll *a* is directly limited by the internal nutrient quota in order to compensate for the enhanced demand required to maintain the cell structure leading to a reduced investment into the light harvesting capacity.

The excretion of phytoplankton in terms of carbon and chlorophyll *a* is consequently given by:

$$\left.\frac{\partial \overset{\chi}{P}_{\mathbb{C},C}}{\partial t}\right|_{\text{excr}} = \overset{\chi}{\mathcal{Q}}_{\text{excr}} \left.\frac{\partial \overset{\chi}{P}_{\mathbb{C},C}}{\partial t}\right|_{\text{gpp}}. \tag{11}$$

GMDD
8, 7063–7187, 2015
ERSEM 15.06
M. Butenschön et al.

Respiration of phytoplankton is split into respiration at rest, that is proportional to the current biomass by the constant specific rate $\overset{\chi}{r}_{\text{resp}}$ complemented with an activity related term that is a fraction $\overset{\chi}{q}_{\text{aresp}}$ of the assimilated amount of biomass per time unit after excretion:

$$\left.\frac{\partial \overset{\chi}{P}_{\mathrm{C},c}}{\partial t}\right|_{\text{resp}} = \overset{\chi}{r}_{\text{resp}} \; \overset{\chi}{P'}_{\mathrm{C},c} + \overset{\chi}{q}_{\text{aresp}} \left(\left.\frac{\partial \overset{\chi}{P}_{\mathrm{C},c}}{\partial t}\right|_{\text{gpp}} - \left.\frac{\partial \overset{\chi}{P}_{\mathrm{C},c}}{\partial t}\right|_{\text{excr}} \right) . \tag{12}$$

The losses of phytoplankton by lysis are given by

$$\left.\frac{\partial \overset{\chi}{P}_{\mathrm{C},c}}{\partial t}\right|_{\text{lys}} = \overset{\chi}{S}_{\text{lys}} \; \overset{\chi}{P'}_{\mathrm{C},c} \tag{13}$$

while the individual terms of loss through predation of predator Ψ in

$$\left.\frac{\partial \overset{\chi}{P}_{\mathrm{C},c}}{\partial t}\right|_{\text{pred}} = \sum_{\Psi} \mathcal{F}\big|_{\overset{\chi}{P}}^{\Psi} \; \overset{\chi}{P'}_{\mathrm{C},c} . \tag{14}$$

are specified in the sections of the respective predators in Eqs. (29) and (168).

Nutrient demand (with the exception of silicate) is computed from assimilation demand at maximum quota $\overset{\chi}{q}_{\max_{\mathrm{N,P,F:C}}}$ complemented by a regulation term relaxing the internal quota towards the maximum quota and compensating for rest respiration:

$$\begin{aligned} \mathcal{F}_{\text{demand}}\big|_{N_{\mathrm{N,P,F}}}^{\overset{\chi}{P}_{\mathrm{N,P,F}}} = & \overset{\chi}{S}_{\text{gpp}} \left(1 - \overset{\chi}{Q}_{\text{excr}}\right) \left(1 - \overset{\chi}{q}_{\text{aresp}}\right) \overset{\chi}{q}_{\max_{\mathrm{N,P,F:C}}} \; \overset{\chi}{P}_{\mathrm{C}} \\ & + r_{\text{nlux}} \left(\overset{\chi}{q}_{\max_{\mathrm{N,P,F:C}}} \; \overset{\chi}{P}_{\mathrm{C}}' - \overset{\chi}{P'}_{\mathrm{N,P,F}} \right) - \overset{\chi}{r}_{\text{resp}} \; \overset{\chi}{P'}_{\mathrm{N,P,F}} \end{aligned} \tag{15}$$

GMDD
8, 7063–7187, 2015
ERSEM 15.06
M. Butenschön et al.

where r_{nlux} is the tendency of nutrient luxuary uptake towards the maximum quota.

Note, that these terms may turn negative when rest respiration exceeds the effective assimilation rate $\overset{\chi}{S}_{\mathrm{gpp}}\left(1-\overset{\chi}{Q}_{\mathrm{excr}}\right)\left(1-\overset{\chi}{q}_{\mathrm{aresp}}\right)\overset{\chi}{P}_{\mathbb{C}}$ or the internal nutrient content exceeds the maximum quota resulting in nutrient excretion in dissolved inorganic from. The maximum quota for nitrogen and phosphorus may exceed the optimal quota allowing for luxury storage while it is identical to the optimum quota for iron and silicate.

$\left.\frac{\partial \overset{\chi}{P}_{\mathbb{N},\mathbb{P},\mathbb{F}}}{\partial t}\right|_{\mathrm{upt}}$ is capped at the maximum achievable uptake depending on the nutrient affinities $\overset{\chi}{r}_{\mathrm{aff}_{\mathbb{P},\mathbb{F},n,a}}$ and the external dissolved nutrient concentrations:

$$\mathcal{F}_{\mathrm{avail}}\big|^{\overset{\chi}{P}_{\mathbb{P},\mathbb{F}}}_{N_{\mathbb{P},\mathbb{F}}} = \overset{\chi}{r}_{\mathrm{aff}_{\mathbb{P},\mathbb{F}}} N'_{\mathbb{P},\mathbb{F}}\ \overset{\chi}{P}_{\mathbb{C}}\,, \tag{16}$$

$$\mathcal{F}_{\mathrm{avail}}\big|^{\overset{\chi}{P}_{\mathbb{N}}}_{N_{\mathbb{N}}} = \left(\overset{\chi}{r}_{\mathrm{aff}_n}\ \overset{\mathrm{ox}}{N'}_{\mathbb{N}} + \overset{\chi}{r}_{\mathrm{aff}_a}\ \overset{\mathrm{amm}}{N'}_{\mathbb{N}}\right)\overset{\chi}{P}_{\mathbb{C}}\,, \tag{17}$$

where the nitrogen need is satisfied by uptake in oxidised and reduced form in relation to the respective affinities and external availability.

The resulting net uptake of nitrogen, phosphorus and iron is then

$$\left.\frac{\partial \overset{\chi}{P}_{\mathbb{N},\mathbb{P},\mathbb{F}}}{\partial t}\right|_{\mathrm{upt}} = \min\left(\mathcal{F}_{\mathrm{demand}}\big|^{\overset{\chi}{P}_{\mathbb{N},\mathbb{P},\mathbb{F}}}_{N_{\mathbb{N},\mathbb{P},\mathbb{F}}}, \mathcal{F}_{\mathrm{avail}}\big|^{\overset{\chi}{P}_{\mathbb{N},\mathbb{P},\mathbb{F}}}_{N_{\mathbb{N},\mathbb{P},\mathbb{F}}}\right) \tag{18}$$

GMDD
8, 7063–7187, 2015
ERSEM 15.06
M. Butenschön et al.

Lysis and predation losses are computed analogous to the carbon component:

$$\left.\frac{\partial \overset{\chi}{P}_{\mathbb{N},\mathbb{P},\mathbb{F}}}{\partial t}\right|_{\text{lys}} = \overset{\chi}{S}_{\text{lys}} \; \overset{\chi}{P'}_{\mathbb{N},\mathbb{P},\mathbb{F}}\,, \tag{19}$$

$$\left.\frac{\partial \overset{\chi}{P}_{\mathbb{N},\mathbb{P},\mathbb{F}}}{\partial t}\right|_{\text{pred}} = \sum_{\Psi} \mathcal{F}|^{\Psi}_{\overset{\chi}{P}} \; \overset{\chi}{P'}_{\mathbb{N},\mathbb{P},\mathbb{F}}\,. \tag{20}$$

The silicate component of diatoms is given by the equations:

$$\left.\frac{\partial \overset{\text{dia}}{P}_{\mathbb{S}}}{\partial t}\right|_{\text{upt}} = \max\left(0, \overset{\text{dia}}{q}_{\text{ref}_{\mathbb{S}:\mathbb{C}}} \; \overset{\text{dia}}{S}_{\text{growth}}\right) - \max\left(0, \overset{\text{dia}}{P'}_{\mathbb{S}} - \overset{\text{dia}}{q}_{\text{ref}_{\mathbb{S}:\mathbb{C}}} \; \overset{\text{dia}}{P'}_{\mathbb{C}}\right), \tag{21}$$

$$\left.\frac{\partial \overset{\text{dia}}{P}_{\mathbb{S}}}{\partial t}\right|_{\text{lys}} = \overset{\text{dia}}{S}_{\text{lys}} \; \overset{\text{dia}}{P'}_{\mathbb{S}}\,, \tag{22}$$

$$\left.\frac{\partial \overset{\text{dia}}{P}_{\mathbb{S}}}{\partial t}\right|_{\text{pred}} = \sum_{\Psi} \mathcal{F}|^{\Psi}_{\overset{\text{dia}}{P}} \; \overset{\text{dia}}{P'}_{\mathbb{S}}\,, \tag{23}$$

where $\overset{\text{dia}}{q}_{\text{ref}_{\mathbb{S}:\mathbb{C}}}$ is the reference silicate to carbon quota of diatoms.

A formulation to model the impact of an increased atmospheric p_{CO_2} on phytoplankton carbon uptake that was introduced in Artioli et al. (2014) is available via the CENH preprocessing option. In this case gross carbon uptake (Eq. 8) and activity respiration (the second term in Eq. 12) are enhanced by the factor $\gamma_{\text{enh}\mathbb{C}}$ defined as:

$$\gamma_{\text{enh}\mathbb{C}} = 1.0 + p_{CO_2} - 379.48 \times 0.0005\,. \tag{24}$$

GMDD
8, 7063–7187, 2015
ERSEM 15.06
M. Butenschön et al.

3.2 Predators

Predator dynamics are largely based on the descriptions of Baretta-Bekker et al. (1995) and Broekhuizen et al. (1995) described by the equations:

$$\left.\frac{\partial \overset{\chi}{Z}_{\mathbb{C}}}{\partial t}\right|_{\text{bgc}} = \left.\frac{\partial \overset{\chi}{Z}_{\mathbb{C}}}{\partial t}\right|_{\text{upt}} - \left.\frac{\partial \overset{\chi}{Z}_{\mathbb{C}}}{\partial t}\right|_{\text{excr}} - \left.\frac{\partial \overset{\chi}{Z}_{\mathbb{C}}}{\partial t}\right|_{\text{resp}} - \left.\frac{\partial \overset{\chi}{Z}_{\mathbb{C}}}{\partial t}\right|_{\text{mort}} - \left.\frac{\partial \overset{\chi}{Z}_{\mathbb{C}}}{\partial t}\right|_{\text{pred}}, \tag{25}$$

$$\left.\frac{\partial \overset{\chi}{Z}_{\mathbb{N},\mathbb{P}}}{\partial t}\right|_{\text{bgc}} = \left.\frac{\partial \overset{\chi}{Z}_{\mathbb{N},\mathbb{P}}}{\partial t}\right|_{\text{upt}} - \left.\frac{\partial \overset{\chi}{Z}_{\mathbb{N},\mathbb{P}}}{\partial t}\right|_{\text{excr}} - \left.\frac{\partial \overset{\chi}{Z}_{\mathbb{N},\mathbb{P}}}{\partial t}\right|_{\text{rel}} - \left.\frac{\partial \overset{\chi}{Z}_{\mathbb{N},\mathbb{P}}}{\partial t}\right|_{\text{mort}} - \left.\frac{\partial \overset{\chi}{Z}_{\mathbb{N},\mathbb{P}}}{\partial t}\right|_{\text{pred}}. \tag{26}$$

Note, that the iron and silicate cycles are simplified in a way that the iron/silicate content of phytoplankton subject to predation is directly turned into particulate organic matter (see Eqs. 66 and 67).

The pelagic predators considered in ERSEM are composed of three size classes of zooplankton categorised as heterotrophic flagellates, microzooplankton and mesozooplankton. According to size, these are capable of predating on different prey types including cannibalism as given in Table 3.

The total prey available to each zooplankton type χ is composed of the preys ψ using type II Michaelis–Menten type uptake capacities (Gentleman et al., 2003) as

$$\overset{\chi}{\text{Pr}}_{\mathbb{C},\mathbb{N},\mathbb{P}} = \sum_{\psi} f_{\text{pr}}\Big|_{\psi}^{\overset{\chi}{Z}} \frac{\psi'_{\mathbb{C}}}{\psi'_{\mathbb{C}} + \overset{\chi}{f}_{\text{min}}} \psi'_{\mathbb{C},\mathbb{N},\mathbb{P}}, \tag{27}$$

where $f_{\text{pr}}\big|_{\psi}^{\overset{\chi}{Z}}$ are the food preferences and $\overset{\chi}{f}_{\text{min}}$ is a food half-saturation constant reflecting the detection capacity of predator χ of individual prey types.

GMDD
8, 7063–7187, 2015
ERSEM 15.06
M. Butenschön et al.

The specific uptake capacity for each zooplankton type χ is then given by:

$$\overset{\chi}{S}_{\text{growth}} = \overset{\chi}{g}_{\max}\ \overset{\chi}{l}_{\text{T}} \frac{\overset{\chi}{Z}_{\mathbb{C}}}{\overset{\chi}{\text{Pr}}_{\mathbb{C}} + \overset{\chi}{h}_{\text{up}}}\,, \tag{28}$$

where $\overset{\chi}{g}_{\max}$ is the maximum uptake capacity of each type at the reference temperature, $\overset{\chi}{l}_{\text{T}}$ is the metabolic temperature response (Eq. 231), $\overset{\chi}{h}_{\text{up}}$ is a predation efficiency constant limiting the chances of encountering prey. Introducing the specific fluxes from prey ψ to predator χ

$$\mathcal{F}|^{\chi}_{\psi} = \overset{\chi}{S}_{\text{growth}}\, f_{\text{pr}}\big|^{\overset{\chi}{Z}}_{\psi} \frac{\psi'_{\mathbb{C}}}{\psi'_{\mathbb{C}} + \overset{\chi}{f}_{\min}} \tag{29}$$

the zooplankton uptake can then be written as:

$$\left.\frac{\partial \overset{\chi}{Z}_{\mathbb{C},\mathbb{N},\mathbb{P}}}{\partial t}\right|_{\text{upt}} = \sum_{\psi} \mathcal{F}|^{\overset{\chi}{Z}}_{\psi} \psi'_{\mathbb{C},\mathbb{N},\mathbb{P}}\,. \tag{30}$$

Note, that in contrast to previous parametrisations, we now normalise the sum of the food preferences for each predator $\overset{\chi}{Z}$ to

$$\sum_{\psi} f_{\text{pr}}\big|^{\overset{\chi}{Z}}_{\psi} = 1\,, \tag{31}$$

as non-normalised preferences lead to a hidden manipulation of the predation efficiency and at low prey concentrations of the maximum uptake capacity $\overset{\chi}{g}_{\max}$.

GMDD
8, 7063–7187, 2015
ERSEM 15.06
M. Butenschön et al.

Zooplankton ingestion of prey is subject to inefficiencies, leading to excretion:

$$\left.\frac{\partial \overset{\chi}{Z}_{\mathbb{C},\mathbb{N},\mathbb{P}}}{\partial t}\right|_{\text{excr}} = \left(1 - \overset{\chi}{q}_{\text{eff}}\right) \overset{\chi}{q}_{\text{excr}} \left.\frac{\partial \overset{\chi}{Z}_{\mathbb{C},\mathbb{N},\mathbb{P}}}{\partial t}\right|_{\text{upt}}, \tag{32}$$

where $\overset{\chi}{q}_{\text{eff}}$ is the carbon uptake efficiency and $\overset{\chi}{q}_{\text{excr}}$ the excreted fraction of inefficiency losses.

Zooplankton respiration is composed of an activity related term given by the remainder of the inefficiency losses and a rest respiration term that is proportional to the biomass by the constant factor $\overset{\chi}{r}_{\text{resp}}$ multiplied with the metabolic temperature response (Eq. 231):

$$\left.\frac{\partial \overset{\chi}{Z}_{\mathbb{C}}}{\partial t}\right|_{\text{resp}} = \left(1 - \overset{\chi}{q}_{\text{eff}}\right)\left(1 - \overset{\chi}{q}_{\text{excr}}\right) \left.\frac{\partial \overset{\chi}{Z}_{\mathbb{C}}}{\partial t}\right|_{\text{growth}} + \overset{\chi}{r}_{\text{resp}} \; \overset{\chi}{l}_{\text{T}} \; \overset{\chi}{Z'}_{\mathbb{C}}. \tag{33}$$

Nitrogen and phosphorus are released regulating the internal stoichiometric quota:

$$\left.\frac{\partial \overset{\chi}{Z}_{\mathbb{N},\mathbb{P}}}{\partial t}\right|_{\text{rel}} = \min\left(0, \overset{\chi}{Z'}_{\mathbb{N},\mathbb{P}} - \overset{\chi}{q}_{\mathbb{N},\mathbb{P}:\mathbb{C}} \; \overset{\chi}{Z'}_{\mathbb{C}}\right) \overset{\chi}{r}_{\text{rel}\mathbb{N},\mathbb{P}}, \tag{34}$$

where $\overset{\chi}{r}_{\text{rel}\mathbb{P},\mathbb{N}}$ are the relaxation rates of release into dissolved inorganic form (see Eqs. 103 and 106).

GMDD
8, 7063–7187, 2015
ERSEM 15.06
M. Butenschön et al.

Mortality is proportional to biomass based on a basal rate $\overset{\chi}{p}_{\text{mort}}$ enhanced up to $\overset{\chi}{p}_{\text{mort}\mathbb{O}} + \overset{\chi}{p}_{\text{mort}}$ under oxygen limitation $\overset{\chi}{l}_{\mathbb{O}}$ (Eq. 241) as:

$$\left.\frac{\partial \overset{\chi}{Z}_{\mathbb{C},\mathbb{N},\mathbb{P}}}{\partial t}\right|_{\text{mort}} = \left(\left(1 - \overset{\chi}{l}_{\mathbb{O}}\right)\overset{\chi}{p}_{\text{mort}\mathbb{O}} + \overset{\chi}{p}_{\text{mort}}\right)\overset{\chi}{Z}'_{\mathbb{C},\mathbb{N},\mathbb{P}} \,. \tag{35}$$

Biomass lost to other predators Ψ is computed as:

$$\left.\frac{\partial \overset{\chi}{Z}_{\mathbb{C},\mathbb{N},\mathbb{P}}}{\partial t}\right|_{\text{pred}} = \sum_{\Psi} \mathcal{F}|^{\Psi}_{\overset{\chi}{Z}} \; \overset{\chi}{Z}'_{\mathbb{C},\mathbb{N},\mathbb{P}} \,. \tag{36}$$

Mesozooplankton

The top-level predator mesozooplankton takes a special role in the predator group in three respects:

It is capable of scavenging on medium size organic matter whose uptake inefficiency is subject to the enhanced uptake inefficiency $\overset{\text{MESO}}{q}_{\text{Rexcr}}$:

$$\left.\frac{\partial \overset{\text{MESO}}{Z}_{\mathbb{C}}}{\partial t}\right|_{\text{excr}} = \left(1 - \overset{\text{MESO}}{q}_{\text{eff}}\right)\overset{\text{MESO}}{q}_{\text{excr}} \sum_{\psi}^{\psi \neq \overset{\text{med}}{R}} \mathcal{F}|^{\overset{\text{MESO}}{Z}}_{\psi} \; \boldsymbol{\psi}'_{\mathbb{C},\mathbb{N},\mathbb{P}} + \overset{\text{MESO}}{q}_{\text{Rexcr}} \mathcal{F}|^{\overset{\text{MESO}}{Z}}_{\overset{\text{med}}{R}} \; \overset{\text{med}}{\boldsymbol{R}}'_{\mathbb{C},\mathbb{N},\mathbb{P}} \tag{37}$$

The second particularity is that it involves an optional hibernation state, that can be activated by the switch `Z4_OW_SW` for over-wintering. In this case the vertically inte-

GMDD
8, 7063–7187, 2015
ERSEM 15.06
M. Butenschön et al.

grated prey availability to mesozooplankton is computed according to:

$$\overset{\mathrm{ow}}{\mathrm{Pr}}_{\mathrm{av}} = \int_{\mathrm{seafloor}}^{0} \overset{\mathrm{MESO}}{\mathrm{Pr}}_{\mathbb{C}} \tag{38}$$

triggering the hibernation state when it falls below the threshold $\overset{\mathrm{ow}}{p}_{\mathrm{min}}$.

In hibernation (overwintering) state the only active processes for mesozooplankton are respiration and mortality. The basal rates of respiration and mortality (r_{owresp} and r_{owmort}) are modified with respect to the active state:

$$\left.\frac{\partial \overset{\mathrm{MESO}}{Z}_{\mathbb{C}}}{\partial t}\right|_{\mathrm{resp}} = r_{\mathrm{owresp}} \overset{\mathrm{MESO}}{Z'}_{\mathbb{C}} \tag{39}$$

$$\left.\frac{\partial \overset{\mathrm{MESO}}{Z}_{\mathbb{C}}}{\partial t}\right|_{\mathrm{mort}} = r_{\mathrm{owmort}} \overset{\mathrm{MESO}}{Z'}_{\mathbb{C}} \tag{40}$$

Finally, mesozooplankton have a fixed nutrient to carbon quota and therefore the process rates are adjusted replacing the nutrient release terms with exudation according to Eqs. (260) and (261) by balancing superfluous carbon uptake as large particulate matter excretion and superfluous nutrients as phosphate or ammonium excretion based on the net fluxes of carbon and nutrients. This results in the following equations for mesozooplankton dynamics:

GMDD
8, 7063–7187, 2015
ERSEM 15.06
M. Butenschön et al.

$$\left.\frac{\partial\, {}^{\mathrm{MESO}}Z_{\mathbb{C}}}{\partial t}\right|_{\mathrm{bgc}} = \left.\frac{\partial\, {}^{\mathrm{MESO}}Z_{\mathbb{C}}}{\partial t}\right|_{\mathrm{upt}} - \left.\frac{\partial\, {}^{\mathrm{MESO}}Z_{\mathbb{C}}}{\partial t}\right|_{\mathrm{excr}} - \left.\frac{\partial\, {}^{\mathrm{MESO}}Z_{\mathbb{C}}}{\partial t}\right|_{\mathrm{resp}} - \left.\frac{\partial\, {}^{\mathrm{MESO}}Z_{\mathbb{C}}}{\partial t}\right|_{\mathrm{mort}} - \left.\frac{\partial\, {}^{\mathrm{MESO}}Z_{\mathbb{C}}}{\partial t}\right|_{\mathrm{pred}} - \left.\frac{\partial\, {}^{\mathrm{MESO}}Z_{\mathbb{C}}}{\partial t}\right|_{\mathrm{exu}}, \tag{41}$$

$$\left.\frac{\partial {}^{\mathrm{MESO}}Z_{\mathbb{N},\mathbb{P}}}{\partial t}\right|_{\mathrm{bgc}} = \left.\frac{\partial {}^{\mathrm{MESO}}Z_{\mathbb{N},\mathbb{P}}}{\partial t}\right|_{\mathrm{upt}} - \left.\frac{\partial {}^{\mathrm{MESO}}Z_{\mathbb{N},\mathbb{P}}}{\partial t}\right|_{\mathrm{excr}} - \left.\frac{\partial {}^{\mathrm{MESO}}Z_{\mathbb{N},\mathbb{P}}}{\partial t}\right|_{\mathrm{mort}} - \left.\frac{\partial {}^{\mathrm{MESO}}Z_{\mathbb{N},\mathbb{P}}}{\partial t}\right|_{\mathrm{pred}} - \left.\frac{\partial {}^{\mathrm{MESO}}Z_{\mathbb{N},\mathbb{P}}}{\partial t}\right|_{\mathrm{exu}}. \tag{42}$$

3.3 Heterotrophic bacteria

The biogeochemical dynamics of heterotrophic bacteria are given by the equations:

$$\left.\frac{\partial B_{\mathbb{C}}}{\partial t}\right|_{\mathrm{bgc}} = \left.\frac{\partial B_{\mathbb{C}}}{\partial t}\right|_{\mathrm{upt}} - \left.\frac{\partial B_{\mathbb{C}}}{\partial t}\right|_{\mathrm{resp}} - \left.\frac{\partial B_{\mathbb{C}}}{\partial t}\right|_{\mathrm{mort}} - \left.\frac{\partial B_{\mathbb{C}}}{\partial t}\right|_{\mathrm{pred}}, \tag{43}$$

$$\left.\frac{\partial B_{\mathbb{N},\mathbb{P}}}{\partial t}\right|_{\mathrm{bgc}} = \left.\frac{\partial B_{\mathbb{N},\mathbb{P}}}{\partial t}\right|_{\mathrm{upt}} - \left.\frac{\partial B_{\mathbb{N},\mathbb{P}}}{\partial t}\right|_{\mathrm{rel}} - \left.\frac{\partial B_{\mathbb{N},\mathbb{P}}}{\partial t}\right|_{\mathrm{mort}} - \left.\frac{\partial B_{\mathbb{N},\mathbb{P}}}{\partial t}\right|_{\mathrm{pred}}. \tag{44}$$

Two alternative sub-modules for decomposition of organic material by bacteria are available in the ERSEM model:

3.3.1 Original version

In this version (Baretta-Bekker et al., 1997; Allen, 2002; Blackford et al., 2004) bacteria feed explicitly only on labile dissolved organic matter $\overset{\mathrm{lab}}{R}$. This is sufficient to create

GMDD
8, 7063–7187, 2015
ERSEM 15.06
M. Butenschön et al.

microbial loop dynamics in the model opening the pathway from dissolved organic matter (DOM) over bacteria to zooplankton, while the other forms of substrate are recycled implicitly (see Eq. 64).

Bacterial uptake of DOM is given by the potential uptake regulated by temperature and limited by nutrient and oxygen conditions, capped at a maximum turn-over rate r^B_{lab} for the labile dissolved organic matter by bacteria:

$$\overset{B}{\mathcal{S}}_{\text{upt}} = \min\left(\overset{B}{g}_{\max}\ \overset{B}{l}_{\text{T}}\ \overset{B}{l}_{\text{O}} \min\left(\overset{B}{l}_{\text{P}}, \overset{B}{l}_{\text{N}}\right) \frac{B_{\text{C}}}{\underset{\text{dis}}{R_{\text{C}}}}, r^B_{\text{lab}}\right), \tag{45}$$

$$\left.\frac{\partial B_{\text{C,N,P}}}{\partial t}\right|_{\text{upt}} = \overset{B}{\mathcal{S}}_{\text{upt}}\ \overset{\text{lab}}{R'}_{\text{C,N,P}}, \tag{46}$$

where $\overset{B}{g}_{\max}$ is the maximum specific uptake of bacteria.

Mortality is given as a constant fraction of bacteria biomass:

$$\left.\frac{\partial B_{\text{C,N,P}}}{\partial t}\right|_{\text{mort}} = \overset{B}{r}_{\text{mort}} B'_{\text{C,N,P}}, \tag{47}$$

where $\overset{B}{r}_{\text{mort}}$ is a constant specific mortality rate for bacteria.

Bacteria respiration is computed according to activity respiration as an investment of activity in growth dependent on the oxygen state and a basal part:

$$\left.\frac{\partial B_{\text{C}}}{\partial t}\right|_{\text{resp}} = \left(1 - \overset{B}{q}_{\text{highO}}\ \overset{B}{l}_{\text{O}} - \overset{B}{q}_{\text{lowO}}\left(1 - \overset{B}{l}_{\text{O}}\right)\right)\left.\frac{\partial B_{\text{C}}}{\partial t}\right|_{\text{upt}} + \overset{B}{r}_{\text{resp}}\ \overset{B}{l}_{\text{T}} B'_{\text{C}}, \tag{48}$$

where $\overset{B}{r}_{\text{resp}}$ is the specific basal respiration rate at rest and $\overset{B}{q}_{\text{highO,lowO}}$ are the bacterial efficiencies at high and low oxygen levels.

GMDD
8, 7063–7187, 2015
ERSEM 15.06
M. Butenschön et al.

Poor nutritional quality of the substrate may result in deprivation of nitrogen or phosphorus resulting in competition with phytoplankton for external dissolved nutrient sources, otherwise bacteria releases superfluous nutrients to the environment. The internal stoichiometric quota of phosphorus is consequently balanced according to:

$$\left.\frac{\partial B_{\mathbb{P}}}{\partial t}\right|_{\text{rel}} = \begin{cases} \overset{B}{r}_{\text{lab}} \left(\overset{B}{q}_{\mathbb{P}:\mathbb{C}} - \overset{B}{q}_{\max_{\mathbb{P}:\mathbb{C}}} \right) B'_{\mathbb{C}} & \text{if } \overset{B}{q}_{\mathbb{P}:\mathbb{C}} \geq \overset{B}{q}_{\max_{\mathbb{P}:\mathbb{C}}} \\ \overset{B}{r}_{\text{lab}} \left(\overset{B}{q}_{\mathbb{P}:\mathbb{C}} - \overset{B}{q}_{\max_{\mathbb{P}:\mathbb{C}}} \right) B_{\mathbb{C}} \frac{N'_{\mathbb{P}}}{N'_{\mathbb{P}} + \overset{B}{h}_{\mathbb{P}}} & \text{if } \overset{B}{q}_{\mathbb{P}:\mathbb{C}} < \overset{B}{q}_{\max_{\mathbb{P}:\mathbb{C}}} \end{cases} \tag{49}$$

with $q_{\max_{\mathbb{P}:\mathbb{C}}}$ being the optimal phosphorus to carbon quota of bacteria and $\overset{B}{r}_{\text{rel}}$ being the specific release rate.

For nitrogen the internal stoichiometric quota is balanced using ammonium:

$$\left.\frac{\partial B_{\mathbb{N}}}{\partial t}\right|_{\text{rel}} = \begin{cases} \overset{B}{r}_{\text{lab}} \left(\overset{B}{q}_{\mathbb{N}:\mathbb{C}} - \overset{B}{q}_{\max_{\mathbb{N}:\mathbb{C}}} \right) B'_{\mathbb{C}} & \text{if } \overset{B}{q}_{\mathbb{N}:\mathbb{C}} \geq \overset{B}{q}_{\max_{\mathbb{N}:\mathbb{C}}} \\ \overset{B}{r}_{\text{lab}} \left(\overset{B}{q}_{\mathbb{N}:\mathbb{C}} - \overset{B}{q}_{\max_{\mathbb{N}:\mathbb{C}}} \right) B_{\mathbb{C}} \frac{\overset{\text{amm}}{N'_{\mathbb{N}}}}{\overset{\text{amm}}{N'_{\mathbb{N}}} + \overset{B}{h}_{\mathbb{N}}} & \text{if } \overset{B}{q}_{\mathbb{N}:\mathbb{C}} < \overset{B}{q}_{\max_{\mathbb{N}:\mathbb{C}}} \end{cases} \tag{50}$$

Predation on bacteria occurs only by heterotrophic flagellates and is given by:

$$\left.\frac{\partial B_{\mathbb{C},\mathbb{P},\mathbb{F},\mathbb{N}}}{\partial t}\right|_{\text{pred}} = \mathcal{F}|_{B}^{\overset{\text{HET}}{Z}} B'_{\mathbb{C},\mathbb{P},\mathbb{F},\mathbb{N}}. \tag{51}$$

3.3.2 Dynamic decomposition version

In this version, activated with the `DOCDYN` preprocessing definition, the decomposition of particulate organic matter is directly mediated by bacteria and the partition between labile dissolved organic matter and dissolved matter with longer degradation time scales (including the additional state of semi-refractory carbon) occurrs in relation

GMDD
8, 7063–7187, 2015
ERSEM 15.06
M. Butenschön et al.

to the nutritional status of bacteria as opposed to the fixed, parametric decomposition and partition of particles in the standard model. The formulation includes the bacteria mediated production of recalcitrant dissolved organic carbon (DOC) (Hansell, 2013) and therefore provides the conceptual framework for an implementation of the microbial carbon pump (Jiao et al., 2014, 2010). However, the fractions of recalcitrant DOM with long turnover time ($\gg 1$ year) are not considered in the current formulation. The sub-model is an extended version of the formulation in Polimene et al. (2006, 2007) with bacteria feeding on all forms of particulate and dissolved organic matter:

$$\tilde{R}_{\mathbb{C},\mathbb{P},\mathbb{N}} = \overset{\text{lab}}{R}_{\mathbb{C},\mathbb{P},\mathbb{N}} + q_{\underset{M}{\text{slab}}} \overset{\text{slab}}{R}_{\mathbb{C},\mathbb{P},\mathbb{N}} + q_{\underset{R}{\text{srefr}}} \overset{\text{srefr}}{R}_{\mathbb{C},\mathbb{P},\mathbb{N}} + q_{\underset{R}{\text{small}}} \overset{\text{small}}{R}_{\mathbb{C},\mathbb{P},\mathbb{N}} + q_{\underset{R}{\text{med}}} \overset{\text{med}}{R}_{\mathbb{C},\mathbb{P},\mathbb{N}} + q_{\underset{R}{\text{large}}} \overset{\text{large}}{R}_{\mathbb{C},\mathbb{P},\mathbb{N}}, \tag{52}$$

where the parameters $q_{\underset{M}{\psi}}$ are non-dimensional turn-over rates relative to $\overset{\text{lab}}{R}$ turn-over, leading to the equations:

$$\overset{B}{S}_{\text{upt}} = \min\left(\overset{B}{g}_{\text{max}} \; \overset{B}{l}_{\text{T}} \; \overset{B}{l}_{\text{O}} \frac{B_{\mathbb{C}}}{\tilde{R}_{\mathbb{C}}}, \overset{B}{r}_{\text{dis}}\right) \tag{53}$$

$$\left.\frac{\partial B_{\mathbb{C},\mathbb{N},\mathbb{P}}}{\partial t}\right|_{\text{upt}} = \overset{B}{S}_{\text{upt}} \tilde{R}_{\mathbb{C},\mathbb{P},\mathbb{N}}, \tag{54}$$

In this case the bacteria losses towards organic carbon differ with respect to the standard model in two ways:

- the growth is not nutrient limited as the internal stoichiometric quota of bacteria is balanced directly through the regulating fluxes releasing carbon into semi-labile organic matter,
- semi-refractory matter is produced as release of capsular material proportionally to the activity respiration by a factor of q_{srefr},

GMDD
8, 7063–7187, 2015
ERSEM 15.06
M. Butenschön et al.

leading to the alternative equations:

$$\left.\frac{\partial B_{\mathbb{C}}}{\partial t}\right|_{\text{bgc}} = \left.\frac{\partial B_{\mathbb{C}}}{\partial t}\right|_{\text{upt}} - \left.\frac{\partial B_{\mathbb{C}}}{\partial t}\right|_{\text{rel}} - \left.\frac{\partial B_{\mathbb{C}}}{\partial t}\right|_{\text{resp}} - \left.\frac{\partial B_{\mathbb{C}}}{\partial t}\right|_{\text{mort}} - \left.\frac{\partial B_{\mathbb{C}}}{\partial t}\right|_{\text{pred}}, \tag{55}$$

$$\left.\frac{\partial B_{\mathbb{C}}}{\partial t}\right|_{\text{rel}} = \overset{B}{r}_{\text{dis}} \max\left(0, \max\left(1 - \frac{q_{\mathbb{P}:\mathbb{C}}}{q_{\max_{\mathbb{P}:\mathbb{C}}}}, 1 - \frac{q_{\mathbb{N}:\mathbb{C}}}{q_{\max_{\mathbb{N}:\mathbb{C}}}}\right)\right) B_{\mathbb{C}}$$
$$+ q_{\text{srefr}}\left(1 - \overset{B}{q}_{\text{high}\mathbb{O}}\ \overset{B}{l}_{\mathbb{O}} - \overset{B}{q}_{\text{low}\mathbb{O}}\left(1 - \overset{B}{l}_{\mathbb{O}}\right)\right) \left.\frac{\partial B_{\mathbb{C}}}{\partial t}\right|_{\text{growth}}. \tag{56}$$

3.4 Particulate organic matter

The particulate matter ($\overset{\chi}{R}$: χ = small, medium or large) fluxes resulting from the above processes are composed of excretion and mortality inputs and decomposition and scavenging losses (for medium size particulate matter only) complemented by inputs resulting from mesozooplankton regulation of the internal stoichiometric ratio for large particulate matter. As the consumer types for simplicity do not include an internal component for iron or silicate, the corresponding component fluxes resulting from predation are directed to particulate matter as indirect excretion.

$$\left.\frac{\partial \overset{\chi}{R}_{\mathbb{C},\mathbb{N},\mathbb{P}}}{\partial t}\right|_{\text{bgc}} = \left.\frac{\partial \overset{\chi}{R}_{\mathbb{C},\mathbb{N},\mathbb{P}}}{\partial t}\right|_{\text{excr}} + \left.\frac{\partial \overset{\chi}{R}_{\mathbb{C},\mathbb{N},\mathbb{P}}}{\partial t}\right|_{\text{mort}} - \left.\frac{\partial \overset{\chi}{R}_{\mathbb{C},\mathbb{N},\mathbb{P}}}{\partial t}\right|_{\text{decomp}}$$

GMDD
8, 7063–7187, 2015
ERSEM 15.06
M. Butenschön et al.

$$\left[-\left. \frac{\partial \overset{\text{med}}{R}_{\mathbb{C},\mathbb{N},\mathbb{P}}}{\partial t} \right|_{\text{scav}} \right] \left[+\left. \frac{\partial \overset{\text{large}}{R}_{\mathbb{C}}}{\partial t} \right|_{\text{adj}} \right], \tag{57}$$

$$\left. \frac{\partial \overset{\chi}{R}_{\mathbb{F}}}{\partial t} \right|_{\text{bgc}} = \left. \frac{\partial \overset{\chi}{R}_{\mathbb{F}}}{\partial t} \right|_{\text{excr}} + \left. \frac{\partial \overset{\chi}{R}_{\mathbb{F}}}{\partial t} \right|_{\text{mort}} - \left. \frac{\partial \overset{\chi}{R}_{\mathbb{F}}}{\partial t} \right|_{\text{decomp}} \left[-\left. \frac{\partial \overset{\text{med}}{R}_{\mathbb{F}}}{\partial t} \right|_{\text{scav}} \right]. \tag{58}$$

$$\left. \frac{\partial \overset{\text{med}}{R}_{\mathbb{S}}}{\partial t} \right|_{\text{bgc}} = \left. \frac{\partial \overset{\text{med}}{R}_{\mathbb{S}}}{\partial t} \right|_{\text{excr}} + \left. \frac{\partial \overset{\text{med}}{R}_{\mathbb{S}}}{\partial t} \right|_{\text{mort}}. \tag{59}$$

Only the excretion of zooplankton (Eq. 32) results in particulate matter by a fraction of $1-\overset{\Psi}{q}_{\text{dloss}}$, while mortality of phytoplankton (Eqs. 13 and 19) and zooplankton (Eqs. 35 and 40) both have a particulate component ($\overset{\psi}{q}_{\text{plys}}$ or $1-\overset{\Psi}{q}_{\text{dloss}}$ respective):

$$\left. \frac{\partial \overset{\chi}{R}_{\mathbb{C}}}{\partial t} \right|_{\text{excr}} = \sum_{\Psi} \left(1 - \overset{\Psi}{q}_{\text{dloss}} \right) \left. \frac{\partial \overset{\Psi}{Z}_{\mathbb{C}}}{\partial t} \right|_{\text{excr}} \tag{60}$$

$$\left. \frac{\partial \overset{\chi}{R}_{\mathbb{N},\mathbb{P}}}{\partial t} \right|_{\text{excr}} = \sum_{\Psi} \left(1 - \overset{\text{lab}}{p}_{\text{cyto}_{\mathbb{N},\mathbb{P}}} \overset{\Psi}{q}_{\text{dloss}} \right) \left. \frac{\partial \overset{\Psi}{Z}_{\mathbb{N},\mathbb{P}}}{\partial t} \right|_{\text{excr}} \tag{61}$$

$$\left. \frac{\partial \overset{\chi}{R}_{\mathbb{C},\mathbb{N},\mathbb{P},\mathbb{F},\mathbb{S}}}{\partial t} \right|_{\text{mort}} = \sum_{\psi} \overset{\psi}{q}_{\text{plys}} \left. \frac{\partial \overset{\psi}{P}_{\mathbb{C},\mathbb{N},\mathbb{P},\mathbb{F},\mathbb{S}}}{\partial t} \right|_{\text{lys}} + \sum_{\Psi} \left(1 - \overset{\Psi}{q}_{\text{dloss}} \right) \left. \frac{\partial \overset{\Psi}{Z}_{\mathbb{C},\mathbb{N},\mathbb{P}}}{\partial t} \right|_{\text{mort}}, \tag{62}$$

GMDD
8, 7063–7187, 2015
ERSEM 15.06
M. Butenschön et al.

where $\overset{\text{lab}}{p}_{\text{cyto}_{\mathbb{N},\mathbb{P}}}$ reflects the relative nitrogen or phosphorus content of cytoplasm with respect to the structural components assuming that the dissolved losses of zooplankton through excretion are largely of cytoplasm origin and $\overset{\Psi}{q}_{\text{dloss}}$ is the dissolved fraction of zooplankton losses. The size classes of particulate organic matter χ in these equations originate from the phytoplankton types $\overset{\psi}{P}$ and zooplankton types $\overset{\Psi}{Z}$ as given in Table 4.

Scavenging of mesozooplankton on medium size particulate organic matter results from Eq. (29):

$$\left.\frac{\partial \overset{\text{med}}{R}_{\mathbb{C},\mathbb{N},\mathbb{P},\mathbb{F},\mathbb{S}}}{\partial t}\right|_{\text{scav}} = \mathcal{F}\Big|_{\overset{\text{med}}{R}}^{\overset{\text{MESO}}{Z}} \overset{\text{med}}{R'}_{\mathbb{C},\mathbb{N},\mathbb{P},\mathbb{F},\mathbb{S}}. \tag{63}$$

Additional large particulate organic matter may result from the mesozooplankton exudation flux $\left.\frac{\partial \overset{\text{large}}{R}_{\mathbb{C}}}{\partial t}\right|_{\text{exu}} = \left.\frac{\partial \overset{\text{MESO}}{Z}_{\mathbb{C}}}{\partial t}\right|_{\text{exu}}$ (Eq. 260).

The decomposition of particulate matter is dependent on the bacteria sub-model applied. In case of the **standard bacteria model** (Sect. 3.3.1) it is converted to dissolved organic matter proportionally to the amount of substrate available by the rate $\overset{\chi}{r}_{\text{decomp}}$ and modified by the nutritional status of the substrate in relation to the Redfield Ratio $q_{\text{ref}_{\mathbb{C}:\mathbb{N}}}$:

$$\left.\frac{\partial \overset{\chi}{R}_{\mathbb{C},\mathbb{N},\mathbb{P},\mathbb{F}}}{\partial t}\right|_{\text{decomp}} = q_{\text{ref}_{\mathbb{C}:\mathbb{N}}} q_{\mathbb{N}:\mathbb{C}} \overset{\chi}{r}_{\text{decomp}} \overset{\chi}{R'}_{\mathbb{C},\mathbb{P},\mathbb{N},\mathbb{F}}. \tag{64}$$

For the **model with dynamic decomposition** (Sect. 3.3.2) directly mediated by bacteria, the decomposition fluxes are given by the bacterial uptake resulting from

GMDD
8, 7063–7187, 2015
ERSEM 15.06
M. Butenschön et al.

Eqs. (52), (53), (54) as:

$$\left.\frac{\partial \overset{\chi}{R}_{\mathbb{C},\mathbb{N},\mathbb{P},\mathbb{F}}}{\partial t}\right|_{\text{decomp}} = -\overset{B}{\mathcal{S}}_{\text{growth}} r_{\overset{\chi}{M}} \overset{\chi}{R}'_{\mathbb{C},\mathbb{P},\mathbb{N},\mathbb{F}} \,. \tag{65}$$

The iron and silicate component of phytoplankton taken up by zooplankton in Eqs. (20) and (23) are for simplicity directly converted to particulate matter:

$$\left.\frac{\partial \overset{\chi}{R}_{\mathbb{F}}}{\partial t}\right|_{\text{excr}} = \sum_{\psi,\Psi} \mathcal{F}|^{\overset{\Psi}{Z}}_{\overset{\psi}{P}} \overset{\psi'}{P}_{\mathbb{F}} \tag{66}$$

$$\left.\frac{\partial \overset{\chi}{R}_{\mathbb{S}}}{\partial t}\right|_{\text{excr}} = \sum_{\psi,\Psi} \mathcal{F}|^{\overset{\Psi}{Z}}_{\overset{\psi}{P}} \overset{\psi'}{P}_{\mathbb{S}} \,. \tag{67}$$

In the case of silicate the particulate organic matter types are given by the size relation analogous to the zooplankton excretion:

- Small particulate organic matter ($\overset{\text{small}}{R}$): heterotrophic flagellates ($\overset{\text{HET}}{Z}$),
- Medium size particulate organic matter ($\overset{\text{med}}{R}$): microzooplankton ($\overset{\text{MICRO}}{Z}$),
- Large particulate organic matter ($\overset{\text{large}}{R}$): mesozooplankton ($\overset{\text{MESO}}{Z}$),

while for iron they are analogous to phytoplankton lysis:

- Small particulate organic matter ($\overset{\text{small}}{R}$): nano- and picophytoplankton ($\overset{\text{nano}}{P}$, $\overset{\text{pico}}{P}$),
- Medium size particulate organic matter ($\overset{\text{med}}{R}$): microphytoplankton and diatoms ($\overset{\text{micro}}{P}$, $\overset{\text{dia}}{P}$),

GMDD
8, 7063–7187, 2015
ERSEM 15.06
M. Butenschön et al.

– Large particulate organic matter ($\overset{\text{large}}{R}$): none.

3.5 Dissolved organic matter

The fluxes of dissolved organic matter are affected by excretion, mortality and decomposition. The partition of labile dissolved, semi-labile and semi-refractory carbon originating from bacteria substantially differs in between the **standard bacteria model** (Sect. 3.3.1) and the **bacteria model with dynamic decomposition** (Sect. 3.3.2).

For the **standard bacteria model** losses of bacteria, phytoplankton and zooplankton in dissolved carbon are fractionated at a constant quota q_{dis} in between labile and semi-labile DOC. Excretion towards the dissolved forms of organic matter may originate from phytoplankton (Eq. 11), or zooplankton (Eq. 32):

$$\left.\frac{\partial \overset{\text{lab}}{R}_{\mathbb{C}}}{\partial t}\right|_{\text{excr}} = q_{\text{dis}} \left(\sum_{\psi} \left.\frac{\partial \overset{\psi}{P}_{\mathbb{C}}}{\partial t}\right|_{\text{excr}} + \sum_{\Psi} \overset{\Psi}{q}_{\text{dloss}} \left.\frac{\partial \overset{\Psi}{Z}_{\mathbb{C}}}{\partial t}\right|_{\text{excr}} \right) \tag{68}$$

$$\left.\frac{\partial \overset{\text{slab}}{R}_{\mathbb{C}}}{\partial t}\right|_{\text{excr}} = (1 - q_{\text{dis}}) \left(\sum_{\psi} \left.\frac{\partial \overset{\psi}{P}_{\mathbb{C}}}{\partial t}\right|_{\text{excr}} + \sum_{\Psi} \overset{\Psi}{q}_{\text{dloss}} \left.\frac{\partial \overset{\Psi}{Z}_{\mathbb{C}}}{\partial t}\right|_{\text{excr}} \right), \tag{69}$$

where $\overset{\Psi}{q}_{\text{dloss}}$ is the dissolved fraction of the zooplankton losses.

Mortality input may originate from all three trophic levels (Eqs. 47, 13, 35, 39):

$$\left.\frac{\partial \overset{\text{lab}}{R}_{\mathbb{C}}}{\partial t}\right|_{\text{mort}} = q_{\text{lab}} \left(\left.\frac{\partial B_{\mathbb{C}}}{\partial t}\right|_{\text{mort}} + \sum_{\psi} \left(1 - \overset{\psi}{q}_{\text{plys}}\right) \left.\frac{\partial \overset{\psi}{P}_{\mathbb{C}}}{\partial t}\right|_{\text{mort}} + \sum_{\Psi} \overset{\Psi}{q}_{\text{dloss}} \left.\frac{\partial \overset{\Psi}{Z}_{\mathbb{C}}}{\partial t}\right|_{\text{mort}} \right) \tag{70}$$

GMDD
8, 7063–7187, 2015

$$\left.\frac{\partial \overset{\text{slab}}{R}_{\mathbb{C}}}{\partial t}\right|_{\text{mort}} = (1-q_{\text{lab}})\left(\left.\frac{\partial B_{\mathbb{C}}}{\partial t}\right|_{\text{mort}} + \sum_{\psi}\left(1-\overset{\psi}{q}_{\text{plys}}\right)\left.\frac{\partial \overset{\psi}{P}_{\mathbb{C}}}{\partial t}\right|_{\text{mort}} + \sum_{\Psi}\overset{\Psi}{q}_{\text{dloss}}\left.\frac{\partial \overset{\Psi}{Z}_{\mathbb{C}}}{\partial t}\right|_{\text{mort}}\right). \quad (71)$$

In addition, the decomposition of the particulate matter types ($\overset{\Psi}{R}$: Ψ= small, medium or large, Eq. 64) and of semi-labile dissolved organic carbon $\overset{\text{slab}}{R}_{\mathbb{C}}$ is directly converted to labile dissolved organic matter ($\overset{\text{lab}}{R}$) according to

$$\left.\frac{\partial \overset{\text{lab}}{R}_{\mathbb{C},\mathbb{N},\mathbb{P}}}{\partial t}\right|_{\text{decomp}} = \sum_{\Psi}\left.\frac{\partial \overset{\Psi}{R}_{\mathbb{C},\mathbb{N},\mathbb{P}}}{\partial t}\right|_{\text{decomp}} + \left.\frac{\partial \overset{\text{slab}}{R}_{\mathbb{C}}}{\partial t}\right|_{\text{decomp}} \quad (72)$$

$$\left.\frac{\partial \overset{\text{slab}}{R}_{\mathbb{C}}}{\partial t}\right|_{\text{decomp}} = \overset{\text{slab}}{r}_{\text{decomp}}\overset{\text{slab}}{R'}_{\mathbb{C}} \quad (73)$$

without explicit mediation of bacteria.

In the **dynamic decomposition model** the fractionation of dissolved organic matter originating from bacteria and phytoplankton is based on the originating process. This reflects the capacity of bacteria to utilise different forms of substrate and discarding the less digestible forms adding semi-refractory organic matter to the set of state variables. This is reflected in lysis/mortality contributing to the labile DOM pool, while excretion of carbon occurs in semi-labile form. Zooplankton losses are treated identically with respect to the standard bacteria model. Excretion of DOC may originate from the phyto- and zooplankton excretion (Eqs. 11 and 32), the regulation of the bacterial

GMDD
8, 7063–7187, 2015
ERSEM 15.06
M. Butenschön et al.

stoichiometric quota (Eq. 56) and excess bacterial growth:

$$\left.\frac{\partial \overset{\text{lab}}{R}_{\mathbb{C}}}{\partial t}\right|_{\text{excr}} = \sum_{\Psi} q_{\text{dis}}\ \overset{\Psi}{q}_{\text{dloss}} \left.\frac{\partial \overset{\Psi}{Z}_{\mathbb{C}}}{\partial t}\right|_{\text{excr}} \tag{74}$$

$$\left.\frac{\partial \overset{\text{slab}}{R}_{\mathbb{C}}}{\partial t}\right|_{\text{excr}} = \left.\frac{\partial B_{\mathbb{C}}}{\partial t}\right|_{\text{rel}} + \sum_{\psi} \left.\frac{\partial \overset{\psi}{P}_{\mathbb{C}}}{\partial t}\right|_{\text{excr}} + \sum_{\Psi} (1 - q_{\text{dis}})\, \overset{\Psi}{q}_{\text{dloss}} \left.\frac{\partial \overset{\Psi}{Z}_{\mathbb{C}}}{\partial t}\right|_{\text{excr}} \tag{75}$$

$$\left.\frac{\partial \overset{\text{srefr}}{R}_{\mathbb{C}}}{\partial t}\right|_{\text{excr}} = p_{\text{srefr}} \left(1 - \overset{B}{q}_{\text{high}\mathbb{O}}\ \overset{B}{l}_{\mathbb{O}} - \overset{B}{q}_{\text{low}\mathbb{O}} \left(1 - \overset{B}{l}_{\mathbb{O}}\right)\right) \left.\frac{\partial B_{\mathbb{C}}}{\partial t}\right|_{\text{growth}}, \tag{76}$$

while the non-particulate part of mortality/lysis is split according to:

$$\left.\frac{\partial \overset{\text{lab}}{R}_{\mathbb{C}}}{\partial t}\right|_{\text{mort}} = \left.\frac{\partial B_{\mathbb{C}}}{\partial t}\right|_{\text{mort}} + \sum_{\psi} \left(1 - \overset{\psi}{q}_{\text{plys}}\right) \left.\frac{\partial \overset{\psi}{P}_{\mathbb{C}}}{\partial t}\right|_{\text{lysis}} + \sum_{\Psi} q_{\text{dis}}\ \overset{\Psi}{q}_{\text{dloss}} \left.\frac{\partial \overset{\Psi}{Z}_{\mathbb{C}}}{\partial t}\right|_{\text{mort}} \tag{77}$$

$$\left.\frac{\partial \overset{\text{slab}}{R}_{\mathbb{C}}}{\partial t}\right|_{\text{mort}} = \sum_{\Psi} (1 - q_{\text{dis}})\, \overset{\Psi}{q}_{\text{dloss}} \left.\frac{\partial \overset{\Psi}{Z}_{\mathbb{C}}}{\partial t}\right|_{\text{mort}}. \tag{78}$$

Uptake of labile dissolved matter by bacteria is given by

$$\left.\frac{\partial \overset{\text{lab}}{R}_{\mathbb{C},\mathbb{N},\mathbb{P}}}{\partial t}\right|_{\text{upt}} = \overset{B}{\mathcal{S}}_{\text{growth}}\ \overset{\text{lab}}{R'}_{\mathbb{C},\mathbb{N},\mathbb{P}}, \tag{79}$$

GMDD
8, 7063–7187, 2015
ERSEM 15.06
M. Butenschön et al.

where the substrate-specific uptake of bacteria $\overset{B}{S}_{\text{growth}}$ is given in Eq. (45) for the **standard decomposition** model and in Eq. (53) for the **dynamic decomposition model**.

All other terms are identical for both decomposition sub-models. Excretion and mortality of nitrogen and phosphorus result in the dissolved fluxes

$$\left.\frac{\partial \overset{\text{lab}}{R}_{\text{IN,IP}}}{\partial t}\right|_{\text{excr}} = \sum_{\Psi} \overset{\Psi}{q}_{\text{dloss}} \, \overset{\text{lab}}{p}_{\text{cyto}_{\text{IN,IP}}} \left.\frac{\partial \overset{\Psi}{Z}_{\text{IN,IP}}}{\partial t}\right|_{\text{excr}} \tag{80}$$

$$\left.\frac{\partial \overset{\text{lab}}{R}_{\text{IN,IP}}}{\partial t}\right|_{\text{mort}} = \left.\frac{\partial B_{\text{IN,IP}}}{\partial t}\right|_{\text{mort}} + \sum_{\psi} \left(1 - \overset{\psi}{q}_{\text{plys}}\right) \left.\frac{\partial \overset{\psi}{P}_{\text{IN,IP}}}{\partial t}\right|_{\text{mort}} + \sum_{\Psi} \overset{\Psi}{q}_{\text{dloss}} \left.\frac{\partial \overset{\Psi}{Z}_{\text{IN,IP}}}{\partial t}\right|_{\text{mort}} . \tag{81}$$

Remineralisation of dissolved organic nutrients into inorganic form is given by fixed specific remineralisation rates $r_{\text{rem}_{N,\text{IP}}}$:

$$\left.\frac{\partial \overset{\text{lab}}{R}_{\text{IN,IP}}}{\partial t}\right|_{\text{remin}} = r_{\text{rem}_{\text{IN,IP}}} \, \overset{\text{dis}}{R'}_{\text{IN,IP}} . \tag{82}$$

GMDD
8, 7063–7187, 2015
ERSEM 15.06
M. Butenschön et al.

In summary, for the **standard model** the balance equations for dissolved organic matter are given as:

$$\left.\frac{\partial^{\text{lab}} R_{\mathbb{C},\mathbb{N},\mathbb{P}}}{\partial t}\right|_{\text{bgc}} = \left.\frac{\partial^{\text{lab}} R_{\mathbb{C},\mathbb{N},\mathbb{P}}}{\partial t}\right|_{\text{excr}} + \left.\frac{\partial^{\text{lab}} R_{\mathbb{C},\mathbb{N},\mathbb{P}}}{\partial t}\right|_{\text{mort}} + \left.\frac{\partial^{\text{lab}} R_{\mathbb{C},\mathbb{N},\mathbb{P}}}{\partial t}\right|_{\text{decomp}} - \left.\frac{\partial^{\text{lab}} R_{\mathbb{C},\mathbb{N},\mathbb{P}}}{\partial t}\right|_{\text{upt}} - \left.\frac{\partial^{\text{lab}} R_{\mathbb{C},\mathbb{N},\mathbb{P}}}{\partial t}\right|_{\text{remin}}, \tag{83}$$

$$\left.\frac{\partial^{\text{slab}} R_{\mathbb{C}}}{\partial t}\right|_{\text{bgc}} = \left.\frac{\partial^{\text{slab}} R_{\mathbb{C}}}{\partial t}\right|_{\text{excr}} + \left.\frac{\partial^{\text{slab}} R_{\mathbb{C}}}{\partial t}\right|_{\text{mort}} - \left.\frac{\partial^{\text{slab}} R_{\mathbb{C}}}{\partial t}\right|_{\text{decomp}}, \tag{84}$$

while for the **dynamic model** they are given by:

$$\left.\frac{\partial^{\text{lab}} R_{\mathbb{C},\mathbb{N},\mathbb{P}}}{\partial t}\right|_{\text{bgc}} = \left.\frac{\partial^{\text{lab}} R_{\mathbb{C},\mathbb{N},\mathbb{P}}}{\partial t}\right|_{\text{excr}} + \left.\frac{\partial^{\text{lab}} R_{\mathbb{C},\mathbb{N},\mathbb{P}}}{\partial t}\right|_{\text{mort}} - \left.\frac{\partial^{\text{lab}} R_{\mathbb{C},\mathbb{N},\mathbb{P}}}{\partial t}\right|_{\text{upt}} \left[- \left.\frac{\partial^{\text{lab}} R_{\mathbb{N},\mathbb{P}}}{\partial t}\right|_{\text{remin}} \right], \tag{85}$$

GMDD
8, 7063–7187, 2015
ERSEM 15.06
M. Butenschön et al.

$$\left.\frac{\partial\, {}^{\text{slab}}R_{\mathbb{C}}}{\partial t}\right|_{\text{bgc}} = \left.\frac{\partial\, {}^{\text{slab}}R_{\mathbb{C}}}{\partial t}\right|_{\text{excr}} + \left.\frac{\partial\, {}^{\text{slab}}R_{\mathbb{C}}}{\partial t}\right|_{\text{mort}} - \left.\frac{\partial\, {}^{\text{upt}}R_{\mathbb{C}}}{\partial t}\right|_{\text{upt}}, \tag{86}$$

$$\left.\frac{\partial\, {}^{\text{srefr}}R_{\mathbb{C}}}{\partial t}\right|_{\text{bgc}} = \left.\frac{\partial\, {}^{\text{lab}}R_{\mathbb{C}}}{\partial t}\right|_{\text{excr}} - \left.\frac{\partial\, {}^{\text{lab}}R_{\mathbb{C}}}{\partial t}\right|_{\text{upt}}. \tag{87}$$

3.6 Calcification

The model in its current form does not include calcifiers as a dedicated functional group. Nevertheless, the process of calcification is treated implicitly by considering part of the nanophytoplankton to act as calcifiers. Calcification processes are inferred from the system dynamics based on the assumption of a given quota between particulate inorganic carbon over particulate organic carbon in sedimenting material, usually referred to as rain-ratio. Here this ratio is used as a proxy for the calcite production matching the local increase of POC originating from nanophytoplankton.

In this context the local rain-ratio is based on a reference ratio q_{rain0} that varies according to the regulating factors ${}^{\text{calc}}f_{\mathbb{C}}$, ${}^{\text{calc}}f_{\text{T}}$ and ${}^{\text{calc}}f_{\langle \text{INP} \rangle}$ given in Eqs. (252) or (254), (256) and (257):

$$q_{\text{rain}} = \max\left(\frac{1}{200}, q_{\text{rain0}}\, {}^{\text{calc}}f_{\mathbb{C}}\, {}^{\text{calc}}f_{\text{T}}\, {}^{\text{calc}}f_{\langle \text{INP} \rangle}\right), \tag{88}$$

where

$$\left.\frac{\partial\, {}^{\text{calc}}R_{\mathbb{C}}}{\partial t}\right|_{\text{bgc}} = \left.\frac{\partial\, {}^{\text{calc}}R_{\mathbb{C}}}{\partial t}\right|_{\text{lys}} + \left.\frac{\partial\, {}^{\text{calc}}R_{\mathbb{C}}}{\partial t}\right|_{\text{pred}} + \left.\frac{\partial\, {}^{\text{calc}}R_{\mathbb{C}}}{\partial t}\right|_{\text{sed}} - \left.\frac{\partial\, {}^{\text{calc}}R_{\mathbb{C}}}{\partial t}\right|_{\text{dis}} \tag{89}$$

GMDD
8, 7063–7187, 2015
ERSEM 15.06
M. Butenschön et al.

The contribution of nanophytoplankton lysis to calcite production is proportional to the particulate fraction of lysis (compare Eq. 62) by the rain ratio

$$\left.\frac{\partial \overset{\text{calc}}{R}_{\mathrm{C}}}{\partial t}\right|_{\text{lys}} = q_{\text{rain}}\ \overset{\text{nano}}{q}_{\text{plys}}\left.\frac{\partial \overset{\text{nano}}{P}_{\mathrm{C}}}{\partial t}\right|_{\text{lys}} \tag{90}$$

Ingestion of nanophytoplankton and subsequent dissolution in zooplankton guts contributes with a fraction q_{gutdiss} of the excreted part of nanophytoplankton uptake by the various zooplankton groups (compare Eqs. 14 and 32):

$$\left.\frac{\partial \overset{\text{calc}}{R}_{\mathrm{C}}}{\partial t}\right|_{\text{pred}} = q_{\text{rain}} q_{\text{gutdiss}} \left(1 - \overset{\chi}{q}_{\text{eff}}\right) \overset{\chi}{q}_{\text{excr}} \sum_{\Psi} \mathcal{F}|^{\overset{\Psi}{Z}}_{\overset{\text{nano}}{P}}\ \overset{\text{nano}}{P'_{\mathrm{C}}} \tag{91}$$

As sedimentation of nanophytoplankton contributes to the organic carbon considered in the rain-ratio the matching contribution to calcite production is computed as

$$\left.\frac{\partial \overset{\text{calc}}{R}_{\mathrm{C}}}{\partial t}\right|_{\text{sed}} = q_{\text{rain}} \left.\frac{\partial \overset{\text{nano}}{P}_{\mathrm{C}}}{\partial t}\right|_{\text{sed}} \tag{92}$$

with the sinking rate $\left.\frac{\partial \overset{\text{nano}}{P}_{\mathrm{C}}}{\partial t}\right|_{\text{sed}}$ given in Eq. (136).

Dissolution of calcite is proportional to the current concentration of calcite with a maximum rate of r_{dis}, regulated by $\overset{\text{calc}}{I}_{\mathrm{C}}$ (Eqs. 253 or 255):

$$\left.\frac{\partial \overset{\text{calc}}{R}_{\mathrm{C}}}{\partial t}\right|_{\text{dis}} = r_{\text{dis}}\ \overset{\text{dis}}{I}_{\mathrm{C}}\ \overset{\text{calc}}{R'_{\mathrm{C}}} \tag{93}$$

The solution of the calcite dynamics is optional and activated by the preprocessing switch CALC.

GMDD
8, 7063–7187, 2015
ERSEM 15.06
M. Butenschön et al.

3.7 Inorganic components

The dynamics of dissolved inorganic nutrients in the model are given by uptake of phytoplankton and bacteria and are resupplied locally by remineralisation and excretion

$$\left.\frac{\partial \overset{\text{ox}}{N}_{\text{IN}}}{\partial t}\right|_{\text{bgc}} = \left.\frac{\partial \overset{\text{ox}}{N}_{\text{IN}}}{\partial t}\right|_{\text{nitr}} - \left.\frac{\partial \overset{\text{ox}}{N}_{\text{IN}}}{\partial t}\right|_{\text{upt}}, \tag{94}$$

$$\left.\frac{\partial \overset{\text{amm}}{N}_{\text{IN}}}{\partial t}\right|_{\text{bgc}} = \left.\frac{\partial \overset{\text{amm}}{N}_{\text{IN}}}{\partial t}\right|_{\text{remin}} + \left.\frac{\partial \overset{\text{amm}}{N}_{\text{IN}}}{\partial t}\right|_{\text{rel}} - \left.\frac{\partial \overset{\text{amm}}{N}_{\text{IN}}}{\partial t}\right|_{\text{upt}} - \left.\frac{\partial \overset{\text{amm}}{N}_{\text{IN}}}{\partial t}\right|_{\text{nitr}}, \tag{95}$$

$$\left.\frac{\partial N_{\text{IP}}}{\partial t}\right|_{\text{bgc}} = \left.\frac{\partial N_{\text{IP}}}{\partial t}\right|_{\text{remin}} + \left.\frac{\partial N_{\text{IP}}}{\partial t}\right|_{\text{rel}} - \left.\frac{\partial N_{\text{IP}}}{\partial t}\right|_{\text{upt}}, \tag{96}$$

$$\left.\frac{\partial N_{\text{S}}}{\partial t}\right|_{\text{bgc}} = \left.\frac{\partial N_{\text{S}}}{\partial t}\right|_{\text{rel}} - \left.\frac{\partial N_{\text{S}}}{\partial t}\right|_{\text{upt}}, \tag{97}$$

$$\left.\frac{\partial N_{\text{IF}}}{\partial t}\right|_{\text{bgc}} = \left.\frac{\partial N_{\text{IF}}}{\partial t}\right|_{\text{remin}} + \left.\frac{\partial N_{\text{IF}}}{\partial t}\right|_{\text{rel}} - \left.\frac{\partial N_{\text{IF}}}{\partial t}\right|_{\text{upt}} - \left.\frac{\partial N_{\text{IF}}}{\partial t}\right|_{\text{scav}}. \tag{98}$$

Oxidised nitrogen in the water-column is taken up only by the four phytoplankton types $\overset{\psi}{P}$ following Eq. (18) according to external availability:

$$\left.\frac{\partial \overset{\text{ox}}{N}_{\text{IN}}}{\partial t}\right|_{\text{upt}} = \sum_{\psi} \frac{\overset{\psi}{r}_{\text{aff}_n} \overset{\text{ox}}{N'}_{\text{IN}}}{\left(\overset{\psi}{r}_{\text{aff}_n} \overset{\text{ox}}{N'}_{\text{IN}} + \overset{\psi}{r}_{\text{aff}_a} \overset{\text{amm}}{N'}_{\text{IN}}\right)} \max\left(0, \left.\frac{\partial \overset{\psi}{P}_{\text{IN}}}{\partial t}\right|_{\text{upt}}\right) \tag{99}$$

GMDD
8, 7063–7187, 2015
ERSEM 15.06
M. Butenschön et al.

and regenerated exclusively by nitrification:

$$\left.\frac{\partial \overset{\mathrm{ox}}{N}_{\mathbb{N}}}{\partial t}\right|_{\mathrm{nitr}} = \overset{B}{r}_{\mathrm{nitr}}\ \overset{B\,\mathrm{nitr}}{l}_{\mathrm{T}}\overset{\mathrm{nitr}}{l}_{\mathbb{O}}\overset{\mathrm{nitr}}{l}_{\mathbb{N}}l_{\mathrm{pH}}\overset{\mathrm{amm}}{N'}_{\mathbb{N}}, \tag{100}$$

where $\overset{B}{r}_{\mathrm{nitr}}$ is the maximum specific nitrification rate at reference temperature. The various regulation and limitation factors $\overset{B}{l}_{\mathrm{T}}$, $\overset{\mathrm{nitr}}{l}_{\mathbb{O}}$, $\overset{\mathrm{nitr}}{l}_{\mathbb{N}}$ and l_{pH} are given in Sect. 6.1.

Ammonium is taken up by phytoplankton as the reduced part of total nitrogen uptake (Eq. 18) and bacteria when nitrogen limited

$$\left.\frac{\partial \overset{\mathrm{amm}}{N}_{\mathbb{N}}}{\partial t}\right|_{\mathrm{upt}} = \sum_{\psi} \frac{\overset{\psi}{r}_{\mathrm{aff}_n}\ \overset{\mathrm{amm}}{N'}_{\mathbb{N}}}{\left(\overset{\psi}{r}_{\mathrm{aff}_n}\ \overset{\mathrm{ox}}{N'}_{\mathbb{N}} + \overset{\psi}{r}_{\mathrm{aff}_a}\ \overset{\mathrm{amm}}{N'}_{\mathbb{N}}\right)} \max\left(0, \left.\frac{\partial \overset{\psi}{P}_{\mathbb{N}}}{\partial t}\right|_{\mathrm{upt}}\right) - \min\left(0, \left.\frac{\partial B_{\mathbb{N}}}{\partial t}\right|_{\mathrm{rel}}\right) \tag{101}$$

and remineralised according to Eq. (82)

$$\left.\frac{\partial \overset{\mathrm{amm}}{N}_{\mathbb{N}}}{\partial t}\right|_{\mathrm{remin}} = r_{\mathrm{rem}_{\mathbb{N}}}\ \overset{\mathrm{lab}}{R'}_{\mathbb{N}}. \tag{102}$$

Ammonium is released by the phytoplankton types ψ (Eq. 18) when above their luxury storage capacity and by the zooplankton types Ψ (Eqs. 34 and 261) and bacteria

GMDD
8, 7063–7187, 2015
ERSEM 15.06
M. Butenschön et al.

(Eq. 50) when above their optimal quota

$$\left.\frac{\partial^{\mathrm{amm}} N_{\mathbb{N}}}{\partial t}\right|_{\mathrm{rel}} = -\sum_{\psi} \min\left(0, \left.\frac{\partial^{\psi} P_{\mathbb{N}}}{\partial t}\right|_{\mathrm{upt}}\right) + \left.\sum_{\Psi} \frac{\partial^{\Psi} Z_{\mathbb{N}}}{\partial t}\right|_{\mathrm{rel}} + \min\left(0, \left.\frac{\partial B_{\mathbb{N}}}{\partial t}\right|_{\mathrm{rel}}\right). \quad (103)$$

Ammonium concentrations may be further reduced by nitrification:

$$\left.\frac{\partial^{\mathrm{amm}} N_{\mathbb{N}}}{\partial t}\right|_{\mathrm{nitr}} = {}^{B}r_{\mathrm{nitr}}\ {}^{B}l_{\mathrm{T}} l_{\mathbb{O}_{\mathrm{nitr}}} l_{\mathbb{N}_{\mathrm{nitr}}} l_{\mathrm{pH}}\, {}^{\mathrm{amm}}N'_{\mathbb{N}}. \quad (104)$$

Phosphorus dynamics are analogous to nitrogen dynamics but simplified with only one dissolved inorganic pool being considered in the model. It is taken up according to Eqs. (18) and (49)

$$\left.\frac{\partial N_{\mathbb{P}}}{\partial t}\right|_{\mathrm{upt}} = \sum_{\psi} \max\left(0, \left.\frac{\partial^{\psi} P_{\mathbb{P}}}{\partial t}\right|_{\mathrm{upt}}\right) - \min\left(0, \left.\frac{\partial B_{\mathbb{P}}}{\partial t}\right|_{\mathrm{rel}}\right), \quad (105)$$

released following Eqs. (18), (49), (34) and (35)

$$\left.\frac{\partial N_{\mathbb{P}}}{\partial t}\right|_{\mathrm{rel}} = \left.\sum_{\Psi} \frac{\partial^{\Psi} Z_{\mathbb{P}}}{\partial t}\right|_{\mathrm{rel}} - \sum_{\psi} \min\left(0, \left.\frac{\partial^{\psi} P_{\mathbb{P}}}{\partial t}\right|_{\mathrm{upt}}\right) + \max\left(0, \left.\frac{\partial B_{\mathbb{P}}}{\partial t}\right|_{\mathrm{rel}}\right) \quad (106)$$

GMDD
8, 7063–7187, 2015
ERSEM 15.06
M. Butenschön et al.

and remineralised as given in Eq. (50)

$$\left.\frac{\partial N_{\mathbb{P}}}{\partial t}\right|_{\text{remin}} = r_{\text{rem}_{\mathbb{P}}} \overset{\text{lab}}{R'}_{\mathbb{P}} . \tag{107}$$

Iron is taken up only by phytoplankton (Eq. 18)

$$\left.\frac{\partial N_{\mathbb{F}}}{\partial t}\right|_{\text{upt}} = \sum_{\psi} \max\left(0, \left.\frac{\partial \overset{\psi}{P}_{\mathbb{F}}}{\partial t}\right|_{\text{upt}}\right) \tag{108}$$

and subject to scavenging due to hydroxide, treated similarly as in Aumont et al. (2003) and Vichi et al. (2007):

$$\left.\frac{\partial N_{\mathbb{F}}}{\partial t}\right|_{\text{scav}} = r_{\mathbb{F}\text{scav}} \max\left(0, N'_{\mathbb{F}}\right) , \tag{109}$$

where $r_{\mathbb{F}\text{scav}}$ is a threshold concentration over which scavenging occurs, here fixed at $0.6 \frac{\mu\text{mol}}{\text{m}^3}$.

Iron is released by phytoplankton (Eq. 18)

$$\left.\frac{\partial N_{\mathbb{F}}}{\partial t}\right|_{\text{rel}} = -\sum_{\psi} \min\left(0, \left.\frac{\partial \overset{\psi}{P}_{\mathbb{F}}}{\partial t}\right|_{\text{upt}}\right) \tag{110}$$

and implicitly remineralised by mesozooplankton scavenging of particulate organic matter (Eq. 63) and bacterial consumption of particulate matter (Eqs. 64 and 65)

$$\left.\frac{\partial N_{\mathbb{F}}}{\partial t}\right|_{\text{remin}} = \mathcal{F}\Big|_{\substack{\text{med} \\ R}}^{\text{MESO}} \overset{\text{med}}{Z} R'_{\mathbb{F}} \left[+ \left.\frac{\partial \overset{\chi}{R}_{\mathbb{C},\mathbb{N},\mathbb{P},\mathbb{F}}}{\partial t}\right|_{\text{decomp}} \right] . \tag{111}$$

GMDD
8, 7063–7187, 2015
ERSEM 15.06
M. Butenschön et al.

Silicate is taken up

$$\left.\frac{\partial N_{\mathrm{S}}}{\partial t}\right|_{\mathrm{uptake}} = \max\left(0, {}^{\mathrm{dia}}q_{\mathrm{ref}_{\mathrm{S:C}}} \, {}^{\mathrm{dia}}S_{\mathrm{growth}}\right) \tag{112}$$

and released

$$\left.\frac{\partial N_{\mathrm{S}}}{\partial t}\right|_{\mathrm{rel}} = \max\left(0, P'^{\mathrm{dia}}_{\mathrm{S}} - {}^{\mathrm{dia}}q_{\mathrm{ref}_{\mathrm{S:C}}} \, P'^{\mathrm{dia}}_{\mathrm{C}}\right) \tag{113}$$

exclusively by diatoms (Eq. 21). It is not remineralised in the pelagic part of the system.

The dynamics of DIC are given by photosynthesis and respiration of the organisms considered and calcification and dissolution of calcite:

$$\begin{aligned}\left.\frac{\partial O_{\mathrm{C}}}{\partial t}\right|_{\mathrm{bgc}} = &\left.\frac{\partial B_{\mathrm{C}}}{\partial t}\right|_{\mathrm{resp}} + \sum_{\psi} \left.\frac{\partial {}^{\psi}P_{\mathrm{C}}}{\partial t}\right|_{\mathrm{resp}} + \sum_{\Psi} \left.\frac{\partial {}^{\Psi}Z_{\mathrm{C}}}{\partial t}\right|_{\mathrm{resp}} \\ &- \sum_{\psi} \left.\frac{\partial {}^{\chi}P_{\mathrm{C}}}{\partial t}\right|_{\mathrm{gpp}} + \left.\frac{\partial {}^{\mathrm{calc}}R_{\mathrm{C}}}{\partial t}\right|_{\mathrm{dis}} - \left.\frac{\partial {}^{\mathrm{calc}}R_{\mathrm{C}}}{\partial t}\right|_{\mathrm{calc}},\end{aligned} \tag{114}$$

where the respiration terms $\left.\frac{\partial B_{\mathrm{C}}}{\partial t}\right|_{\mathrm{resp}}$, $\left.\frac{\partial {}^{\psi}P_{\mathrm{C}}}{\partial t}\right|_{\mathrm{resp}}$ and $\left.\frac{\partial {}^{\Psi}Z_{\mathrm{C}}}{\partial t}\right|_{\mathrm{resp}}$ are given in Eqs. (48), (12), (33) and (39), synthesis of carbon is given in Eq. (8), the dissolution of calcite is given in Eq. (93) and precipitation of DIC into calcite is given by the sum of the calcification terms

$$\left.\frac{\partial {}^{\mathrm{calc}}R_{\mathrm{C}}}{\partial t}\right|_{\mathrm{calc}} = \left.\frac{\partial {}^{\mathrm{calc}}R_{\mathrm{C}}}{\partial t}\right|_{\mathrm{lys}} + \left.\frac{\partial {}^{\mathrm{calc}}R_{\mathrm{C}}}{\partial t}\right|_{\mathrm{graz}} + \left.\frac{\partial {}^{\mathrm{calc}}R_{\mathrm{C}}}{\partial t}\right|_{\mathrm{sed}} \tag{115}$$

GMDD
8, 7063–7187, 2015
ERSEM 15.06
M. Butenschön et al.

given in Eqs. (90), (91) and (92).

Rates of change of oxygen are implied from the corresponding carbon fluxes converted by stoichiometric factors taking into account different efficiencies for respiration $\overset{\text{resp}}{p}_{\mathbb{O}}$ and photosynthesis $\overset{\text{syn}}{p}_{\mathbb{O}}$.

The pelagic oxygen cycle is reduced to the consumption of dissolved oxygen in respiration (Eqs. 48, 12, 33 and 39) and the production of dissolved oxygen in photosynthesis (Eq. 8):

$$\left.\frac{\partial O_{\mathbb{O}}}{\partial t}\right|_{\text{bgc}} = -\overset{\text{resp}}{p}_{\mathbb{O}} \left.\frac{\partial B_{\mathbb{C}}}{\partial t}\right|_{\text{resp}} - \overset{\text{resp}}{p}_{\mathbb{O}} \sum_{\psi}^{\psi} \left.\frac{\partial P_{\mathbb{C}}}{\partial t}\right|_{\text{resp}} - \overset{\text{resp}}{p}_{\mathbb{O}} \sum_{\Psi}^{\Psi} \left.\frac{\partial Z_{\mathbb{C}}}{\partial t}\right|_{\text{resp}} + \overset{\text{syn}}{p}_{\mathbb{O}} \sum_{\psi}^{\chi} \left.\frac{\partial P_{\mathbb{C}}}{\partial t}\right|_{\text{gpp}} . \tag{116}$$

3.8 The carbonate system

The model for the carbonate system incorprated in ERSEM was introduced in Blackford and Burkill (2002) and further developed in Blackford and Gilbert (2007); Artioli et al. (2012). In this model, the speciation of carbon is calculated from dissolved inorganic carbon $O_{\mathbb{C}}$, total alkalinity $\mathbb{A}_{\text{tot}}$ (which is calculated from a regression of temperature and salinity complemented by modifications due to the biological processes in Eq. 127, if activated) and total boron $\mathbb{B}_{\text{tot}}$ (which is calculated from a linear regression of salinity). It assumes chemical equilibrium between the inorganic carbon species justified by the fast reaction time scales of the underlying chemical reaction compared to the biological and physical rates on the spatial scales the model operates on. The comprehensive set of equations to describe the carbonate system and ways to solve it given specific subsets of known quantities have been extensively described elsewhere (Dickson et al., 2007; Zeebe and Wolf-Gladrow, 2001), here we use a simplified set omitting the components that contribute less under general sea-water conditions (Takahashi et al., 1982).

The three quantities $O_{\mathbb{C}}$, $\mathbb{A}_{\text{tot}}$ and $\mathbb{B}_{\text{tot}}$ are used to derive the partial pressure of carbon dioxide p_{CO_2}, carbonic acid, carbonate and bicarbonate concentrations ($c_{[H_2CO_3]}$,

GMDD
8, 7063–7187, 2015

$c_{\left[CO_3^{2-}\right]}$ and $c_{[HCO_3^-]}$) and pH (using the seawater scale) at chemical equilibrium. These utilise the four equilibrium constants for solubility of carbon dioxide and for the dissociation of carbonic acid, bicarbonate and boric acid derived from empirical environmental relationships (Millero, 1995; Mehrbach et al., 1973; Weiss, 1974; Dickson, 1990) that are detailed in the Supplement for reference. The resulting set of equations to solve is then given by:

$$\mathbb{C}_{\text{tot}} = c_{\left[CO_3^{2-}\right]} + c_{[HCO_3^-]} + c_{[CO_2^*]} \tag{117}$$

$$\mathbb{A}_{\text{tot}} = c_{[HCO_3^-]} + 2c_{\left[CO_3^{2-}\right]} + c_{[B(OH)_4^-]} \tag{118}$$

$$\mathbb{B}_{\text{tot}} = c_{[B(OH)_3]} + c_{[B(OH)_4^-]} \tag{119}$$

$$c_{B(OH)_3} = \frac{c_{[H^+]} c_{[B(OH)_4^-]}}{k_b} \tag{120}$$

$$c_{CO_2^*} = \frac{c_{[H^+]} c_{[HCO_3^-]}}{k_1} \tag{121}$$

$$c_{HCO_3^-} = \frac{c_{[H^+]} c_{\left[CO_3^{2-}\right]}}{k_2} \tag{122}$$

$$\text{pH} = -\log_{10}\left(c_{[H^+]}\right) \tag{123}$$

$$p_{CO_2} = k_0 c_{[CO_2^*]} \tag{124}$$

The system is solved using the HALTAFALL algorithm (Ingri et al., 1967) by using the equilibrium relations 120 to 122 to eliminate the unknowns $c_{[B(OH)_3]}$, $c_{[CO_2^*]}$ and $c_{[HCO_3^-]}$. The balance equations for DIC and total boron are then used to express $c_{\left[CO_3^{2-}\right]}$ and $c_{[B(OH)_4^-]}$ in the balance equation for alkalinity (Eq. 118) as functions of the only remaining unknown $c_{[H^+]}$. This equation is solved for the logarithm of the unknown variable (allowing only positive real numbers as solution) applying a combination of the bisection method to narrow down the solution to a sufficiently small interval in $c_{[H^+]}$ to permit

GMDD
8, 7063–7187, 2015
ERSEM 15.06
M. Butenschön et al.

linear approximation followed by the bisection method reducing the solution residual to the desired tolerance.

Calcite saturation is computed from the product of calcium and carbonate concentrations ($c_{\left[Ca^{2+}\right]}$ and $c_{\left[CO_3^{2-}\right]}$) divided by their product in chemical equilibrium k_{calc}

$$\Omega_{calc} = \frac{c_{\left[Ca^{2+}\right]} c_{\left[CO_3^{2-}\right]}}{k_{calc}} \tag{125}$$

Similarly, the aragonite saturation state is determined by the equation

$$\Omega_{calc} = \frac{c_{\left[Ca^{2+}\right]} c_{\left[CO_3^{2-}\right]}}{k_{arag}} \tag{126}$$

The different variants of alkalinity regressions available from the scientific literature (Borges and Frankignoulle, 1999; Bellerby et al., 2005; Millero et al., 1998; Lee et al., 2006), the total boron regression and the empirical equilibrium constants k are given in the Supplement.

The changes of alkalinity due to biological processes can be traced in the model (activated by the preprocessor definition `BIOALK`) using a dedicated state variable. Its changes are given by sources and sinks of phosphate, oxidised nitrogen and ammonium as well as calcification and dissolution of calcite:

$$\left.\frac{\partial A_{bio}}{\partial t}\right|_{bgc} = \left.\frac{\partial N_{\mathbb{N}}^{amm}}{\partial t}\right|_{bgc} + 2\left.\frac{\partial L_{\mathbb{C}}^{calc}}{\partial t}\right|_{diss} - \left.\frac{\partial R_{\mathbb{P}}}{\partial t}\right|_{bgc} - \left.\frac{\partial R_{\mathbb{N}}^{ox}}{\partial t}\right|_{bgc} - 2\left.\frac{\partial R_{\mathbb{C}}^{calc}}{\partial t}\right|_{calc}. \tag{127}$$

3.9 Light extinction

Light in the water column is attenuated according to the Beer–Lambert formulation computing PAR as:

$$E_{PAR} = q_{PAR} I_{surf} e^{\int_0^z K_d(\xi) d\xi}, \tag{128}$$

GMDD
8, 7063–7187, 2015
ERSEM 15.06
M. Butenschön et al.

where I_{surf} is the short-wave radiation at sea-surface level, q_{PAR} is a parameter for the photosynthetically active fraction and K_d is the spatially varying attenuation coefficient. The latter incorporates light attenuation by the modelled living and non-living optically active components as well as background extinction due to clear sea-water and other components not explicitly modelled. Two alternative models are available for the computation of K_d:

1. a model based on specific attenuation coefficients for the relevant functional types, not modelled inorganic matter and background attenuation of clear sea water; this model is used in previous ERSEM versions (Blackford et al., 2004) and is the default choice,

2. a model based on broadband inherent optical properties (absorption and backscatter), activated by the preprocessing definition `IOPMODEL`.

For the default model based on specific attenuation coefficients K_d is computed according to:

$$K_d = \sum_{\chi} \lambda_{\chi_P} \overset{\chi}{P}_{\mathbb{C}} + \sum_{\Psi} \lambda_R \overset{\Psi}{R}_{\mathbb{C}} + \lambda_{R_{susp}} R_{susp} + \Lambda_{sea}\,, \tag{129}$$

where the λs are the specific attenuation coefficients of the optically active components, i.e. the phytoplankton types χ and the particulate organic matter types Ψ. Λ_{sea} is the background attenuation of sea water and R_{susp} is the concentration of non-modelled optically active substances, mostly suspended matter.

The model based on inherent optical properties (activated by the preprocessing switch `IOPMODEL`) uses the light attenuation model proposed in Lee et al. (2005):

$$K_d = (1 + 0.005\theta_{zen})a + 4.18\left(1.0 - 0.52e^{-10.8a}\right) b_b\,, \tag{130}$$

GMDD
8, 7063–7187, 2015

where θ_{zen} is the zenith angle at the given time and location. Absorption a and back-scatter b_b are composed as:

$$a = \sum_{\chi} a^*_{\substack{\chi \\ P}} \overset{\chi}{P_C} + \sum_{\Psi} a^*_{\substack{\Psi \\ R}} \overset{\Psi}{R_C} + a_{M_{susp}} + a_{sea}\,, \tag{131}$$

$$b_b = \sum_{\chi} b^*_{\substack{\chi \\ P}} \overset{\chi}{P_C} + \sum_{\Psi} b^*_{R} \overset{\Psi}{R_C} + b_k + b_{sea} \tag{132}$$

with a^* and b^* being the specific absorption and back-scatter coefficients of the respective components, a_{sea} and b_{sea} being the broadband absorption and back-scatter of clear sea-water, $a_{M_{susp}}$ the constant absorption of non-modelled suspended matter and b_k a constant amount of background back-scatter in the water column.

In both optical models the attenuation of optically active matter that is not modelled by ERSEM (R_{susp}, mostly inorganic suspended particulate matter) can be provided homogeneously through a namelist parameter or spatially variable through the physical driver by filling and updating the ESS variable.

The combination of the attenuation of particulate organic matter and the non-modelled particles may be provided externally through the physical driver using the preprocessing definition ADYTRACER. This option introduces the state variable a_{ady} and Eq. (129) reduces to

$$K_d = \sum_{\chi} \lambda_{\substack{\chi \\ P}} \overset{\chi}{P_C} + a_{ady} + \Lambda_{sea}\,, \tag{133}$$

or in case of the model based on inherent optical properties

$$a = \sum_{\chi} a^*_{\substack{\psi \\ P}} \overset{\chi}{P_C} + a_{ady} + a_{sea}\,, \tag{134}$$

$$b_b = \sum_{\chi} b^*_{\substack{\psi \\ b,P}} \overset{\chi}{P_C} + b_{b,k} + b_{b,sea}\,, \tag{135}$$

GMDD
8, 7063–7187, 2015
ERSEM 15.06
M. Butenschön et al.

neglecting the backscatter component of particulate and non-modelled matter (see Eqs. 131 and 132).

3.10 Gravitational sinking

The sinking of model states is incorporated using a simple upwind scheme for the equation

$$\left.\frac{\partial c_\mathrm{p}}{\partial t}\right|_\mathrm{sed} = \overset{c_\mathrm{p}}{w}_\mathrm{sed} \cdot \frac{\partial c_\mathrm{p}}{\partial z} \tag{136}$$

and adding the resulting rate to the biogeochemical rates that are passed to the physical driver for integration.

The sedimenting states in the model are given by the particulate organic types $\overset{\Psi}{R}_{\mathbb{C},\mathbb{N},\mathbb{P},\mathbb{F},\mathbb{S}}$, the phytoplankton types $\overset{\chi}{P}_{\mathbb{C},\mathbb{N},\mathbb{P},\mathbb{F},\mathbb{S},\mathcal{C}}$ and calcite $\overset{\mathrm{calc}}{L}_{\mathbb{C}}$. Sinking velocities are constant velocities $\overset{\psi}{w}_0$ for each particulate matter type ψ, while for the phytoplankton states χ they are composed of a constant velocity complemented by a variable component subject to nutrient limitation beyond the threshold $\overset{\chi}{p}_\mathrm{sink}$:

$$\overset{\chi}{w}_\mathrm{sed} = \overset{\chi}{w}_0 + \overset{\chi}{w}_\mathrm{lim} \max\left(0, \overset{\chi}{p}_\mathrm{sink} - \overset{\chi}{l}_{\langle \mathbb{N}\mathbb{P} \rangle}\right) \tag{137}$$

4 The benthic system

Two benthic models are currently included in ERSEM. The first one is a full benthic model predicated on muddy sediments of the continental shelf, including zoobenthos, bacteria, different forms of organic matter and implicit vertical distribution of material within the sea-bed. The second one is a remineralisation model that adsorbs deposing particulate matter and phytoplankton and returns dissolved inorganic nutrients and

GMDD
8, 7063–7187, 2015

carbon to the water column at a given time scale reducing the sediments to a simple buffer layer of organic matter recycling in the sediments.

4.1 Benthic model structure

The full benthic model is a simplified version (Blackford, 1997; Kohlmeier, 2004) of the more complex original model introduced in the original version of ERSEM (Ruardij and Van Raaphorst, 1995; Ebenhöh et al., 1995) assuming near-equilibirum conditions for the inorganic components. Organisms are distinguished in classes on a more functional and less size oriented base than in the pelagic part. The model includes the functional types of aerobic and anaerobic bacteria, three types of zoobenthos (suspension feeders, deposit feeders and meiobenthos), dissolved organic matter and three forms of particulate detritus classified according to their availability and decomposition time scales into slowly degradable, available refractory and buried refractory matter. The model considers three distinct layers, a top, aerobic layer that is oxygenated and delimited by the horizon of dissolved oxygen, an intermediate anaerobic layer with no free oxygen, but oxidised nitrogen available (also referred to as denitrification layer) and delimited by the horizon of oxidised nitrogen and a completely anoxic deep sediment layer. Below these layers, limited by the total depth horizon of the model, no biogeochemical processes take place and only buried refractory matter exists. The vertical distribution of matter is implicitly resolved assuming near-equilibrium conditions for the inorganic components determining the diffusion rate with the overlying water body for the inorganic forms.

The chemical components of the types are identical to the pelagic part consisting of carbon, nitrogen, phosphorus, silicate and iron; the silicate and iron cycles are simplified bypassing the living functional types, similar to the pelagic part of the model. The silicate contained in detritus is remineralised implicitly into inorganic state in the sediments, while the iron in detritus is directly recycled and returned to the water column. A particularity of the benthic model are the dedicated state variables describing the oxygen horizon (the lower limit of the oxygenated layer and the upper limit of the anaerobic

GMDD
8, 7063–7187, 2015

layer), the oxidised nitrogen horizon (the lower limit of the denitrification layer and the upper limit of the strictly anoxic layer) and the mean penetration depths for available refractory carbon, nitrogen and phosphorus and slowly degradable carbon, nitrogen, phosphorus and silicate. A complete list of benthic state variables is given in Tables 5 and 6.

4.2 Implicit vertical distribution of inorganic states in the benthos

In order to determine the dynamics of the oxygen and oxidised nitrogen horizons as well as the inorganic fluxes across the seabed (Sect. 5.1.3), the inorganic components of the benthos are assumed to be close to their equilibrium distributions, in which all source and sink terms of the pore water concentrations of the inorganic components c_{pw} inside the sediments are perfectly balanced by diffusion:

$$v_{\mathrm{idiff}} \frac{\partial^2 c_{\mathrm{pw}}}{\partial \zeta^2} = \frac{1}{\Delta d} \frac{\partial c_{\mathrm{b}}}{\partial t}\bigg|_{\mathrm{bgc}} \tag{138}$$

where c_{b} is the layer content. This partial differential equation has a general parabolic solution in z taking the source-sink term $\frac{\partial c_{\mathrm{b}}}{\partial t}\Big|_{\mathrm{bgc}}$ as a fixed equilibrium rate independent of time. This is a reasonable assumption when the diffusive rates are significantly faster than the biogeochemical processes (v_{idiff} is the diffusivity of dissolved inorganic components in the benthos depending on bioirrigation, see Eq. 206). The equations apply to each of the three sediment layers and the resulting system of piece-wise parabolic continuous profiles can be solved using two boundary conditions per layer: the surface concentration at the upper boundary starting with sediment surface concentrations and the flux across the lower boundary which is equal to the sum of all source and sink processes below the layer under consideration (by definition, no fluxes can occur across the bottom of the sediments so that all sources and sinks have to be compensated from above). The sediment surface concentrations are estimated from

GMDD
8, 7063–7187, 2015
ERSEM 15.06
M. Butenschön et al.

the corresponding pelagic concentration modified by diffusive correction for the non homogenous distribution towards the seabed. In cases when the benthic biogeochmical rates of the inorganic state c_b result in a net source the concentration at the sea bed c_{bed} is approximated from the pelagic concentration nearest to the sea bed (c_p) by

$$c_{bed} = c_p + p_{vmix} \left. \frac{\partial c_b}{\partial t} \right|_{bgc} \tag{139}$$

while for cases when they act as net sink it is given by

$$c_{bed} = c_p \frac{c_p}{c_p - p_{vmix} \left. \frac{\partial c_b}{\partial t} \right|_{bgc}} \tag{140}$$

where p_{vmix} is an inverse mixing velocity constant.

The resulting equilibrium pore water concentrations $\widetilde{c}_{pw}$ in each layer are converted into the full equilibrium layer contents using the layer thickness and the conversion factor

$$v_{\mathbb{N},\mathbb{P}} = p_{poro} p_{ads} \,, \tag{141}$$

where p_{poro} and p_{ads} are porosity and adsorption factors that may vary spatially in case of porosity and adsorption of phosphorus while they are constants for all other adsorptions.

The dynamics of the oxygen and oxidised nitrogen horizons are determined by a relaxation towards their equilibrium values $\overset{oxy}{d}_{eq}$ and $\overset{denit}{d}_{eq}$, which are the depths where the

GMDD
8, 7063–7187, 2015
ERSEM 15.06
M. Butenschön et al.

pore water equilibrium concentrations are 0. Their time evolution is then described by

$$\frac{\partial \overset{\text{oxy}}{D}}{\partial t} = \frac{1}{\tau_{\text{oxy}}} \left(\overset{\text{oxy}}{d_{\text{eq}}} - \overset{\text{oxy}}{D} \right) \tag{142}$$

$$\frac{\partial \overset{\text{denit}}{D}}{\partial t} = \frac{1}{\tau_{\text{denit}}} \left(\overset{\text{denit}}{d_{\text{eq}}} - \overset{\text{denit}}{D} \right), \tag{143}$$

where τ_{ox} and τ_{denit} are the respective relaxation time scales.

4.3 Implicit vertical distribution of organic matter in the benthos

The penetration of organic matter into the sediments is assumed as exponential decay of a concentration γ from a sediment surface value c_0 as function of the mean penetration depth $\overset{\psi}{D}$ of matter ψ.

Total content c and mean penetration depth are then given by the integrals

$$c_{\text{b}} = c_0 \int_0^{d_{\text{tot}}} e^{-\frac{\zeta}{\overset{\psi}{D}}} \mathrm{d}\zeta \tag{144}$$

and

$$\overset{\psi}{D} = \frac{1}{c_{\text{b}}} c_0 \int_0^{d_{\text{tot}}} \zeta e^{-\frac{\zeta}{\overset{\psi}{D}}} \mathrm{d}\zeta \,. \tag{145}$$

For $d_{\text{tot}} \to \infty$ follows

$$c_{\text{b}} = c_0 \overset{\psi}{D}, \tag{146}$$

GMDD
8, 7063–7187, 2015
ERSEM 15.06
M. Butenschön et al.

so assuming $D \ll d_{\mathrm{tot}}$ the vertical distribution of detritus can be expressed as

$$c(\zeta) = c_0 e^{-\frac{\zeta}{\overset{\psi}{D}}} \tag{147}$$

and the mean penetration depth is given by the e-folding depth of the distribution function.

The change of penetration depth due to sources or sink fluxes f_i occurring at depth d_i and bioturbation can then be approximated by the equation

$$\frac{\partial \overset{\psi}{D}}{\partial t} = \sum_i (d_i - \overset{\psi}{D}) \frac{f_i}{c_{\mathrm{b}}} + \left.\frac{\partial \overset{\psi}{D}}{\partial t}\right|_{\mathrm{bturb}} . \tag{148}$$

Bioturbation is acting over a characteristic length scale δ_{bturb} and assumed of the shape

$$\gamma = \nu_{\mathrm{bturb}} \frac{1}{c_{\mathrm{b}}} (c_0 - \gamma(\delta_{\mathrm{bturb}})) , \tag{149}$$

which, still assuming that $\overset{\psi}{D} \ll d_{\mathrm{tot}}$, takes the form

$$\left.\frac{\partial \overset{\psi}{D}}{\partial t}\right|_{\mathrm{bturb}} = \frac{\nu_{\mathrm{bturb}}}{\overset{\psi}{D}} \left(1 - e^{-\frac{\delta_{\mathrm{bturb}}}{\overset{\psi}{D}}}\right) , \tag{150}$$

where ν_{bturb} is the bioturbation diffusivity of particulate matter (208).

The fraction of organic matter contained between two given depth levels can then be computed as

$$\frac{c_{\mathrm{b}}|_{d_{\mathrm{up}}}^{d_{\mathrm{low}}}}{c_{\mathrm{b}}} = \frac{1}{c_{\mathrm{b}}} \int_{d_{\mathrm{up}}}^{d_{\mathrm{low}}} \gamma(z) \mathrm{d}z = \frac{e^{-\frac{d_{\mathrm{up}}}{\overset{\psi}{D}}} - e^{-\frac{d_{\mathrm{low}}}{\overset{\psi}{D}}}}{1 - e^{-\frac{d_{\mathrm{tot}}}{\overset{\psi}{D}}}} , / \tag{151}$$

GMDD
8, 7063–7187, 2015
ERSEM 15.06
M. Butenschön et al.

where the total content was approximated as

$$c_b = \int_0^{d_{tot}} \gamma(\zeta) d\zeta = c_0 \overset{\psi}{D} \left(1 - e^{-\frac{d_{tot}}{\overset{\psi}{D}}} \right) \tag{152}$$

For consistency with the model assumptions and to avoid numerical issues the penetrations depths are constrained to values between $\overset{\psi}{D}_0$ and d_{tot}.

Dissolved organic matter is assumed to reside entirely in the oxygenated layer.

4.4 Heterotrophic bacteria

Benthic decomposers consist of aerobic bacteria living in the upper sediment layer down to the oxygen horizon and anaerobic bacteria living in the denitrification layer and anoxic layer. Their dynamics are summarised by the equations

$$\left.\frac{\partial \overset{\chi}{H}_{\mathbb{C}}}{\partial t}\right|_{bgc} = \left.\frac{\partial \overset{\chi}{H}_{\mathbb{C}}}{\partial t}\right|_{upt} - \left.\frac{\partial \overset{\chi}{H}_{\mathbb{C}}}{\partial t}\right|_{excr} - \left.\frac{\partial \overset{\chi}{H}_{\mathbb{C}}}{\partial t}\right|_{resp} - \left.\frac{\partial \overset{\chi}{H}_{\mathbb{C}}}{\partial t}\right|_{mort} - \left.\frac{\partial \overset{\chi}{H}_{\mathbb{C}}}{\partial t}\right|_{pred} - \left.\frac{\partial \overset{\chi}{H}_{\mathbb{C}}}{\partial t}\right|_{exu}, \tag{153}$$

$$\left.\frac{\partial \overset{\chi}{H}_{\mathbb{N},\mathbb{P}}}{\partial t}\right|_{bgc} = \left.\frac{\partial \overset{\chi}{H}_{\mathbb{N},\mathbb{P}}}{\partial t}\right|_{upt} - \left.\frac{\partial \overset{\chi}{H}_{\mathbb{N},\mathbb{P}}}{\partial t}\right|_{excr} - \left.\frac{\partial \overset{\chi}{H}_{\mathbb{N},\mathbb{P}}}{\partial t}\right|_{mort} - \left.\frac{\partial \overset{\chi}{H}_{\mathbb{N},\mathbb{P}}}{\partial t}\right|_{pred} - \left.\frac{\partial \overset{\chi}{H}_{\mathbb{N},\mathbb{P}}}{\partial t}\right|_{exu}. \tag{154}$$

Specific bacterial uptake is regulated by the sediment surface temperature, oxygen availability (in free or bound form) and the nutritional state of the substrate (through the regulating factors $\overset{\chi}{I}_T$, $\overset{\chi}{I}_O$ and $\overset{\chi}{I}_{\langle \mathbb{N}\mathbb{P} \rangle}$, Eqs. 231, 244, 239) and the amount of bacteria in

GMDD
8, 7063–7187, 2015
ERSEM 15.06
M. Butenschön et al.

the given location:

$$\mathcal{F}\big|^{\overset{\chi}{H}}_{\underset{Q}{\text{dis}}} = r_{\text{up}}\big|^{\overset{\chi}{H}}_{\underset{Q}{\text{dis}}}\ \overset{\chi}{l}_{\text{T}}\ \overset{\chi}{l}_{\text{O}}\ \overset{\chi}{H}_{\text{C}} \tag{155}$$

$$\mathcal{F}\big|^{\overset{\chi}{H}}_{\underset{Q}{\text{refr}}} = r_{\text{up}}\big|^{\overset{\chi}{H}}_{\underset{Q}{\text{refr}}}\ \overset{\chi}{l}_{\text{T}}\ \overset{\chi}{l}_{\text{O}}\ \overset{\chi}{H}_{\text{C}} \tag{156}$$

$$\mathcal{F}\big|^{\overset{\chi}{H}}_{\underset{Q}{\text{slow}}} = \left(r_{\text{fast}}\big|^{\overset{\chi}{H}}_{\underset{Q}{\text{slow}}}\ \overset{\chi}{l}_{\langle \text{INP} \rangle} + r_{\text{up}}\big|^{\overset{\chi}{H}}_{\underset{Q}{\text{slow}}} \right) \overset{\chi}{l}_{\text{T}}\ \overset{\chi}{l}_{\text{O}}\ \overset{\chi}{H}_{\text{C}}\,, \tag{157}$$

where $r_{\text{up}}\big|^{\overset{\chi}{H}}_{\underset{Q}{\psi}}$ are the bacteria and substrate mass specific reference uptake rates. These are generally high for the dissolved form and low for refractory matter. Decomposition of slowly degradable matter has a slow basal component complemented by a fast component $r_{\text{fast}}\big|^{\overset{\chi}{H}}_{\underset{Q}{\text{slow}}}$ subject to nutrient regulation.

To obtain the uptake rates these specific rates are multiplied by the substrate concentrations available in the respective layer (given by Eq. 151):

$$\left.\frac{\partial \overset{\chi}{H}_{\text{C}}}{\partial t}\right|_{\text{upt}} = \sum_{\psi} \mathcal{F}\big|^{\overset{\chi}{H}}_{\underset{R}{\psi}} \overset{\psi}{R}'_{\text{C}} \Big|^{d_{\text{low}}}_{d_{\text{up}}} \tag{158}$$

where the layer limits d_{low},d_{up} are 0, $\overset{\text{oxy}}{D}$ for aerobic bacteria and $\overset{\text{oxy}}{D}$, d_{tot} for anaerobic bacteria. Aerobic bacteria feed on dissolved and particulate substrate, while anaerobic bacteria feed exclusively on the particulate form.

The uptake of organic nitrogen and phosphate is enhanced by a nutrient preference factor $\overset{\chi}{p}_{\text{nup}}$ and is complemented by the uptake of inorganic forms when organic matter is nutrient-poor with respect to the fixed bacterial stoichiometric ratio. Inorganic uptake of nutrients by each bacteria type is regulated by Michaelis–Menten terms of the

GMDD
8, 7063–7187, 2015
ERSEM 15.06
M. Butenschön et al.

pore water inorganic nutrient content within the oxygenated or anaerobic layer with the Redfield equivalent of carbon uptake as the half-saturation term:

$$\left.\frac{\partial \overset{\chi}{H}_{\mathbb{N},\mathbb{P}}}{\partial t}\right|_{\text{upt}} = \sum_{\psi} \overset{\chi}{p}_{\text{nup}} \mathcal{F}\big|_{\substack{\psi \\ Q}}^{\overset{\chi}{H}} \overset{\psi}{H}'_{\mathbb{N},\mathbb{P}} \Big|_{d_{\text{up}}}^{d_{\text{low}}} + \overset{\chi}{q}_{\text{ref}_{\mathbb{N},\mathbb{P}:\mathbb{C}}} \left.\frac{\partial \overset{\chi}{H}_{\mathbb{C}}}{\partial t}\right|_{\text{upt}} \frac{\frac{1}{\nu_{\mathbb{N},\mathbb{P}}} \overset{\text{amm},}{K}_{\mathbb{N},\mathbb{P}} \Big|_{d_{\text{up}}}^{d_{\text{low}}}}{\frac{1}{\nu_{\mathbb{N},\mathbb{P}}} \overset{\text{amm},}{K}_{\mathbb{N},\mathbb{P}} \Big|_{d_{\text{up}}}^{d_{\text{low}}} + \overset{\chi}{q}_{\text{ref}_{\mathbb{N},\mathbb{P}:\mathbb{C}}} \left.\frac{\partial \overset{\chi}{H}_{\mathbb{C}}}{\partial t}\right|_{\text{upt}}}, \tag{159}$$

where $\overset{\text{amm},}{K}_{\mathbb{N}}\Big|_{d_{\text{up}}}^{d_{\text{low}}}$, $K_{\mathbb{P}}\big|_{d_{\text{up}}}^{d_{\text{low}}}$ are the respective layer contents of ammonium or phosphate between the depth d_{up} and d_{low} and $\nu_{\mathbb{N},\mathbb{P}}$ is a volume correction factor (Eq. 141) reducing the total layer content to the pore water content.

Anaerobic bacteria is feeding on and excreting only in particulate form, so that the above rates are for gross uptake in the case of aerobic bacteria followed by excretion in dissolved form, while for anaerobic bacteria they are net rates with no subsequent excretion. Excretion occurs at fixed fractions $\overset{\text{aer}}{q}_{\text{sexcr}}$, $\overset{\text{aer}}{q}_{\text{rexcr}}$ of the aerobic bacteria uptake according to:

$$\left.\frac{\partial \overset{\text{aer}}{H}_{\mathbb{C},\mathbb{N},\mathbb{P}}}{\partial t}\right|_{\text{excr}} = \overset{\text{aer}}{q}_{\text{sexcr}} \mathcal{F}\big|_{\substack{\overset{\text{aer}}{H}_{\text{slow}} \\ Q}} \overset{\text{slow}}{Q}'_{\mathbb{C},\mathbb{N},\mathbb{P}} \Big|_{d_{\text{up}}}^{d_{\text{low}}} + \overset{\text{aer}}{q}_{\text{rexcr}} \mathcal{F}\big|_{\substack{\overset{\text{aer}}{H}_{\text{refr}} \\ Q}} \overset{\text{refr}}{Q}'_{\mathbb{C},\mathbb{N},\mathbb{P}} \Big|_{d_{\text{up}}}^{d_{\text{low}}}. \tag{160}$$

$$\left.\frac{\partial \overset{\text{anaer}}{H}_{\mathbb{C},\mathbb{N},\mathbb{P}}}{\partial t}\right|_{\text{excr}} = 0. \tag{161}$$

GMDD
8, 7063–7187, 2015
ERSEM 15.06
M. Butenschön et al.

Respiration of bacteria is given by activity respiration as a fraction of gross uptake $\overset{\chi}{q}_{\mathrm{aresp}}$ and temperature regulated basal respiration at rest proportional to the bacteria biomass by the factor $\overset{\chi}{r}_{\mathrm{resp}}$:

$$\left.\frac{\partial \overset{\chi}{H}_{\mathbb{C}}}{\partial t}\right|_{\mathrm{resp}} = \overset{\chi}{q}_{\mathrm{aresp}} \left.\frac{\partial \overset{\chi}{H}_{\mathbb{C}}}{\partial t}\right|_{\mathrm{upt}} + \overset{\chi}{r}_{\mathrm{resp}}\ \overset{\chi}{l}_{\mathrm{T}}\ \overset{\chi}{H'}_{\mathbb{C}} \tag{162}$$

Bacterial mortality is fully regulated by oxygen proportional to the bacteria biomass by factor $\overset{\chi}{r}_{\mathrm{mort}}$:

$$\left.\frac{\partial \overset{\chi}{H}_{\mathbb{C},\mathbb{N},\mathbb{P}}}{\partial t}\right|_{\mathrm{mort}} = \overset{\chi}{r}_{\mathrm{mort}} \left(1 - \overset{\chi}{l}_{\mathbb{O}}\right) \overset{\chi}{H'}_{\mathbb{C},\mathbb{N},\mathbb{P}} \,. \tag{163}$$

Benthic bacteria are held at a fixed stoichiometric quota $\overset{\chi}{q}_{\mathrm{ref}_{\mathbb{N},\mathbb{P}:\mathbb{C}}}$, so that any chemical component flux in excess of the reference quota is exudated according to Eqs. (260) and (261), in dissolved form for the nutrients and in the form of organic matter for carbon.

4.5 Predators

The general biogeochemical dynamics of the zoobenthos types χ are given by the equations

$$\left.\frac{\partial \overset{\chi}{Y}_{\mathbb{C}}}{\partial t}\right|_{\mathrm{bgc}} = \left.\frac{\partial \overset{\chi}{Y}_{\mathbb{C}}}{\partial t}\right|_{\mathrm{upt}} - \left.\frac{\partial \overset{\chi}{Y}_{\mathbb{C}}}{\partial t}\right|_{\mathrm{excr}} - \left.\frac{\partial \overset{\chi}{Y}_{\mathbb{C}}}{\partial t}\right|_{\mathrm{resp}} - \left.\frac{\partial \overset{\chi}{Y}_{\mathbb{C}}}{\partial t}\right|_{\mathrm{mort}} - \left.\frac{\partial \overset{\chi}{Y}_{\mathbb{C}}}{\partial t}\right|_{\mathrm{pred}} - \left.\frac{\partial \overset{\chi}{Y}_{\mathbb{C}}}{\partial t}\right|_{\mathrm{exu}} , \tag{164}$$

GMDD
8, 7063–7187, 2015
ERSEM 15.06
M. Butenschön et al.

$$\left.\frac{\partial \overset{\chi}{Y}_{\mathrm{IN,IP}}}{\partial t}\right|_{\mathrm{bgc}} = \left.\frac{\partial \overset{\chi}{Y}_{\mathrm{IN,IP}}}{\partial t}\right|_{\mathrm{upt}} - \left.\frac{\partial \overset{\chi}{Y}_{\mathrm{IN,IP}}}{\partial t}\right|_{\mathrm{excr}} - \left.\frac{\partial \overset{\chi}{Y}_{\mathrm{IN,IP}}}{\partial t}\right|_{\mathrm{rel}} - \left.\frac{\partial \overset{\chi}{Y}_{\mathrm{IN,IP}}}{\partial t}\right|_{\mathrm{mort}} - \left.\frac{\partial \overset{\chi}{Y}_{\mathrm{IN,IP}}}{\partial t}\right|_{\mathrm{pred}} - \left.\frac{\partial \overset{\chi}{Y}_{\mathrm{IN,IP}}}{\partial t}\right|_{\mathrm{exu}} . \quad (165)$$

The benthic predators considered in ERSEM are deposit feeders, suspension feeders and meiobenthos, distinguished by their prey fields and preferences, the depth section they live in and their respective metabolic rates. The prey fields available to each type are given in Table 7, where organic matter is scavenged only in the accesible depth sections indicated for each predator type and d_{SUSP} indicates the range of suspension feeders into the water column assuming homogenous prey distribution over this scale and $\overset{\mathrm{DEPO}}{d_Z}$, $\overset{\mathrm{SUSP}}{d_Z}$, $\overset{\mathrm{MEIO}}{d_Z}$ are parameters describing the depth sections where the predators reside.

The total prey available to each zoobenthos type χ is composed of the individual preys ψ as

$$\overset{\chi}{\mathrm{Pr}}_{\mathrm{C,IN,IP}} = \sum_{\psi} f_{\mathrm{pr}}\Big|_{\psi}^{\overset{\chi}{Z}} \frac{f_{\mathrm{pr}}\Big|_{\psi}^{\overset{\chi}{Z}} \psi'_{\mathbb{C}}}{f_{\mathrm{pr}}\Big|_{\psi}^{\overset{\chi}{Z}} \psi'_{\mathbb{C}} + \overset{\chi}{f}_{\mathrm{min}}} \psi'_{\mathrm{C,IN,IP}} , \quad (166)$$

where $f_{\mathrm{pr}}\Big|_{\psi}^{\overset{\chi}{Z}}$ are the food preferences and $\overset{\chi}{f}_{\mathrm{min}}$ is a food half-saturation constant limiting the detection capacity of predator χ of individual prey types.

The specific uptake capacity for each zooplanton type χ is then given by:

$$\overset{\chi}{S}_{\mathrm{upt}} = \overset{\chi}{g}_{\mathrm{max}} \, \overset{\chi}{l}_{\mathrm{T}} \, \overset{\chi}{l}_{\mathbb{O}} \, \overset{\chi}{l}_{\mathrm{crowd}} \frac{\overset{\chi}{Y}_{\mathbb{C}}}{\overset{\chi}{\mathrm{Pr}}_{\mathbb{C}} + \overset{\chi}{h}_{\mathrm{up}}} , \quad (167)$$

where $\overset{\chi}{g}_{\mathrm{max}}$ is the maximum uptake capacity of each type at reference temperature, $\overset{\chi}{l}_{\mathrm{T}}$ is the metabolic temperature response (Eq. 231), $\overset{\chi}{l}_{\mathbb{O}}$ is the limitation of oxygen (Eq. 242),

GMDD
8, 7063–7187, 2015

$\overset{\chi}{l}_{\text{crowd}}$ is a growth limiting penalty function accounting for overcrowding effects (Eq. 259, absent for meiobenthos as this type is capable to feed on itself), $\overset{\chi}{h}_{\text{up}}$ is a predation efficiency limiting the chances of encountering the prey available ($\overset{\chi}{\text{Pr}}_{\mathbb{C}}$).

Introducing the specific fluxes from prey ψ to predator $\overset{\chi}{Y}$

$$\mathcal{F}\big|_{\psi}^{\overset{\chi}{Y}} = \overset{\chi}{S}_{\text{upt}}\, f_{\text{pr}}\big|_{\psi}^{\overset{\chi}{Y}} \frac{f_{\text{pr}}\big|_{\psi}^{\overset{\chi}{Y}} \psi'_{\mathbb{C}}}{f_{\text{pr}}\big|_{\psi}^{\overset{\chi}{Y}} \psi'_{\mathbb{C}} + \overset{\chi}{f}_{\text{min}}} \tag{168}$$

with $f_{\text{pr}}\big|_{\psi}^{\overset{\chi}{Y}}$ being the food preference of predator $\overset{\chi}{Y}$ for prey ψ, $\overset{\chi}{f}_{\text{min}}$ being a half-saturation constant reflecting the detection capacity of predator χ, the zooplankton uptake can then be written as:

$$\left.\frac{\partial \overset{\chi}{Y}_{\mathbb{C},\mathbb{N},\mathbb{P}}}{\partial t}\right|_{\text{upt}} = \sum_{\psi} \mathcal{F}\big|_{\psi}^{\overset{\chi}{Y}} \psi'_{\mathbb{C},\mathbb{N},\mathbb{P}}\,. \tag{169}$$

Zoobenthos excretion is given by:

$$\left.\frac{\partial \overset{\chi}{Y}_{\mathbb{C}}}{\partial t}\right|_{\text{excr}} = \sum_{\psi}^{\psi \neq Q,R}{}^{\text{slow med}} \overset{\chi}{q}_{\text{excr}} \left.\frac{\partial \overset{\chi}{Y}_{\mathbb{C}}}{\partial t}\right|_{\text{upt}} + \sum_{\psi}^{\psi = Q,R}{}^{\text{slow med}} \overset{\chi}{q}_{\text{pexcr}} \left.\frac{\partial \overset{\chi}{Y}_{\mathbb{C}}}{\partial t}\right|_{\text{upt}} \tag{170}$$

$$\left.\frac{\partial \overset{\chi}{Y}_{\mathbb{N},\mathbb{P}}}{\partial t}\right|_{\text{excr}} = \overset{\chi}{q}_{\text{dil}} \left(\sum_{\psi}^{\psi \neq Q,R}{}^{\text{slow med}} \overset{\chi}{q}_{\text{excr}} \left.\frac{\partial \overset{\chi}{Y}_{\mathbb{C}}}{\partial t}\right|_{\text{upt}} + \sum_{\psi}^{\psi = Q,R}{}^{\text{slow med}} \overset{\chi}{q}_{\text{pexcr}} \left.\frac{\partial \overset{\chi}{Y}_{\mathbb{C}}}{\partial t}\right|_{\text{upt}} \right) \tag{171}$$

GMDD
8, 7063–7187, 2015
ERSEM 15.06
M. Butenschön et al.

where $\overset{\chi}{q}_{\mathrm{excr}}$ is a fixed proportion of gross uptake excreted and $\overset{\chi}{q}_{\mathrm{dil}}$ an additional dilution coefficient taking into account a reduced amount of nutrients in the fecal pellets with respect to the uptake quota.

Respiration of zoobenthos is given by activity respiration as a fraction of net uptake $\overset{\chi}{q}_{\mathrm{aresp}}$ and temperature regulated respiration at rest proportional to the zoobenthos biomass by the factor $\overset{\chi}{r}_{\mathrm{resp}}$:

$$\left.\frac{\partial \overset{\chi}{Y}_{\mathbb{C}}}{\partial t}\right|_{\mathrm{resp}} = \overset{\chi}{q}_{\mathrm{aresp}}\left(1-\overset{\chi}{q}_{\mathrm{excr}}\right)\left.\frac{\partial \overset{\chi}{Y}_{\mathbb{C}}}{\partial t}\right|_{\mathrm{upt}} + \overset{\chi}{r}_{\mathrm{resp}}\ \overset{\chi}{I}_{\mathrm{T}}\ \overset{\chi}{Y}'_{\mathbb{C}} \tag{172}$$

Zoobenthos mortality is regulated by temperature and oxygen and composed of a basal part enhanced under oxygen deficiency and cold temperatures by the factors $\overset{\chi}{r}_{\mathrm{mort}\mathbb{O}}$, $\overset{\chi}{r}_{\mathrm{mortT}}$:

$$\left.\frac{\partial \overset{\chi}{Y}_{\mathbb{C},\mathbb{N},\mathbb{P}}}{\partial t}\right|_{\mathrm{mort}} = \left(\overset{\chi}{r}_{\mathrm{mort}}\ \overset{\chi}{I}_{\mathrm{T}} + \overset{\chi}{r}_{\mathrm{mort}\mathbb{O}}\ \overset{\chi}{I}_{\mathrm{T}}\left(1-\overset{\chi}{I}_{\mathbb{O}}\right) + \overset{\chi}{r}_{\mathrm{mortT}} e^{-\frac{\mathrm{T}}{\overset{\chi}{\mathrm{T}}_{\mathrm{cold}}}}\right)\overset{\chi}{Y}'_{\mathbb{C},\mathbb{N},\mathbb{P}}\,. \tag{173}$$

Also, zoobenthos types are kept at a fixed stoichiometric quota $\overset{\chi}{q}_{\mathrm{ref}_{\mathbb{N},\mathbb{P}:\mathbb{C}}}$ according to Eqs. (260) and (261) resulting in the exudation of nutrients in inorganic form and carbon in the form of slowly degradable organic matter.

4.6 Organic matter

The cycling of carbon, nitrogen and phosphorus through the benthic food-web by the processes of uptake, scavenging, excretion, mortality, exudation and burial results in the following organic matter fluxes:

GMDD
8, 7063–7187, 2015
ERSEM 15.06
M. Butenschön et al.

Uptake of all forms of organic matter by bacteria is given by Eqs. (155)–(157) as

$$\left.\frac{\partial \overset{\psi}{Q}_{\mathbb{C},\mathbb{N},\mathbb{P}}}{\partial t}\right|_{\text{upt}} = \mathcal{F}|^{\overset{\text{aer}}{H}}_{\overset{\psi}{Q}} \overset{\psi}{Q'}_{\mathbb{C},\mathbb{N},\mathbb{P}} \Big|_{0}^{\overset{\text{ox}}{D}} + \mathcal{F}|^{\overset{\text{anaer}}{H}}_{\overset{\psi}{Q}} \overset{\psi}{Q'}_{\mathbb{C},\mathbb{N},\mathbb{P}} \Big|_{\overset{\text{ox}}{D}}^{d_{\text{tot}}} . \tag{174}$$

The excretion of aerobic bacteria is directed to dissolved organic matter, while for the zoobenthos types $\overset{\Psi}{Y}$ it is directed to slowly degradable matter:

$$\left.\frac{\partial \overset{\text{dis}}{Q}_{\mathbb{C},\mathbb{N},\mathbb{P}}}{\partial t}\right|_{\text{excr}} = \left.\frac{\partial \overset{\text{aer}}{H}_{\mathbb{C},\mathbb{N},\mathbb{P}}}{\partial t}\right|_{\text{excr}} \tag{175}$$

$$\left.\frac{\partial \overset{\text{slow}}{Q}_{\mathbb{C},\mathbb{N},\mathbb{P}}}{\partial t}\right|_{\text{excr}} = \sum_{\Psi} \left.\frac{\partial \overset{\Psi}{Y}_{\mathbb{C},\mathbb{N},\mathbb{P}}}{\partial t}\right|_{\text{excr}} , \tag{176}$$

using Eqs. (160), (161), (170), (171).

The mortality of aerobic bacteria is partioned between a particulate part directed to slowly degradable matter and a dissolved part $\overset{\text{aer}}{q}_{\text{dmort}}$, while for the zoobenthos types

GMDD
8, 7063–7187, 2015
ERSEM 15.06
M. Butenschön et al.

$\overset{\Psi}{Y}$ and anaerobic bacteria it is entirely directed to slowly degradable matter:

$$\left.\frac{\partial \overset{\text{dis}}{Q}_{\mathbb{C},\mathbb{N},\mathbb{P}}}{\partial t}\right|_{\text{mort}} = \overset{\text{aer}}{q}_{\text{dmort}} \left.\frac{\partial \overset{\text{aer}}{H}_{\mathbb{C},\mathbb{N},\mathbb{P}}}{\partial t}\right|_{\text{mort}} \tag{177}$$

$$\left.\frac{\partial \overset{\text{slow}}{Q}_{\mathbb{C},\mathbb{N},\mathbb{P}}}{\partial t}\right|_{\text{mort}} = \left(1 - \overset{\text{aer}}{q}_{\text{dmort}}\right) \left.\frac{\partial \overset{\text{aer}}{H}_{\mathbb{C},\mathbb{N},\mathbb{P}}}{\partial t}\right|_{\text{mort}} + \left.\frac{\partial \overset{\text{anaer}}{H}_{\mathbb{C},\mathbb{N},\mathbb{P}}}{\partial t}\right|_{\text{mort}} + \sum_{\Psi} \left.\frac{\partial \overset{\Psi}{Y}_{\mathbb{C},\mathbb{N},\mathbb{P}}}{\partial t}\right|_{\text{mort}} \tag{178}$$

using Eqs. (163) and (173).

Slowly degradable matter is scavenged by zoobenthos according to Eq. (168)

$$\left.\frac{\partial \overset{\text{slow}}{Q}_{\mathbb{C},\mathbb{N},\mathbb{P}}}{\partial t}\right|_{\text{scav}} = \sum_{\Psi} \mathcal{F}|^{\overset{\Psi}{Y}}_{\overset{\text{slow}}{Q}} \overset{\text{slow}'}{Q}_{\mathbb{C},\mathbb{N},\mathbb{P}} . \tag{179}$$

In addition, slowly degradable carbon may be produced by the stoichiometric adjustment (Eq. 260) of bacteria or zoobenthos:

$$\left.\frac{\partial \overset{\text{slow}}{Q}_{\mathbb{C}}}{\partial t}\right|_{\text{exu}} = \sum_{\chi} \left.\frac{\partial \overset{\chi}{H}_{\mathbb{C}}}{\partial t}\right|_{\text{exu}} + \sum_{\Psi} \left.\frac{\partial \overset{\Psi}{Y}_{\mathbb{C}}}{\partial t}\right|_{\text{exu}} . \tag{180}$$

Refractory organic matter may be buried by the transfer of matter across the total depth horizon d_{tot} resulting from the redistribution of organic matter by diffusion and

GMDD
8, 7063–7187, 2015
ERSEM 15.06
M. Butenschön et al.

bioturbation (Eq. 208). Note, that this process (activated by the `ISWbur` switch) removes biomass from the biogeochemically active part of the model, as there are no processes connected to buried organic matter and the model currently doesn't consider remobilisation. This means that during long term simulations the loss of nutrients needs to be compensated, e.g. by riverine inputs or atmospheric deposition (carbon is restored by air–sea exchange). The amount of material buried may be approximated by the product of the concentration at the total depths and the burial velocity by which this level is shifted by the diffusive processes. The concentration at the total depths is computed using Eq. (147) with $z = d_{\mathrm{tot}}$, while the burial velocity may be approximated in first order from the rate of change of the refractory organic matter penetration depth $\left.\frac{\partial\, {}^{\mathrm{refr}}D_{\mathrm{C,IN,IP}}}{\partial t}\right|_{\mathrm{diff}}$. The rate of vertical displacement is not homogeneous over depth, as the concentrations are generally not identical along z. The characteristic time scale τ_{bur} of redistribution at any depth z can be computed using Eq. (147) as:

$$\frac{1}{\tau_{\mathrm{bur}}(z)} = \frac{1}{{}^{\mathrm{refr}}q_{\mathrm{C,IN,IP}}(\zeta)} \frac{\partial\, {}^{\mathrm{refr}}q_{\mathrm{C,IN,IP}}(z)}{\partial t} = \frac{z}{{}^{\mathrm{refr}}D_{\mathrm{C,IN,IP}}{}^{2}} \frac{\partial\, {}^{\mathrm{refr}}D_{\mathrm{C,IN,IP}}}{\partial t}, \tag{181}$$

where ${}^{\mathrm{refr}}q_{\mathrm{C,IN,IP}}(\zeta)$ is the concentration of refractory organic carbon at sediment depth ζ.

The burial velocity can then be estimated scaling the rate of change of the penetration depth with $\frac{\tau_{\mathrm{bur}}({}^{\mathrm{refr}}D_{\mathrm{C,IN,IP}})}{\tau_{\mathrm{bur}}(d_{\mathrm{tot}})} = \frac{d_{\mathrm{tot}}}{{}^{\mathrm{refr}}D_{\mathrm{C,IN,IP}}}$ resulting in a burial flux of:

$$\left.\frac{\partial\, {}^{\mathrm{refr}}Q_{\mathrm{C,IN,IP}}}{\partial t}\right|_{\mathrm{bur}} = \frac{{}^{\mathrm{refr}}Q_{\mathrm{C,IN,IP}}}{{}^{\mathrm{refr}}D_{\mathrm{C,IN,IP}}\left(1 - e^{-\frac{d_{\mathrm{tot}}}{{}^{\mathrm{refr}}D_{\mathrm{C,IN,IP}}}}\right)} e^{-\frac{d_{\mathrm{tot}}}{{}^{\mathrm{refr}}D_{\mathrm{C,IN,IP}}}} \frac{d_{\mathrm{tot}}}{{}^{\mathrm{refr}}D_{\mathrm{C,IN,IP}}} \left.\frac{\partial\, {}^{\mathrm{refr}}D_{\mathrm{C,IN,IP}}}{\partial t}\right|_{\mathrm{diff}} \tag{182}$$

GMDD
8, 7063–7187, 2015
ERSEM 15.06
M. Butenschön et al.

using again Eqs. (147) and (152).

In summary, the dissolved organic matter is produced by excretion and mortality and reduced by bacterial uptake

$$\left.\frac{\partial^{\mathrm{dis}} Q_{\mathbb{C},\mathbb{N},\mathbb{P}}}{\partial t}\right|_{\mathrm{dis}} = \left.\frac{\partial^{\mathrm{dis}} Q_{\mathbb{C},\mathbb{N},\mathbb{P}}}{\partial t}\right|_{\mathrm{excr}} + \left.\frac{\partial^{\mathrm{dis}} Q_{\mathbb{C},\mathbb{N},\mathbb{P}}}{\partial t}\right|_{\mathrm{mort}} - \left.\frac{\partial^{\mathrm{dis}} Q_{\mathbb{C},\mathbb{N},\mathbb{P}}}{\partial t}\right|_{\mathrm{upt}}, \tag{183}$$

slowly degradable matter is generated by excretion and mortality of zoobenthos and aerobic bacteria and exudation fluxes, taken up by bacteria, and scavenged by zoobenthos

$$\left.\frac{\partial^{\mathrm{slow}} Q_{\mathbb{C},\mathbb{N},\mathbb{P}}}{\partial t}\right|_{\mathrm{bgc}} = \left.\frac{\partial^{\mathrm{slow}} Q_{\mathbb{C},\mathbb{N},\mathbb{P}}}{\partial t}\right|_{\mathrm{excr}} + \left.\frac{\partial^{\mathrm{slow}} Q_{\mathbb{C},\mathbb{N},\mathbb{P}}}{\partial t}\right|_{\mathrm{mort}} - \left.\frac{\partial^{\mathrm{slow}} Q_{\mathbb{C},\mathbb{N},\mathbb{P}}}{\partial t}\right|_{\mathrm{upt}} - \left.\frac{\partial^{\mathrm{slow}} Q_{\mathbb{C},\mathbb{N},\mathbb{P}}}{\partial t}\right|_{\mathrm{scav}} \left[+ \left.\frac{\partial^{\mathrm{slow}} Q_{\mathbb{C}}}{\partial t}\right|_{\mathrm{exu}} \right] \tag{184}$$

GMDD
8, 7063–7187, 2015
ERSEM 15.06
M. Butenschön et al.

and refractory matter is taken up by bacteria and modified by burying across the total depth horizon

$$\left.\frac{\partial Q^{\mathrm{refr}}_{\mathbb{C},\mathbb{N},\mathbb{P}}}{\partial t}\right|_{\mathrm{bgc}} = -\left.\frac{\partial Q^{\mathrm{refr}}_{\mathbb{C},\mathbb{N},\mathbb{P}}}{\partial t}\right|_{\mathrm{upt}} - \left.\frac{\partial Q^{\mathrm{refr}}_{\mathbb{C},\mathbb{N},\mathbb{P}}}{\partial t}\right|_{\mathrm{bur}} . \tag{185}$$

The abbreviated cycles for iron and silicate simplify all biogeochemical processes in the benthos into a simple remineralisation of slowly degradable organic matter into dissolved inorganic iron or silicate at a fixed rate $r_{\mathbb{F}\mathrm{remin}}$ or $r_{\mathbb{S}\mathrm{remin}}$:

$$\left.\frac{\partial Q^{\mathrm{slow}}_{\mathbb{F}}}{\partial t}\right|_{\mathrm{bgc}} = -r_{\mathbb{F}\mathrm{remin}}\, Q'^{\mathrm{slow}}_{\mathbb{F}} \tag{186}$$

$$\left.\frac{\partial Q^{\mathrm{slow}}_{\mathbb{S}}}{\partial t}\right|_{\mathrm{bgc}} = -r_{\mathbb{S}\mathrm{remin}}\, Q'^{\mathrm{slow}}_{\mathbb{S}} . \tag{187}$$

GMDD
8, 7063–7187, 2015
ERSEM 15.06
M. Butenschön et al.

4.7 Inorganic components

The dynamics of benthic nutrients are given by the following equations (see Eq. 187 for the remineralisation of silicate):

$$\left.\frac{\partial K_{\mathbb{N}}^{ox}}{\partial t}\right|_{bgc} = \left.\frac{\partial K_{\mathbb{N}}^{ox}}{\partial t}\right|_{nitr} - \left.\frac{\partial K_{\mathbb{N}}^{ox}}{\partial t}\right|_{denit} \tag{188}$$

$$\left.\frac{\partial K_{\mathbb{N}}^{amm}}{\partial t}\right|_{bgc} = -\left.\frac{\partial K_{\mathbb{N}}^{amm}}{\partial t}\right|_{nitr} - \left.\frac{\partial K_{\mathbb{N}}^{amm}}{\partial t}\right|_{upt} + \left.\frac{\partial K_{\mathbb{N}}^{amm}}{\partial t}\right|_{exu} \tag{189}$$

$$\left.\frac{\partial K_{\mathbb{P}}}{\partial t}\right|_{bgc} = -\left.\frac{\partial K_{\mathbb{P}}}{\partial t}\right|_{upt} + \left.\frac{\partial K_{\mathbb{P}}}{\partial t}\right|_{exu} \tag{190}$$

$$\left.\frac{\partial K_{\mathbb{S}}}{\partial t}\right|_{bgc} = r_{\mathbb{S}remin}\, Q'^{slow}_{\mathbb{S}} \tag{191}$$

while the biogeochemistry of dissolved carbon, oxygen and dinitrogen are given by

$$\left.\frac{\partial G_{\mathbb{C}}}{\partial t}\right|_{bgc} = \left.\frac{\partial G_{\mathbb{C}}}{\partial t}\right|_{resp} \tag{192}$$

$$\left.\frac{\partial G_{\mathbb{O}}}{\partial t}\right|_{bgc} = -\left.\frac{\partial G_{\mathbb{O}}}{\partial t}\right|_{resp} - \left.\frac{\partial G_{\mathbb{O}}}{\partial t}\right|_{nitr} \tag{193}$$

$$\left.\frac{\partial G_{\mathbb{N}}}{\partial t}\right|_{bgc} = \left.\frac{\partial G_{\mathbb{N}}}{\partial t}\right|_{denit}. \tag{194}$$

GMDD
8, 7063–7187, 2015
ERSEM 15.06
M. Butenschön et al.

The respiration terms of dissolved inorganic carbon and dissolved oxygen are given by Eqs. (162) and (172) as

$$\left.\frac{\partial G_{\mathbb{C}}}{\partial t}\right|_{\text{resp}} = \sum_{\chi} \left.\frac{\partial \overset{\chi}{H}_{\mathbb{C}}}{\partial t}\right|_{\text{resp}} + \sum_{\Psi} \left.\frac{\partial \overset{\Psi}{Y}_{\mathbb{C}}}{\partial t}\right|_{\text{resp}} \tag{195}$$

$$\left.\frac{\partial G_{\mathbb{O}}}{\partial t}\right|_{\text{resp}} = -q_{\mathbb{O}:\mathbb{C}} \left(\left.\frac{\partial \overset{\text{aer}}{H}_{\mathbb{C}}}{\partial t}\right|_{\text{resp}} + \sum_{\Psi} \left.\frac{\partial \overset{\Psi}{Y}_{\mathbb{C}}}{\partial t}\right|_{\text{resp}} \right) \tag{196}$$

where $q_{\mathbb{O}:\mathbb{C}}$ is the oxygen to carbon conversion coefficient.

Nitrification in the benthos is computed similar to the pelagic nitrification from a maximum specific nitrification rate $\overset{\mathcal{B}}{r}_{\text{nitr}}$ at reference temperature depending on the ammonium available in the oxygenated layer, approximated as $\frac{\overset{\text{oxy}}{D}}{d_{\text{tot}}} \overset{\text{amm}}{K'}_{\mathbb{N}}$:

$$\left.\frac{\partial \overset{\text{ox}}{K}_{\mathbb{N}}}{\partial t}\right|_{\text{nitr}} = \left.\frac{\partial \overset{\text{amm}}{K}_{\mathbb{N}}}{\partial t}\right|_{\text{nitr}} = \overset{H}{r}_{\text{nitr}} \; \overset{\text{bnitr}}{l}_{\mathbb{T}} \; \overset{\text{bnitr}}{l}_{\mathbb{N}} \frac{\overset{\text{oxy}}{D}}{d_{\text{tot}}} \overset{\text{amm}}{K'}_{\mathbb{N}}, \tag{197}$$

$$\left.\frac{\partial G_{\mathbb{O}}}{\partial t}\right|_{\text{nitr}} = 2 \left.\frac{\partial \overset{\text{ox}}{K}_{\mathbb{N}}}{\partial t}\right|_{\text{nitr}} \tag{198}$$

where $\overset{\text{bnitr}}{l}_{\mathbb{N}}$ and $\overset{\text{bnitr}}{l}_{\mathbb{T}}$ are the nitrification limitation due to the presence of high concentrations of oxidised nitrogen and temperature regulation (Eqs. 249 and 231).

GMDD
8, 7063–7187, 2015
ERSEM 15.06
M. Butenschön et al.

Denitrification is calculated from the oxidised nitrogen reduction equivalent required for anaerobic bacteria respiration:

$$\overset{\text{anaer}}{\mathcal{F}}_{\text{req}} = \frac{1}{2\left(1-\overset{H}{q}_{\text{denit}}\right)+\frac{5}{4}\overset{H}{q}_{\text{denit}}}\overset{H}{q}_{\text{red}} q_{O:C}\left.\frac{\partial \overset{\text{anaer}}{H_C}}{\partial t}\right|_{\text{resp}}, \tag{199}$$

where $\overset{H}{q}_{\text{red}}$ is the maximum fraction of anaerobic bacteria respiration resulting in oxidised nitrogen reduction, $\overset{H}{q}_{\text{denit}}$ is fraction of reduction subject to denitrification as opposed to ammonification and 2, $\frac{5}{4}$ are the stoichiometric coefficients of oxygen demand per reduction equivalent for the ammonification and denitrification reactions respectively.

The actual reduction of oxidised nitrogen by denitrification is then further limited by availability of oxidised nitrogen ($\overset{\text{denit}}{I}_{\mathbb{N}}$, Eq. 250) resulting in the following denitrification fluxes:

$$\left.\frac{\partial \overset{\text{ox}}{K}_{\mathbb{N}}}{\partial t}\right|_{\text{denit}} = \overset{\text{denit}}{I}_{\mathbb{N}}\ \overset{\text{anaer}}{\mathcal{F}}_{\text{req}} \tag{200}$$

$$\left.\frac{\partial \overset{\text{amm}}{K}_{\mathbb{N}}}{\partial t}\right|_{\text{denit}} = \left(1-q_{\text{red}N_2}\right)\left.\frac{\partial \overset{\text{ox}}{\mathbb{K}}_{\mathbb{N}}}{\partial t}\right|_{\text{denit}} \tag{201}$$

$$\left.\frac{\partial G_{\mathbb{N}}}{\partial t}\right|_{\text{bgc}} = q_{\text{red}G}\left.\frac{\partial \overset{\text{ox}}{K}_{\mathbb{N}}}{\partial t}\right|_{\text{denit}} \tag{202}$$

where $q_{\text{red}G}$ is the fraction of reduction directed to di-nitrogen. As nitrogen fixation is currently not considered in the model, losses of oxidised nitrogen by denitrification

GMDD
8, 7063–7187, 2015
ERSEM 15.06
M. Butenschön et al.

are removed from the active cycle and need to be compensated in long term runs by riverine or atmospheric inputs or denitrification needs to be switched off.

Exudation of nutrients caused by stoichiometric adjustment (Eq. 260) of bacteria or zoobenthos are given by:

$$\left.\frac{\partial\, {}^{\mathrm{amm}}K_{\mathbb{N}}}{\partial t}\right|_{\mathrm{exu}} = \sum_{\chi} \left.\frac{\partial\, {}^{\chi}H_{\mathbb{N}}}{\partial t}\right|_{\mathrm{exu}} + \sum_{\Psi} \left.\frac{\partial\, {}^{\Psi}Y_{\mathbb{N}}}{\partial t}\right|_{\mathrm{exu}} \tag{203}$$

$$\left.\frac{\partial K_{\mathbb{P}}}{\partial t}\right|_{\mathrm{exu}} = \sum_{\chi} \left.\frac{\partial\, {}^{\chi}H_{\mathbb{P}}}{\partial t}\right|_{\mathrm{exu}} + \sum_{\Psi} \left.\frac{\partial\, {}^{\Psi}Y_{\mathbb{P}}}{\partial t}\right|_{\mathrm{exu}} . \tag{204}$$

4.8 Bioirrigation

The diffusivity of dissolved inorganic states is given by a basal diffusivity ϑ_{χ} for each layer χ: aer, den, anox that is increased for bioirrigation by the factor p_{bimin}. The activity of deposit feeders and meiofauna cause further enhancement to yield the total bioirigation diffusivity ν_{idiff} (used in Eq. 138):

$$\mathcal{S}_{\mathrm{birr}} = {}^{\mathrm{DEPO}}q_{\mathrm{birr}} \left.\frac{\partial\, {}^{\mathrm{DEPO}}Y_{\mathbb{C}}}{\partial t}\right|_{\mathrm{upt}} + {}^{\mathrm{MEIO}}q_{\mathrm{birr}} \left.\frac{\partial\, {}^{\mathrm{MEIO}}Y_{\mathbb{C}}}{\partial t}\right|_{\mathrm{upt}} \tag{205}$$

$$\nu_{\mathrm{idiff}} = \vartheta_{\chi} \left(p_{\mathrm{bimin}} + p_{\mathrm{bienh}} \frac{\mathcal{S}_{\mathrm{birr}}}{\mathcal{S}_{\mathrm{birr}} + h_{\mathrm{birr}}} \right) , \tag{206}$$

where ${}^{\mathrm{DEPO}}q_{\mathrm{birr}}$ and ${}^{\mathrm{MEIO}}q_{\mathrm{birr}}$ are the fractions of deposit feeder and meiobenthos uptake contributing to bioirrigation, h_{birr} is a half-saturation rate for bioirrigation enhancement and p_{bienh} is the maximum bioturbation enhancement factor of dissolved inorganic diffusion in the benthos.

GMDD
8, 7063–7187, 2015
ERSEM 15.06
M. Butenschön et al.

4.9 Bioturbation

For particulate matter in the benthos sediment diffusion ν_{bturb} in Eq. (150) is based on a background diffusivity $\vartheta_{\mathrm{part}}$ and an enhancement factor of Michaelis–Menten type depending on the bioturbation caused by deposit feeder activity (see Eq. 169):

$$\mathcal{S}_{\mathrm{bturb}} = {}^{\mathrm{DEPO}}q_{\mathrm{bturb}} \left. \frac{\partial\, {}^{\mathrm{DEPO}}Y_{\mathbb{C}}}{\partial t} \right|_{\mathrm{upt}} \tag{207}$$

$$\nu_{\mathrm{bturb}} = \vartheta_{\mathrm{part}} \left(1 + p_{\mathrm{btenh}} \frac{\mathcal{S}_{\mathrm{bturb}}}{\mathcal{S}_{\mathrm{bturb}} + h_{\mathrm{bturb}}} \right), \tag{208}$$

where ${}^{\mathrm{DEPO}}q_{\mathrm{bturb}}$ is the fraction of deposit feeder uptake contributing to bioturbation, h_{bturb} is a half-saturation rate for bioturbation enhancement and p_{btenh} is the maximum bioturbation enhancement factor of particulate matter diffusion in the benthos.

5 Horizontal interfaces

5.1 The benthic-pelagic interface

The boundary condition at the seabed is given by the deposition of sinking particulate organic material, phytoplankton and calcite on the seafloor, the diffusion of inorganic chemical components between the pore water and the pelagic water column and re-suspension of organic matter. All other state variables generally have no flux conditions at the pelagic-benthic interface.

GMDD
8, 7063–7187, 2015
ERSEM 15.06
M. Butenschön et al.

5.1.1 Deposition of organic matter and phytoplankton

Deposition fluxes are taken analogous to the gravitational sinking rates in Eq. (136) where the sinking velocity is replaced by the deposition velocity $\overset{\text{dep}}{w}_{c_\text{p}}$ according to the seabed shear stress τ_bed:

$$\overset{\text{depo}}{w}_{c_\text{p}} = \max\left(1 - \frac{\tau_\text{bed}}{\tau_\text{crit}}, 0\right) \overset{\text{sed}}{w}_{c_\text{p}}, \tag{209}$$

leading to the deposition fluxes

$$\mathcal{F}|^{\text{ben}}_{c_\text{p}} = \overset{\text{depo}}{w}_{c_\text{p}} c'_\text{p}. \tag{210}$$

As for gravitational sinking the only state variables sedimenting onto the seafloor are particulate organic matter, the phytoplankton components and calcite ($\overset{\Psi}{M}_{\mathbb{C},\mathbb{N},\mathbb{P},\mathbb{F},\mathbb{S}}$, $\overset{\chi}{P}_{\mathbb{C},\mathbb{N},\mathbb{P},\mathbb{F},\mathbb{S},c}$, $\overset{\text{calc}}{L}_\mathbb{C}$). The absorption of deposited carbon, nitrogen and phosphorus components into the sediments then results in separation of the organic material into dissolved, slowly degradable and refractory matter according to

$$\mathcal{F}|^{\overset{\text{slow}}{Q_\mathbb{C}}}_{\text{pel}} = \left(1 - \overset{\chi}{q}_\text{ddepo} - \overset{\chi}{q}_\text{rdepo}\right) \sum_\chi \mathcal{F}\Big|^{\text{ben}}_{\overset{\chi}{P_\mathbb{C}}} + \overset{\text{part}}{q}_\text{rdepo} \sum_\chi \mathcal{F}\Big|^{\text{ben}}_{\overset{\chi}{R_\mathbb{C}}} \tag{211}$$

$$\mathcal{F}|^{\overset{\text{refr}}{Q_\mathbb{C}}}_{\text{pel}} = \overset{\chi}{q}_\text{rdepo} \sum_\chi \mathcal{F}\Big|^{\text{ben}}_{\overset{\chi}{P_\mathbb{C}}} + \overset{\text{part}}{q}_\text{rdepo} \sum_\chi \mathcal{F}\Big|^{\text{ben}}_{\overset{\chi}{R_\mathbb{C}}} \tag{212}$$

$$\mathcal{F}|^{\overset{\text{dis}}{Q_\mathbb{C}}}_{\text{pel}} = \overset{\chi}{q}_\text{ddepo} \sum_\chi \mathcal{F}\Big|^{\text{ben}}_{\overset{\chi}{P_\mathbb{C}}}, \tag{213}$$

GMDD
8, 7063–7187, 2015
ERSEM 15.06
M. Butenschön et al.

where $\overset{\chi}{q}_{\text{ddepo}}$ and $\overset{\chi}{q}_{\text{rdepo}}$ are the dissolved and refractory fractions of deposing material. For nitrogen and phosphorus the portioning is modified according to the relative cytoplasm nutrient contents $\overset{\text{lab}}{p}_{\text{cyto}_{\text{N,P}}}$, $\overset{\text{part}}{p}_{\text{cyto}_{\text{N,P}}}$:

$$\mathcal{F}|^{\overset{\text{slow}}{Q}_{\text{N,P}}}_{\text{pel}} = \sum_{\chi}\left(1 - \overset{\chi}{q}_{\text{ddepo}}\ \overset{\text{lab}}{p}_{\text{cyto}_{\text{N,P}}} - \overset{\chi}{q}_{\text{rdepo}}\ \overset{\text{part}}{p}_{\text{cyto}_{\text{N,P}}}\right)\mathcal{F}|^{\text{ben}}_{\underset{\chi}{P}_{\text{N,P}}} \tag{214}$$

$$+ \sum_{\psi}\left(1 - \overset{\text{part}}{q}_{\text{rdepo}}\right)\mathcal{F}|^{\text{ben}}_{\underset{\psi}{R}_{\text{N,P}}} \tag{215}$$

$$\mathcal{F}|^{\overset{\text{refr}}{Q}_{\text{N,P}}}_{\text{pel}} = \sum_{\chi}\overset{\chi}{q}_{\text{rdepo}}\ \overset{\text{part}}{p}_{\text{cyto}_{\text{N,P}}}\mathcal{F}|^{\text{ben}}_{\underset{\chi}{P}_{\text{N,P}}} + \sum_{\psi}\overset{\text{part}}{q}_{\text{rdepo}}\mathcal{F}|^{\text{ben}}_{\underset{\psi}{R}_{\text{N,P}}} \tag{216}$$

$$\mathcal{F}|^{\overset{\text{dis}}{Q}_{\text{N,P}}}_{\text{pel}} = \sum_{\chi}\overset{\chi}{q}_{\text{ddepo}}\ \overset{\text{lab}}{p}_{\text{cyto}_{\text{N,P}}}\mathcal{F}|^{\text{ben}}_{\underset{\chi}{P}_{\text{N,P}}}. \tag{217}$$

The iron and silicate components and phosphorus are entirely directed to slowly degradable matter, the only state considered for these components in the benthic model:

$$\mathcal{F}|^{\overset{\text{slow}}{Q}_{\text{F}}}_{\text{pel}} = \sum_{\chi}\mathcal{F}\Big|^{\text{ben}}_{\underset{\chi}{P}_{\text{F}}} + \mathcal{F}|^{\text{ben}}_{\underset{\text{small}}{R}_{\text{F}}} + \mathcal{F}|^{\text{ben}}_{\underset{\text{med}}{R}_{\text{F}}} \tag{218}$$

$$\mathcal{F}|^{\overset{\text{slow}}{Q}_{\text{S}}}_{\text{pel}} = \mathcal{F}|^{\text{ben}}_{\underset{\text{dia}}{P}_{\text{S}}} + \mathcal{F}|^{\text{ben}}_{\underset{\text{med}}{R}_{\text{S}}} + \mathcal{F}|^{\text{ben}}_{\underset{\text{large}}{R}_{\text{S}}} \tag{219}$$

Calcite deposition is given by

$$\mathcal{F}|^{\overset{\text{calc}}{C}_{\text{C}}}_{\underset{\text{calc}}{L}_{\text{C}}} = \overset{\text{depo}}{w}_{\underset{\text{calc}}{L}_{\text{C}}}\ \overset{\text{calc}}{L'}_{\text{C}}. \tag{220}$$

GMDD
8, 7063–7187, 2015
ERSEM 15.06
M. Butenschön et al.

5.1.2 Resuspension

In case of strong shear stress τ_{bed} at the seafloor part of the sediments may get resuspended into the water column. The erosion flux is calculated proportional to the excess shear stress over a critical threshold τ_{crit} by a reference erosion flux r_{er}. Erosion in terms of particulate organic matter is then approximated as a fraction of the total sediment matter $\overset{sed}{p}_Q + \overset{slow}{Q}_{\mathbb{C}}$:

$$\overset{resusp}{\mathcal{S}} = \frac{r_{er} \max\left(\frac{\tau_{bed}}{\tau_{crit}} - 1, 0\right)}{\overset{sed}{p}_Q + \overset{slow}{Q}_{\mathbb{C}}} \tag{221}$$

$$\overset{resusp}{\mathcal{F}}_{\mathbb{C},\mathbb{N},\mathbb{P},\mathbb{F},\mathbb{S}}\Big|^{\overset{med}{R}}_{\overset{slow}{Q}} = \overset{resusp}{\mathcal{S}}\ \overset{slow}{Q}_{\mathbb{C},\mathbb{N},\mathbb{P},\mathbb{F},\mathbb{S}} \tag{222}$$

The values and approximations used for the three parameters τ_{crit}, r_{er} and $\overset{sed}{p}_Q$ are given in the Supplement.

5.1.3 Inorganic fluxes across the seabed

The diffusion of dissolved inorganic states across the benthos is derived from the equilibrium conditions described in Sect. 4.2. Based on the tendency of the system towards the equilibrium the total flux across the sea-bed is then given by the sum of all sources and sinks and a relaxation towards equilibrium.

$$-\overset{\chi}{\mathcal{F}}\Big|^{pel}_{ben} = \frac{\partial \chi}{\partial t}\Big|_{bgc} + \frac{1}{\overset{\chi}{\tau}_{eq}}\left(\chi - p_{poro} p_{Cads} \widetilde{\chi}_{pw}\right), \tag{223}$$

where χ represents the inorganic states of oxygen, DIC, oxidised nitrogen, ammonium, phosphate and silicate.

GMDD
8, 7063–7187, 2015
ERSEM 15.06
M. Butenschön et al.

For phosphorus, ammonium, silicate and DIC the excess is distributed in parabolic form with 0 surface concentrations and 0 bottom flux, so that the relaxation time scale $\overset{\chi}{\tau}_{eq}$ towards equilibrium conditions is given by the parabolic slope at the surface. For oxidised nitrogen and oxygen the procedure requires modification for two reasons: the separation depths of the oxygenated layer and denitrification layer given by the dissolved oxygen horizon and the horizon of oxidised nitrogen may be considered as fixed parameters for the diffusion–production balance of the other state variables, but not so for dissolved oxygen and oxidised nitrogen whose biogeochemical changes affect the dynamics of these horizons directly. In addition, the system imposes a third boundary condition on the balance equation, i.e. that the concentration at the respective horizon has to be zero by definition (and no sources and sinks exist below these limits), which renders the system overdetermined. For these two variables the relaxation time scale is therefore approximated by the fixed parameters τ_{ox} and τ_{denit} also used to determine the dynamical evolution of oxygen and oxidised nitrogen horizon in Eqs. (142) and (143).

The recycling of iron in the benthos is abbreviated, as there is very little information on the iron cycle in the sea-bed. The only form of iron considered in the benthos is the slowly degradable matter, which is implicitly remineralised and returned to the water column in dissolved form at a fixed remineralisation rate $\overset{\chi}{r}_{remin}$:

$$\overset{remin}{\mathcal{F}_{\mathbb{F}}}\Big|_{\overset{\chi}{Q}_{\mathbb{F}}}^{N_{\mathbb{F}}} = r_{remin\mathbb{F}}\ \overset{\chi}{Q}'_{\mathbb{F}} \tag{224}$$

5.1.4 Remineralistion of calcite

No processes related to the formation or dissolution of calcite in the benthos are currently included in the model, the benthic cylce of calcite is resolved purely implicitly similar to iron as simple linear release to the water column of the calcite deposited

GMDD
8, 7063–7187, 2015

onto the sediments:

$$\overset{\text{remin}}{\mathcal{F}}_{\text{calc}} \Big|_{\overset{\text{calc}}{C_{\mathbb{C}}}}^{\overset{\text{calc}}{L_{\mathbb{C}}}} = \overset{\text{calc}}{r}_{\text{remin}} \overset{\text{calc}}{C}_{\mathbb{C}} \tag{225}$$

5.1.5 Benthic remineralisation sub-model

As an alternative to the full benthic model described in the Sect. 4, a simple benthic closure is available, that implicitly remineralises benthic substrate into dissolved inorganic states, analogous to the treatment of iron and calcite above. The treatment of deposition and resuspension of organic matter on the sea floor in this case is identical to the full benthic model, while the recycling of organic matter occurs as a linear function of the benthic content at a given remineralisation rate $\overset{\chi}{r}_{\text{remin}}$:

$$\overset{\text{remin}}{\mathcal{F}}_{\mathbb{C},\mathbb{P},\mathbb{S}} \Big|_{\overset{\chi}{Q}_{\mathbb{C},\mathbb{P},\mathbb{S}}}^{G_{\mathbb{C}},N_{\mathbb{P}},N_{\mathbb{S}}} = \overset{\chi}{r}_{\text{remin}} \overset{\chi}{Q'}_{\mathbb{C},\mathbb{P},\mathbb{S}} \tag{226}$$

For nitrogen the remineralisition flux is split regenerating oxidised nitrogen and ammonium using the fixed fraction $\overset{\chi}{q}_{\text{remin}}$:

$$\overset{\text{remin}}{\mathcal{F}}_{\mathbb{N}} \Big|_{\overset{\chi}{Q}_{\mathbb{N}}}^{\overset{\text{ox}}{N}_{\mathbb{N}}} = \overset{\text{ox}}{q}_{\text{remin}} \overset{\chi}{r}_{\text{remin}} \overset{\chi}{Q'}_{\mathbb{N}} \tag{227}$$

$$\overset{\text{remin}}{\mathcal{F}}_{\mathbb{N}} \Big|_{\overset{\chi}{Q}_{\mathbb{N}}}^{\overset{\text{amm}}{N}_{\mathbb{N}}} = \left(1 - \overset{\text{ox}}{q}_{\text{remin}}\right) \overset{\chi}{r}_{\text{remin}} \overset{\chi}{Q'}_{\mathbb{N}} \tag{228}$$

With this option no other biogeochemical processes are considered in the benthos. The treament of iron and calcite is identical in between the full benthic model and this simplified benthic closure.

GMDD
8, 7063–7187, 2015
ERSEM 15.06
M. Butenschön et al.

5.2 Sea surface fluxes

The only two boundary fluxes computed in the standard set-up at the air–sea interface are the exchange of oxygen and carbon dioxide. Other processes like atmospheric deposition of nutrients and riverine inputs require spatially varying surface fields and are best provided thourgh the physical driver. (Implementations of this type have been used in Artioli et al., 2012; Edwards et al., 2012; Holt et al., 2012; Wakelin et al., 2012.)

Oxygen is exchanged based on the difference from the saturation state

$$\mathcal{F}_{\mathbb{O}}|_{\text{sea}}^{\text{air}} = k_{\text{air}\mathbb{O}}\left(\mathrm{T},\mathrm{S},\boldsymbol{u}_{\text{wind}}\right)\left(G_{\mathbb{O}} - s_{\mathbb{O}}\right) \tag{229}$$

while the exchange of carbon dioxide is based on the difference in partial pressures

$$\mathcal{F}_{\mathbb{C}}|_{\text{sea}}^{\text{air}} = \rho_{\text{sea}} k_{\text{air}\mathbb{C}}\left(\mathrm{T},\boldsymbol{u}_{\text{wind}}\right)\left(p_{\mathrm{CO}_2} - \overset{\text{air}}{p}_{\mathrm{CO}_2}\right), \tag{230}$$

where $\overset{\text{air}}{p}_{\mathrm{CO}_2}$ maybe be provided by the physical driver or a constant parameter $\overset{\text{air}}{p}_{\mathrm{CO}_2}$.

The empirical gas transfer coefficients $k_{\text{air}\mathbb{O}}$ and $k_{\text{air}\mathbb{C}}$ are taken from Weiss (1970); Nightingale et al. (2000) and given in the Supplement.

6 Generic terms

6.1 Regulation and limitation factors

The regulation of metabolic processes by temperature is modelled using the Q_{10} function introduced in Blackford et al. (2004) that strongly increases at low temperatures and decreases slower at high temperatures representing eznyme degradation:

$$\overset{\chi}{l}_{\mathrm{T}} = \overset{\chi}{p}_{Q_{10}}^{\frac{\mathrm{T}\,[^\circ\mathrm{C}]-10\,^\circ\mathrm{C}}{10\,^\circ\mathrm{C}}} - \overset{\chi}{p}_{Q_{10}}^{\frac{\mathrm{T}\,[^\circ\mathrm{C}]-32\,^\circ\mathrm{C}}{3\,^\circ\mathrm{C}}}, \tag{231}$$

GMDD
8, 7063–7187, 2015

where T [°C] is the water temperature in degrees Celsius and χ represents the respective process or state.

Nitrogen and phosphorus limitation factors for each of the four phytoplankton types are computed as:

$$f^{\chi}_{\mathbb{P}} = \min\left(1, \max\left(0, \frac{q^{\chi}_{\mathbb{P}:\mathbb{C}} - q^{\chi}_{\min_{\mathbb{P}:\mathbb{C}}}}{q^{\chi}_{\mathrm{ref}_{\mathbb{P}:\mathbb{C}}} - q^{\chi}_{\min_{\mathbb{P}:\mathbb{C}}}}\right)\right) \tag{232}$$

$$f^{\chi}_{\mathbb{N}} = \min\left(1, \max\left(0, \frac{q^{\chi}_{\mathbb{N}:\mathbb{C}} - q^{\chi}_{\min_{\mathbb{N}:\mathbb{C}}}}{q^{\chi}_{\mathrm{ref}_{\mathbb{N}:\mathbb{C}}} - q^{\chi}_{\min_{\mathbb{N}:\mathbb{C}}}}\right)\right), \tag{233}$$

where χ represents any phytoplankton type (dia, micro, nano, pico), $q^{\chi}_{\mathrm{ref}_{\mathbb{N},\mathbb{P}:\mathbb{C}}}$ is its reference internal quota and $q^{\chi}_{\min_{\mathbb{N},\mathbb{P}:\mathbb{C}}}$ is its minimal internal quota. These two factors are combined to three alternative forms of co-limitation $f^{\chi}_{\langle\mathbb{N}\mathbb{P}\rangle}$

$$f^{\chi}_{\langle\mathbb{N}\mathbb{P}\rangle} = f\left(f^{\chi}_{\mathbb{N}}, f^{\chi}_{\mathbb{P}}\right), \tag{234}$$

switchable through the namelist switch `LimnutX`:

`LimnutX`= 0: $f^{\chi}_{\langle\mathbb{N}\mathbb{P}\rangle}$ is the geometric mean of $f^{\chi}_{\mathbb{N}}$ and $f^{\chi}_{\mathbb{P}}$,

`LimnutX`= 2: $f^{\chi}_{\langle\mathbb{N}\mathbb{P}\rangle}$ is the harmonic mean of $f^{\chi}_{\mathbb{N}}$ and $f^{\chi}_{\mathbb{P}}$,

`LimnutX`= 1: $f^{\chi}_{\langle\mathbb{N}\mathbb{P}\rangle}$ is the minimum of $f^{\chi}_{\mathbb{N}}$ and $f^{\chi}_{\mathbb{P}}$.

GMDD
8, 7063–7187, 2015
ERSEM 15.06
M. Butenschön et al.

The silicate limitation factor for diatoms is computed from the external availability of dissolved silicate N_S, based on a Michaelis–Menten term with half-saturation $\overset{dia}{h}_S$:

$$\overset{dia}{l}_S = \frac{N_S}{N_S + \overset{dia}{h}_S} \tag{235}$$

The iron limitation factor is computed in the same way as the factors for nitrogen and phosphorus:

$$\overset{\chi}{l}_F = \min\left(1, \max\left(0, \frac{\overset{\chi}{q}_{F:C} - \overset{\chi}{q}_{\min_{F:C}}}{\overset{\chi}{q}_{\mathrm{ref}_{F:C}} - \overset{\chi}{q}_{\min_{F:C}}}\right)\right), \tag{236}$$

with $\overset{\chi}{q}_{\mathrm{ref}_{F:C}}$ as its reference internal quota and $\overset{\chi}{q}_{\min_{F:C}}$ as its minimal internal quota.

Phosphorus and nitrogen limitation $\overset{B}{l}_P$, $\overset{B}{l}_N$ for the standard model of bacteria mediated decomposition can be based on the availability of the resource in dissolved inorganic form (`ISWBlimX` = 1) and substrate or only in inorganic form (`ISWBlimX` = 2):

$$\overset{B}{l}_P = \begin{cases} \min\left(\frac{N_P}{N_P + \overset{B}{h}_P}, \frac{\overset{dis}{R}_P}{\overset{dis}{R}_P + \overset{B}{h}_P}\right) & \text{if } \texttt{ISWBlimX} = 1 \\ \frac{N_P + \overset{dis}{R}_P}{N_P + \overset{dis}{R}_P + \overset{B}{h}_P} & \text{if } \texttt{ISWBlimX} = 2 \end{cases} \tag{237}$$

and analogous:

$$\overset{B}{l}_N = \begin{cases} \min\left(\frac{\overset{amm}{N}_N}{\overset{amm}{N}_N + \overset{B}{h}_N}, \frac{\overset{dis}{R}_N}{\overset{dis}{R}_N + \overset{B}{h}_N}\right) & \text{if } \texttt{ISWBlimX} = 1 \\ \frac{\overset{amm}{N}_N + \overset{dis}{R}_N}{\overset{amm}{N}_N + \overset{dis}{R}_N + \overset{B}{h}_N} & \text{if } \texttt{ISWBlimX} = 2 \end{cases}, \tag{238}$$

GMDD
8, 7063–7187, 2015
ERSEM 15.06
M. Butenschön et al.

where $\overset{B}{h}_{\mathbb{P},\mathbb{N}}$ are the Michaelis–Menten constants for phosphorus and nitrogen limitation.

Nutrient regulation of benthic bacteria occurs based on the nutritional state of the substrate

$$\overset{\chi}{l}_{\mathbb{N}} = \min\left(1, \frac{\overset{\text{slow}}{Q'_{\mathbb{N}}}\Big|_{d_{\text{up}}}^{d_{\text{low}}}}{\overset{\chi}{q}_{\text{ref}_{\mathbb{N}:\mathbb{C}}}\overset{\text{slow}}{Q'_{\mathbb{N}}}\Big|_{d_{\text{up}}}^{d_{\text{low}}}}\right)\min\left(1, \frac{\overset{\text{slow}}{Q'_{\mathbb{P}}}\Big|_{d_{\text{up}}}^{d_{\text{low}}}}{\overset{\chi}{q}_{\text{ref}_{\mathbb{P}:\mathbb{C}}}\overset{\text{slow}}{Q'_{\mathbb{P}}}\Big|_{d_{\text{up}}}^{d_{\text{low}}}}\right). \tag{239}$$

where χ are aerobic and anaerobic bacteria within the layers described in Sect. 4.4.

Oxygen limitation of zooplankton (χ: HET, MICRO, MESO) is computed as function of the relative oxygen saturation state

$$s_{\text{rel}\mathbb{O}} = \min\left(1, \frac{G_{\mathbb{O}}}{s_{\mathbb{O}}}\right) \tag{240}$$

$$\overset{\chi}{l}_{\mathbb{O}} = \frac{s_{\text{rel}\mathbb{O}} + s_{\text{rel}\mathbb{O}}\ \overset{\chi}{h}_{\mathbb{O}}}{s_{\text{rel}\mathbb{O}} + \overset{\chi}{h}_{\mathbb{O}}}, \tag{241}$$

where the oxygen saturation concentration $s_{\mathbb{O}}$ is estimated according to Weiss (1970). (The regression formula used is given in the Supplement).

For zoobenthos (χ: DEPO, SUSP, MEIO) it is given by a cubic Michaelis–Menten response to the oxygen concentration in the overlying water body in relation to a minimum oxygen threshold $\overset{\chi}{p}_{\mathbb{O}\text{min}}$ for each species:

$$\overset{\chi}{l}_{\mathbb{O}} = \left(\frac{\max\left(G_{\mathbb{O}} - \overset{\chi}{p}_{\mathbb{O}\text{min}}, 0\right)}{\max\left(G_{\mathbb{O}} - \overset{\chi}{p}_{\mathbb{O}\text{min}}, 0\right) + \overset{\chi}{h}_{\mathbb{O}}}\right)^3. \tag{242}$$

GMDD
8, 7063–7187, 2015
ERSEM 15.06
M. Butenschön et al.

For pelagic bacteria it is given by a simple Michaelis–Menten term of the relative oxygen saturation state (Eq. 240)

$$f^{B}_{\mathbb{O}} = \frac{s_{\mathrm{rel}\mathbb{O}}}{s_{\mathrm{rel}\mathbb{O}} + h^{B}_{\mathbb{O}}}. \tag{243}$$

For benthic bacteria oxygen regulation occurs through the oxygen and oxidised nitrogen horizons

$$f^{\mathrm{aer}}_{\mathbb{O}} = \frac{D^{\mathrm{oxy}}}{D^{\mathrm{oxy}} + d^{\mathrm{oxy}}_{\mathrm{ref}}}; \quad f^{\mathrm{anaer}}_{\mathbb{O}} = \frac{D^{\mathrm{denit}} - D^{\mathrm{oxy}}}{D^{\mathrm{denit}} - D^{\mathrm{oxy}} + d^{\mathrm{denit}}_{\mathrm{ref}}}, \tag{244}$$

where $d^{\mathrm{oxy}}_{\mathrm{ref}}$ is the aerobic half saturation depth and $d^{\mathrm{denit}}_{\mathrm{ref}}$ the anaerobic half saturation depth for oxygen regulation.

$f^{\mathrm{nitr}}_{\mathbb{O}}$ is the oxygen limitation factor for nitrification:

$$f^{\mathrm{nitr}}_{\mathbb{O}} = \frac{O^3_{\mathbb{O}}}{O^3_{\mathbb{O}} + h^{\mathrm{nitr}}_{\mathbb{O}}} \tag{245}$$

with $h^{\mathrm{nitr}}_{\mathbb{O}}$ being the cubic half-saturation constant for oxygen limitation of nitrification,

$f^{\mathrm{nitr}}_{\mathbb{N}}$ is the substrate limitation factor for nitrification:

$$f^{\mathrm{nitr}}_{\mathbb{N}} = \frac{N^{\mathrm{amm}^3}_{\mathbb{N}}}{N^{\mathrm{amm}^3}_{\mathbb{N}} + h^{\mathrm{nitr}}_{\mathbb{N}}} \tag{246}$$

GMDD
8, 7063–7187, 2015
ERSEM 15.06
M. Butenschön et al.

with h_{INnitr} being the cubic half-saturation constant for substrate limitation of nitrification and l_{pH} is the pH-limitation factor for nitrification:

$$l_{\mathrm{pH}} = \min\left(2, \max\left(0, 0.6111\mathrm{pH} - 3.8889\right)\right). \tag{247}$$

Benthic nitrification is inhibited at high benthic content of oxidised nitrogen according to

$$\overline{{}^{\mathrm{ox}}_{K_{\mathrm{IN}}}} = \frac{{}^{\mathrm{ox}}_{K_{\mathrm{IN}}}}{{}^{\mathrm{oxy}}_{D} + \frac{{}^{\mathrm{denit}}_{D} - {}^{\mathrm{oxy}}_{D}}{3}} \tag{248}$$

$${}^{\mathrm{bnitr}}_{l_{\mathrm{IN}}} = \frac{{}^{\mathrm{bnitr}}_{h_{\mathrm{IN}}}}{{}^{\mathrm{bnitr}}_{h_{\mathrm{IN}}} + \overline{{}^{\mathrm{ox}}_{K_{\mathrm{IN}}}}}, \tag{249}$$

where ${}^{\mathrm{bnitr}}_{h_{\mathrm{IN}}}$ is the oxygenated layer concentration of oxidised nitrogen at which nitrifation is inhibited by 50 %.

Here, it is assumed that some oxidised nitrogen penetrates into the denitrification layer, so that the oxygenated layer concentration is on average three times higher compared to the denitrification layer.

GMDD
8, 7063–7187, 2015
ERSEM 15.06
M. Butenschön et al.

Based on the same assumption, denitrification in the oxidised layer uses a Michaelis–Menten response to the assumed layer content of oxidised nitrogen

$$\overline{K_{\mathrm{IN}}^{\mathrm{denitr}}} = \frac{1}{3} \frac{K_{\mathrm{IN}}'^{\mathrm{ox}}}{D^{\mathrm{oxy}} + \frac{D^{\mathrm{denit}} - D^{\mathrm{ox}}}{3}} \tag{250}$$

$$I_{\mathrm{IN}}^{\mathrm{denitr}} = \frac{\overline{K_{\mathrm{IN}}^{\mathrm{denitr}}}}{\overline{K_{\mathrm{IN}}^{\mathrm{denitr}}} + h_{\mathrm{IN}}^{\mathrm{denitr}}}, \tag{251}$$

where $h_{\mathrm{IN}}^{\mathrm{denitr}}$ is a denitrification half saturation constant.

Calcification and dissolution of calcite occur in relation to the calcite saturation state of the water $\Omega_{\mathrm{calc}} \gtrless 0$ (Eq. 125). The regulating factor of the rain ratio for calcification and the regulation factor for dissolution of calcite can be calculated in two alternative ways chosen by the `ISWCAL = 1` namelist switch. The first option (`ISWCAL = 1`) is based on an exponential term:

$$I_{\mathrm{C}}^{\mathrm{calc}} = \max\left(0, (\Omega_{\mathrm{calc}} - 1)^{n_{\mathrm{calc}}}\right) \tag{252}$$

$$I_{\mathrm{C}}^{\mathrm{dis}} = \max\left(0, (1 - \Omega_{\mathrm{calc}})^{n_{\mathrm{dis}}}\right), \tag{253}$$

where $n_{\mathrm{calc,dis}}$ are calcification/dissolution exponents (Ridgwell et al., 2007; Keir, 1980).

The second option (`ISWCAL = 2`) uses a Michaelis–Menten term:

$$I_{\mathrm{C}}^{\mathrm{calc}} = \max\left(0, \frac{\Omega_{\mathrm{calc}} - 1}{\Omega_{\mathrm{calc}} - 1 + h_{\mathrm{calc}}}\right) \tag{254}$$

$$I_{\mathrm{C}}^{\mathrm{dis}} = \max\left(0, \frac{1 - \Omega_{\mathrm{calc}}}{1 - \Omega_{\mathrm{calc}} + h_{\mathrm{calc}}}\right) \tag{255}$$

GMDD
8, 7063–7187, 2015
ERSEM 15.06
M. Butenschön et al.

where h_{calc} is the half-saturation constant for calcification and dissolution of calcite (Blackford et al., 2010; Gehlen et al., 2007).

The rain ratio (Eq. 88) is regulated by nutrient limitation and temperature to reflect the dependency of the calcifying fraction of nanophytoplankton on the environmental conditions. Temperature regulation is given by

$$\overset{\mathrm{calc}}{I_{\mathrm{T}}} = \frac{\max\left(0, \mathrm{T}[^{\circ}\mathrm{C}]\right)}{\max\left(0, \mathrm{T}[^{\circ}\mathrm{C}]\right) + \overset{\mathrm{calc}}{h_T}}, \tag{256}$$

where the half-saturation constant is set to $\overset{\mathrm{calc}}{h_T} = 2\,^{\circ}\mathrm{C}$. As coccolithophores are reported to have generally higher phosphorus affinity but lower nitrogen acquisition capacity with respect to other phytoplankton (Riegman et al., 2000; Paasche, 1998), limitation of these nutrients has an opposed impact on the rain ratio. This is reflected in our combined nutrient limitation factor for calcification which is obtained from the phosphorus and nitrogen limitation of nanophytoplankton (Eqs. 233 and 232) as

$$\overset{\mathrm{calc}}{I_{\langle \mathrm{IN|P} \rangle}} = \min\left(1 - \overset{\mathrm{nano}}{I_{\mathrm{IP}}}, \overset{\mathrm{nano}}{I_{\mathrm{IN}}}\right). \tag{257}$$

Uptake limitation of suspension and deposit feeders by overcrowding is given by a nested Michaelis–Menten response to the respective biomass:

$$\overset{\chi}{p}_{\mathrm{crowd}} = \left(\overset{\chi}{Y}_{\mathbb{C}} - \overset{\chi}{p}_{\mathbb{C}}\right) \frac{\overset{\chi}{Y}_{\mathbb{C}} - \overset{\chi}{p}_{\mathrm{crowd}}}{\overset{\chi}{Y}_{\mathbb{C}} - \overset{\chi}{p}_{\mathrm{crowd}} + \overset{\chi}{h}_{\mathrm{sat}}} \tag{258}$$

$$\overset{\chi}{I}_{\mathrm{crowd}} = 1 - \frac{\overset{\chi}{p}_{\mathrm{crowd}}}{\overset{\chi}{p}_{\mathrm{crowd}} + \overset{\chi}{h}_{\mathrm{crowd}}}. \tag{259}$$

GMDD
8, 7063–7187, 2015
ERSEM 15.06
M. Butenschön et al.

6.2 Stoichiometric adjustments

For states $\overset{\chi}{\varphi}$ with fixed stoichiometric quota $q_{\mathbb{N},\mathbb{P}:\mathbb{C}}^{\chi}$ (mesozooplankton, benthic bacteria and predators) the processes rates are complemented by exudation fluxes that regulate imbalances with respect to the reference quotas as follows:

$$\left.\frac{\partial \overset{\chi}{\varphi}_{\mathbb{C}}}{\partial t}\right|_{\text{exu}} = \max\left(\left.\frac{\widetilde{\partial \overset{\chi}{\varphi}_{\mathbb{C}}}}{\partial t}\right|_{\text{bgc}} - \frac{1}{q_{\mathbb{P}:\mathbb{C}}^{\chi}}\left.\frac{\widetilde{\partial \overset{\chi}{\varphi}_{\mathbb{P}}}}{\partial t}\right|_{\text{bgc}}, \left.\frac{\widetilde{\partial \overset{\chi}{\varphi}_{\mathbb{C}}}}{\partial t}\right|_{\text{bgc}} - \frac{1}{q_{\mathbb{N}:\mathbb{C}}^{\chi}}\left.\frac{\widetilde{\partial \overset{\chi}{\varphi}_{\mathbb{N}}}}{\partial t}\right|_{\text{bgc}}, 0\right), \tag{260}$$

$$\left.\frac{\partial \overset{\chi}{\varphi}_{\mathbb{N},\mathbb{P}}}{\partial t}\right|_{\text{exu}} = \max\left(\left.\frac{\widetilde{\partial \overset{\chi}{\varphi}_{\mathbb{N},\mathbb{P}}}}{\partial t}\right|_{\text{net}} - q_{\mathbb{N},\mathbb{P}:\mathbb{C}}^{\chi}\left.\frac{\widetilde{\partial \overset{\chi}{\varphi}_{\mathbb{C}}}}{\partial t}\right|_{\text{bgc}}\right) \tag{261}$$

where $\left.\frac{\widetilde{\partial \overset{\chi}{\varphi}_{\mathbb{C}}}}{\partial t}\right|_{\text{net}}$ are the comprehensive biogeochemical process rates prior to adjustments

$$\left.\frac{\widetilde{\partial \overset{\chi}{\varphi}}}{\partial t}\right|_{\text{bgc}} = \left.\frac{\partial \overset{\chi}{\varphi}}{\partial t}\right|_{\text{net}} - \left.\frac{\partial \overset{\chi}{\varphi}}{\partial t}\right|_{\text{exu}}. \tag{262}$$

7 Implementations

Most ecosystem models are tightly bound to a specific physical, hydrodynamic driver that is usually three-dimensional and consequently computationally heavy and cumbersome to test and implement. The ERSEM model comes as an independent library and can in principle be coupled to any physical driver with comparatively little effort. In fact, coupled configurations exist for a variety of drivers in one or three-dimensional

GMDD
8, 7063–7187, 2015
ERSEM 15.06
M. Butenschön et al.

settings amongst which are the NEMO ocean engine (Madec, 2008), the POLCOMS model for shelf seas (Holt and James, 2001), and the GOTM/GETM model (Burchard et al., 2006). While for realistic implementations a full-scale three-dimensional configuration is required, for the stages of process development and qualitative analysis of the functioning of the modelled ecosystem, zero- or one-dimensional frameworks are often beneficial as they provide a light-weight implementation that is easier to grasp, much faster to run, amenable to sensitivity analysis and quicker to analyse.

The model distribution itself includes drivers for two idealised systems: the first is a simple zero dimensional implementation of mesocosm type called the ERSEM-Aquarium with a pelagic box overlying a benthic box, each of them with internally homogeneous conditions. This is essentially a test environment for new users and fast process assessment requiring no external software for the ocean physics. The second is a driver for the vertical one-dimensional GOTM model (http://www.gotm.net – Burchard et al., 2006). It is a more realistic system allowing for full vertical structures in a comparatively lightweight software environment that is capable of running in serial mode on any standard desktop or laptop. It requires a copy of the GOTM code with minor modifications to accommodate ERSEM, which can be obtained for the stable release or the development release of GOTM (see Sect. 9). Here, we use the 0-D framework to illustrate the carbon fluxes through the model food-web under contrasting environmental conditions (Sect. 7.1) and the 1-D implementation to demonstrate the model capacity to reflect the lower trophic level of the marine ecosystem under varying conditions at three different sites, underpinned by a brief validation against in situ time-series data (Sect. 7.2).

Beyond these simpler test cases, the ERSEM model has been implemented in various full-scale three dimensional applications from coastal to global scales, cited above. The descriptions of these configurations would exceed the scope and volume of this paper and are given in the respective publications, but for completeness we give a short example of a simulation based on a previously published configuration in order to illustrate the full potential of the model (Sect. 7.3).

GMDD
8, 7063–7187, 2015

All simulations presented in this section were performed using the same parametrisation, which is given in the Supplement. This parametrisation was developed using size as the main trait to scale the metabolic rates of the pelagic functional groups more widely than in previous parametrisations (Baretta-Bekker et al., 1997; Blackford et al., 2004) and respects the conventional restriction of the food matrix suggested in Eq. (31). A table with all parameter values, their mathematical symbols as used in Sect. 2 and the corresponding name in the model code and namelists is given in the Supplement.

7.1 ERSEM-Aquarium

The simulation of mesocosm type environments is supported through the ERSEM-Aquarium model. The model simulates two 0-D boxes, a pelagic box, which is characterised by its mid-depth below the surface and by the geographical location, and a benthic box beneath it. Seasonal variations in temperature and salinity can be imposed as cosine functions between an extreme value at the first of January in the beginning of the simulation and a second extreme after half a year. The light field can be imposed in the same way as cosine oscillation between two prescribed extreme values, or extracted from the prescribed geographical position using standard astronomical formula ignoring cloud cover. Additionally diurnal oscillations of temperature and light can be superimposed in cosine form by prescribing a daily excursion between midday and midnight. It should be noted that this framework is not designed to deliver realistic simulations of the marine environment in a particular location, but rather to aid the development and quick evaluation of process studies, or to study the model system behaviour in a simplified context without additional complicating factors.

Figure 2 illustrates the carbon fluxes between model compartments for two different simulations using the ERSEM-Aquarium. The first is configured as a representation of tropical oligotrophic conditions characterised by deep and warm waters with high irradiance and low nutrients, while the second roughly corresponds to the shallow coastal eutrophic waters of the Southern North Sea with strong nutrient supply and comparatively low light. Both configurations are run for a thousand years in order to achieve full

GMDD
8, 7063–7187, 2015

equilibrium between the benthic and pelagic environments. The former uses the simple benthic closure scheme for remineralisation (Sect. 5.1.5), which is more appropriate for deep water configurations where the impact of the benthos is of lesser importance, while the latter uses the full benthic model (Sect. 4). All configuration files necessary to replicate these runs are given in the Supplement. Figure 2 gives flux magnitudes in the modelled food-web directly scaled from the annual average of the last year of each simulation. The experiment highlights the substantial quantitative production difference in between the two systems. In addition, it clearly shows the qualitative shift in the model food-web under the contrasting conditions. In the oligotrophic case most of the gross production is excreted to dissolved matter due to strong growth limitation. This leads to a microbial dominated scenario with bacteria as the main food-source for the predators and only small amounts of carbon entering the second trophic level leading to negative community production and low deposition of biomass to the sediments. In the eutrophic case production levels are increased by a level of magnitude. The assimilated carbon is used more efficiently by phytoplankton fueling substantial secondary production with autotrophs as the main food source of zooplankton and significantly more biomass exported to the sediments resulting in positive community production.

7.2 GotmErsem – a model Framework for the water column

The GotmErsem framework provides the possibility to include a more realistic physical environment into the simulations with opposing gradients of nutrient supply from depth and short-wave radiation attenuated as it penetrates through the water column. The GOTM model is a one-dimensional water column model including a variety of turbulence closure schemes for vertical mixing (Burchard et al., 2006). Here, we show three implementations using this framework in contrasting environments to demonstrate the portability of the ERSEM model, one for the Oyster Grounds in the Southern North Sea, a typical shelf sea site; one at the L4 site in the Western English Channel representative of a mid-latitude site with mixed waters of both oceanic and coastal origin; and one in the oligotrophic sub-tropics at the Bermuda Atlantic Time-series Study site.

GMDD
8, 7063–7187, 2015

Each of these sites is supported by extensive in situ data sets for model evaluation. Full configuration files to run these simulations are provided in the Supplement. The validation against in situ data was performed by sub-sampling the daily averaged model output for each in situ data sample. It is presented in target diagrams (Jolliff et al., 2009) for each site showing statistically robust metrics (e.g. Daszykowski et al., 2007) to account for the underlying non-Gaussian asymmetric data distributions and in order to avoid spurious overweighting of outliers. The metrics provided are the median bias (median$(M_i - D_i)$; M_i: model sample, D_i data sample) on the ordinate and the unbiased median absolute error (MAE', median[abs$(M_i - D_i - \text{median}(M_i - D_i))$]) on the abscissa. Both are normalised with the inter-quartile range (IQR) for the scale of the in situ data and the Spearman or rank correlation is represented by the colour code for each data set. The sign on the abscissa is given by the relation of IQRs (sign$(\text{IQR}(M_i) - \text{IQR}(D_i))$).

All three sites are forced with data from the ERA-interim reanalysis (Dee et al., 2011) at the atmospheric boundary condition. The L4 and Oyster Ground configurations use surface pressure data to introduce tidal mixing into the idealised one-dimensional set-ups. The BATS and L4 site were additionally relaxed towards temperature and salinity profiles from CTD measurements (BATS – Steinberg et al., 2001, L4 – Harris, 2010) in order to compensate for the missing hydrodynamic impacts of lateral advection and diffusion. Initial conditions for the sites were derived from the concurrent in situ data where available. As for the ERSEM-Aquarium simulations the benthic remineralisation closure was used for the deep, oligotrophic BATS site, while for the shallow eutrophic sites L4 and Oyster Grounds the full benthic model was used.

7.2.1 Oyster Grounds – (54°24′36″ N, 4°1′12″ E)

This site is located in the Southern North Sea and is influenced by the English Channel and surrounding coastal waters, with seasonal stratification in most summers and an accentuated spring bloom at the onset of stratification that depletes the nutrients from the comparatively stable and isolated water surface layer (Baretta-Bekker et al., 2008).

GMDD
8, 7063–7187, 2015
ERSEM 15.06
M. Butenschön et al.

A comparison with smart buoy data for the years 2000–2009 (Greenwood et al., 2010) reveals a good representation of the local seasonal cycle (Fig. 3). Simulations do not show significant bias in any of the variables, while the MAE' is significantly lower than the in situ data variability (≈ 0.75 of the IQR of the in situ data for chlorophyll *a*, ≈ 0.25 silicate and phosphate and virtually 0 for oxidised nitrogen). Correlations are high for the nutrients (> 0.6), but comparatively low for chlorophyll *a* (> 0.2). The lower skill for the latter is partly caused by a weaker secondary bloom in summer in the simulations compared to the observations and comparatively low observational coverage over the first years of the simulation leading to potential overstressing of singular events in the data sampling and giving a spurious picture of the seasonal cycle when compared to the more consistently covered last three years of the period shown.

7.2.2 L4 – Western English Channel (50°15′ N, 4°13′ W)

The L4 site is a long-term monitoring station near the Northern coast of the Western English Channel. Similar to the Oyster Grounds site, it is seasonally stratified and generally nutrient depleted in summer, but highly affected by episodic events of freshwater inputs of riverine origin (Smyth et al., 2010).

Figure 4 shows the seasonal cycles of oxidised nitrogen, phosphate and chlorophyll *a* at the sea surface for the model simulations and for the in situ data (Smyth et al., 2010 – http://www.westernchannelobservatory.org.uk/) for the years 2007–2011. The model follows the seasonal cycle of nutrient depletion in summer and nutrient resupply in winter revealed by the data in all three nutrients shown. Also the results for chlorophyll *a* follow the bulk seasonality represented by the in situ data, but show deficiencies in capturing the episodic peaks, which appear misplaced with respect to the measurements. Possible reasons for these short-comings include the absence of physical and biogeochemical impacts of lateral processes in such an idealised 1-dimensional setting as well as a sub-optimal representation of the local phytoplankton community by the parametrisation adopted consistently across the contrasting environments. Nevertheless, the model skill expressed in the overall statistics is considerable. The bias and

GMDD
8, 7063–7187, 2015
ERSEM 15.06
M. Butenschön et al.

MAE' for all 4 variables falls well below the variability of the in situ data. Chlorophyll *a* shows a relative bias of about 0.25 and a relative unbiased error of little less than 0.5, while the three nutrients show an error and bias very close to 0.

7.2.3 BATS – Bermuda, Sargasso Sea (31°40′ N, 64°10′ W)

This site in the Sargasso Sea is characterised by a weak geostrophic flow with net down-welling. Strong stratification separates the nutrient-poor surface waters from the nutrient-rich deep water, with the exception of the passing of cold fronts in winter which cause substantial convective mixing with accompanying nutrient entrainment (Steinberg et al., 2001). This is illustrated in the left panel of Fig. 5, which shows the seasonal cycle of chlorophyll *a* from model simulations (on top) and in situ data. The mixing events triggering autotrophic growth initially spread over the upper part of the water column, but they are limited to a rather marked deep-chlorophyll *a* maximum at around 100 m depth when stratification sets in. A summary of the validation against the extensive in situ data available at BATS (Bermuda Time Series Study – Steinberg et al., 2001) for the years 1990–2008 is given in the target diagram on the right of Fig. 5. In contrast to the two shallow sites, in situ data in this case is vertically resolved, which was respected in the matching procedure.

Bias and MAE' for all variables do not exceed the variability of the in situ data. Both metrics are very close to zero for the nitrate, phosphate and chlorophyll *a* and in general most metrics stay below 50 % of the in situ variability with the exception of the bias for oxygen and the MAE' for phosphate. The latter are caused by an underestimated aeriation of the water column and a weaker vertical gradient in phosphate for the model (not shown). However, some weakness in the simulation of the vertical distributions are to be expected given the absence of explicit lateral dynamics and the resulting vertical flows. Correlations lie between 0.4 and 0.6 reflecting the overall satisfactory model performance.

GMDD
8, 7063–7187, 2015
ERSEM 15.06
M. Butenschön et al.

7.2.4 Properties emerging from simulations at all three sites

In order to give an impression of the functioning of the ecosystem dynamics across the three sites, Fig. 6 shows a comparison between some ecosystem properties emerging from data meta-analysis and model simulations, namely the internal stoichiometric quotas of nutrients with respect to carbon in phytoplankton and the phytoplankton community structure. On the left of Fig. 6 we show the range of the internal stoichiometric quotas of nitrogen, phosphorus, silicate and iron with respect to carbon on the abscissa plotted against the average quotas for phytoplankton on the ordinate as an indicator of the modelled phytoplankton plasticity in response to nutrient limitation. Quotas from the simulations (circles) are compared to the results of a meta-analysis (diamonds) provided by Moore et al. (2013) based on observed internal stoichiometric phytoplankton quotas from scientific literature. Results for the three macronutrients are consistent in that the average quotas are well matched while the stoichiometric range is underestimated by approximately half an order of magnitude. This is to be expected given that the case studies included in the model simulations don't cover the full range of natural variability of marine environments. Results for iron show substantial differences in range and average state. The mismatch in average state can be attributed to the fact that the present parametrisation of the iron cycle took into consideration the works of Timmermans et al. (2005) and Veldhuis et al. (2005), which reported comparatively low iron to carbon quotas, but weren't considered in the above meta-analysis, while the huge discrepancy in range is caused by the absence of substantial iron limitation in sites of the case studies.

The right hand side panel of Fig. 6 shows the size fractionated contribution of each phytoplankton group to total chlorophyll *a* across the three sites as a running average over the ordered model samples from all three sites collectively. The procedure is analogous to the meta-analysis provided by Hirata et al. (2011). The results show a domination of the phytoplankton community by picophytoplankton at low chlorophyll *a* and by large phytoplankton at high chlorophyll *a*. Nanophytoplankton is present throughout

GMDD
8, 7063–7187, 2015
ERSEM 15.06
M. Butenschön et al.

the chlorophyll *a* range, reaching a maximum at intermediate values. The emerging modelled community structure compares well to the meta-analysis (compare Fig. 2a–c therein) particularly considering the limited range of marine environments considered in this exercise.

7.3 A full scale implementation for the North-West European Shelf

The previous case studies demonstrate the capability of the model to represent the marine ecosystem with a focus on small scale ecosystem processes. Nevertheless, the full potential of the model unfolds in full-scale applications of coupled dynamical systems linked to hydrodynamic models capturing the full advection and diffusion of the biogeochemical states and thus providing a complete synoptic picture of the large scale biogeochemical cycles and the marine environment. A full description of these systems would exceed the scope of this particular paper. Nevertheless, we give here a brief overview of the model performance on a simulation of the North-West European Shelf Seas using the POLCOMS model for shelf sea circulation (Holt and James, 2001), based on a hindcast configuration identical to the one used and described in Holt et al. (2012) and Artioli et al. (2012), but using the most recent model version presented in this work and the same parametrisation as in the above examples.

The left hand side panel of Fig. 7 shows the mean optical-depth-averaged chlorophyll *a* field of the area to illustrate the model domain as used in the validation exercise, and also to give an idea of the ecosystem characteristics of the area. Model simulations were validated against in situ data for oxidised nitrogen, phosphorus, chlorophyll *a*, oxygen and salinity retrieved from the ICES data base (ICES, 2009) for the period of 1970–2004 using the same metrics as above, summarised in a target diagram on the right of Fig. 7. Results are consistent with the validation results of the 1-D sites with both bias and MAE' generally less than 50 % of the in situ variability, and correlations > 0.4 for all variables confirming the good performance of the model dynamics in a realistic large-scale simulation.

GMDD
8, 7063–7187, 2015

8 Development and testing framework

In addition to the 0- and 1-D ERSEM implementations a framework is provided with the model that allows developers and users of the code to analyse and plot the result of calls to individual ERSEM procedures from Python. This facility is supported through Fortran–C interoperability, that arrived with the Fortran 2003 standard (ISO/IEC 1539-1:2004(E)), and the Python Ctypes package. The ERSEM test harnesses consist of the ERSEM library and a set of C wrappers, which are jointly compiled as a shared library. A Python interface to the shared library permits access to Fortran data structures and procedures from Python. Here we illustrate this feature by examining the photosynthesis model implemented in ERSEM.

The photosynthesis model used in ERSEM is based on Geider et al. (1997), and is described in Sect. 3.1. In the case of diatoms, the carbon specific rate of photosynthesis, $\overset{\text{dia}}{\mathcal{S}}_{\text{gpp}}$ (d^{-1}), is a function of temperature, T (°C); PAR, E_{PAR} (W m); the external silicate concentration, N_{S} (mmol Si m); and the dynamic cellular chlorophyll *a* to carbon ratio, $q^{\chi}_{c:\text{C}}$ ($\text{mg Chl } a \text{ mg C}^{-1}$), as given by Eq. (5). The other primary producer groups use the same photosynthesis model, but without silicate limitation. The sensitivity of the maximum, light-saturated carbon specific photosynthesis rate $\overset{\chi}{g}(\text{T})$ to temperature is modelled by a Q_{10} function (Eq. 231), empirically adapted to mimic enzyme inhibition at high temperatures. The reference temperature, T_0, is set at 10 °C. The model assumes that the light saturated rate of photosynthesis is proportional to the organic carbon content of the cell, while the rate of photosynthesis under light limitation is assumed to be proportional to the product of the chlorophyll *a* to carbon ratio and PAR (Geider et al., 1997). In the model cells are able to regulate the chlorophyll *a* to carbon ratio in response to changes in irradiance, temperature and silicate by modifying the proportion of photosynthate that is directed towards chlorophyll biosynthesis ($\overset{\chi}{\rho}$; see

GMDD
8, 7063–7187, 2015

Eq. 9). Balanced growth is achieved when cells are fully acclimated, in which case:

$$\frac{\mathrm{d}}{\mathrm{d}t}\left(\frac{\overset{\chi}{P}_C}{\overset{\chi}{P}_{\mathbb{C}}}\right) = 0 \tag{263}$$

Chlorophyll *a* biosynthesis is assumed to be up-regulated in response to a reduction in irradiance and down regulated in response to an increase in irradiance. Through this process, cells are able to balance the rate of energy supply through light absorption, and energy demands for growth. The maximum, light saturated photosynthesis rate $\overset{\chi}{g}(\mathrm{T})$ is assumed to be independent of changes in irradiance, which is consistent with observations which indicate Rubisco content is relatively invariant with respect to changes in irradiance (Sukenik et al., 1987), and the hypothesis that these cells are adapted to survive and reproduce in dynamic light environments (Talmy et al., 2014).

Using the ERSEM testing framework, model cells can be artificially acclimated to a given set of environmental conditions by finding a value for $\overset{\chi}{q}_{C:\mathbb{C}}$ which satisfies Eq. (263). Figure 8 shows a plot of $\overset{\chi}{q}_{C:\mathbb{C}}$ vs. $\mathrm{I}_{\mathrm{PAR}}$ for fully photo-acclimated diatoms in ERSEM. Cells were acclimated to a given irradiance by holding cellular carbon fixed and varying the cellular chlorophyll *a* content within the range $\overset{\chi}{q}_{\mathrm{min}_{C:\mathbb{C}}} \leq \overset{\chi}{q} \leq \overset{\chi}{q}_{\varphi\mathrm{max}}$ in order to achieve balanced growth. Overlaid are observations for the diatom T. Pseudonana. No attempt was made to fit the curve to this particular set of observations. The parameter set is the same as used in the simulations of Sect. 7 and is given in the Supplement.

Diatoms are a physiologically and morphologically diverse group, which are characterised by their requirement for silicate, which they use to construct their cell wall. It is perhaps unsurprising that model fits to photosynthesis-irradiance curves for different diatom species result in a range of parameter values, including differences in the maximum light saturated carbon specific photosynthesis rate as a function of temperature, and the initial slope of the photosynthesis-irradiance curve (e.g. Geider et al., 1997).

GMDD
8, 7063–7187, 2015

Ultimately, many of these differences arise due to differences in organism morphology and physiology, with, for example, different pigment compliments or levels of investment in biosynthesis, being reflected in derived parameter values. These within group variations pose a perennial problem to the development of marine ecosystem and biogeochemical models. The diatom group in ERSEM is designed to be representative of diatoms as a whole, and to reflect the important biogeochemical role these organisms perform in nature.

ERSEM includes four phytoplankton functional groups: diatoms, which are characterised by their requirement for silicate, and three further groups which are characterised according to their size. These are the pico-, nano-, and microphytoplankton. The choice to characterise groups according to their size reflects the importance of size as a physiological trait (Litchman et al., 2007, 2010), which influences an organism's competitive ability through its effect on nutrient acquisition, carbon and nutrient storage, the intracellular transport of solutes, photosynthesis rates through pigment packaging effects, and susceptibility to predation (e.g. Chisholm, 1992; Finkel et al., 2010). Figure 9 shows photosynthesis-irradiance curves for ERSEM's four phytoplankton groups under the condition of balanced growth. As with the diatoms, the use of a single parameter set for each size-based group ignores within group variations that are observed in nature. It is important to take such abstractions into consideration when interpreting model outputs.

This example illustrates how ERSEM's testing framework can be used to study and check the implementation of different processes within the code. Importantly, this is achieved without having to rewrite sections of the code in a second language with visualisation capabilities, which is an inherently error prone procedure. This capability is designed to compliment the 0-D and 1-D drivers that simulate more complex time-varying environments, in which it is often difficult to study processes in isolation.

GMDD
8, 7063–7187, 2015
ERSEM 15.06
M. Butenschön et al.

9 Technical Specifications and Code Availability

The ERSEM 15.06 model is written in FORTRAN using the 2008 standard. Output is entirely based on netCDF and the output parsing scripts generating I/O FORTRAN code from plain text lists of variables are written in python.

The model is distributed under the open-source GNU Lesser General Public License through a gitlab server and freely available upon registration through the web-portal www.shelfseasmodelling.org. There are no restrictions or conditions for the registration of individual users, the registration is merely implemented in order to keep track of the user base. The code repository is fully version controlled (using git) and features a bug tracking system open to users. The release code of this publication is available in the master branch of the repository as tag ERSEM-15.06. The GOTM version used in the simulations of this work is also taged as "ERSEM-15.06" on the ERSEM enabled fork of the development version of GOTM which can be downloaded from the same repository server. A quick start guide and user's reference manual are also provided along with the code.

10 Conclusions

In this paper we have provided a full mathematical description of an updated version of ERSEM, one of the most established marine ecosystem models currently in use in the scientific community and in operational systems. Case studies ranging from a mesocosm type zero-dimensional experiment through three one-dimensional water column implementations to a brief three-dimensional full-scale example have illustrated the model dynamics in varying environments.

Qualitative and quantitative validation with in situ data for the basic ecosystem state variables chlorophyll *a* and the macronutrients has demonstrated the capability of the model to represent ecosystems ranging from oligotrophic open oceans to eutrophic coastal conditions. An integral validation of each single component would exceed the

GMDD
8, 7063–7187, 2015

scope of this paper, the main purpose of which is the detailed description of the model ingredients as a reference for scientists, developers and users. Nevertheless, examples of component validations have been published previously and are available in literature (Artioli et al., 2012; Allen and Somerfield, 2009; Allen et al., 2007; de Mora et al., 2013). In addition the testing framework supplied within the model distribution allows for targeted analysis and validation of individual parts of the model down to the level of single equations directly without rewriting or extracting the model code. We have demonstrated this capability here on the example of the PI-curve for phytoplankton growth.

The ERSEM 15.06 model is the only model currently available that provides the structure for simulating in one coherent system the biogeochemical cycles of carbon, the major macronutrients and iron, the carbonate system and calcification, the microbial food-web and the benthic biogeochemistry.

While the range of processes included in the model brings the advantage of suitability for a whole range of applications as different as process studies, regional or global budgets of different chemical elements, habitat maps or risk assessment of environmental hazard, it also points to one of the major drawbacks of the model, i.e. a comparatively heavy structure and high number of parameters, that render it difficult to access for new users and hard to calibrate and parametrise. These problems are being addressed in a fully modular version of the model with streamlined process descriptions that is currently under development. It will allow for an arbitrary number of functional groups and easy replacment of individual sub-models, which can be tuned to the specific application at run-time. These developments will be made available with the next release of the model.

The Supplement related to this article is available online at doi:10.5194/gmdd-8-7063-2015-supplement.

GMDD
8, 7063–7187, 2015

Acknowledgements. The contributions of M. Butenschön, J. Clark, J. N. Aldridge, J. I. Allen, Y. Artioli, J. Blackford, G. Lessin, S. van Leeuwen, J. van der Molen, L. Polimene, S. Sailley and N. Stephens were part-funded by the UK Shelf Seas Biogeochemistry programme (contract no. NE/K001876/1) of the National Environmental Research Council (NERC) and the Deparment for Environment Food and Rural Affairs (DEFRA).

M. Butenschön, J. Clark, J. I. Allen, Y. Artioli, J. Bruggeman, P. Cazenave, S. Ciavatta, S. Kay, G. Lessin, L. de Mora, S. Sailley, N. Stephens and R. Torres were supported by the NERC National Capability in Modelling programme at the Plymouth Marine Laboratory. J. N. Aldridge, S. van Leeuwen and J. van der Molen were also supported through matched funding by DEFRA under contract C6164. J. Blackford and Y. Artioli were part-funded by the Regional Ocean Modelling project (contract no. NE/H017372/1) of the NERC UK Ocean Acidification research programme (UKOA). L. de Mora, M. Butenschön and J. I. Allen were part-funded by the Integrated Global Biogeochemical Modelling Network to support UK Earth System Research (i-MarNet, contract no. NE/K001345/1) project. M. Butenschön and L. Polimene were part-funded by the EU-FP7 MyOcean project (Grant Agreement 283367). J. I. Allen and S. Ciavatta were additionally supported by the UK – National Centre of Earth Observations (NCEO) of NERC.

We gratefully acknowledge the work of the developement team of the original ERSEM versions I and II under the lead of J.W. Baretta providing the baseline versions this model has emerged from over the last two decades.

The SmartBuoy observations at the Oyster Grounds were collected as part of the Marine Ecosystem Connections (MECS) programme led by Cefas and funded by the Department for Environment, Food and Rural affairs (Defra) through contract E3205, see Biogeochemistry 113, Issue 1, 2013 for key publications from MECS. In-situ observation at the L4 site were obtained from the Western English Observatory http://www.westernchannelobservatory.org.uk/). The data of the Bermuda Time Series Site was collected by the Bermuda Institute of Ocean Science Bermuda Time Series Study). Validation data for the North-East Atlantic was retrieved from the Dataset on Ocean Hydrography dsitributed by the International Council for the Exploration of the Sea (ICES).

GMDD
8, 7063–7187, 2015

References

Allen, J., Somerfield, P., and Gilbert, F.: Quantifying uncertainty in high-resolution coupled hydrodynamic-ecosystem models, in: Contributions from Advances in Marine Ecosystem Modelling Research, 27–29 June, 2005, Plymouth, UK AMEMR, 64, 3–14, available at: http://www.sciencedirect.com/science/article/pii/S0924796306001035 (last access: 14 August 2015), 2007. 7066, 7159

Allen, J. I.: Simulating the spring phytoplankton bloom in the Humber Plume (UK) with a variable phytoplankton carbon: chlorophyll-a model, in: Elsevier Oceanography Series, edited by: Fiemming, N., Vallerga, S., Pinardi, N., Behrens, H., Manzella, G., Prandle, D., and Stei, J., vol. 66 of Opertional Oceanography Implementation at the European and Regional Scales Proceedings of the second international Conference on EuroGOOS, 11–13 March 1999, Rome, Italy, 497–504, Elsevier, Amsterdam, available at: http://www.sciencedirect.com/science/article/pii/S0422989402800563 (last access: 13 August 2015), 2002. 7085

Allen, J. I. and Somerfield, P. J.: A multivariate approach to model skill assessment, J. Marine Syst., 76, 83–94, doi:10.1016/j.jmarsys.2008.05.009, 2009. 7066, 7159

Allen, J. I., Blackford, J. C., Holt, J., Proctor, R., Ashworth, M., and Siddorn, J.: A highly spatially resolved ecosystem model for the North West European Continental Shelf, Sarsia, 86, 423–440, 2001. 7065

Artioli, Y., Blackford, J. C., Butenschön, M., Holt, J. T., Wakelin, S. L., Thomas, H., Borges, A. V., and Allen, J. I.: The carbonate system in the North Sea: sensitivity and model validation, J. Marine Syst., 102–104, 1–13, doi:10.1016/j.jmarsys.2012.04.006, 2012. 7065, 7073, 7105, 7138, 7154, 7159

Artioli, Y., Blackford, J. C., Nondal, G., Bellerby, R. G. J., Wakelin, S. L., Holt, J.T., Butenschön, M., and Allen, J. I.: Heterogeneity of impacts of high CO_2 on the North Western European Shelf, Biogeosciences Discuss., 10, 9389–9413, doi:10.5194/bgd-10-9389-2013, 2013. 7066

Artioli, Y., Blackford, J. C., Nondal, G., Bellerby, R. G. J., Wakelin, S. L., Holt, J. T., Butenschön, M., and Allen, J. I.: Heterogeneity of impacts of high CO_2 on the North Western European Shelf, Biogeosciences, 11, 601–612, doi:10.5194/bg-11-601-2014, 2014. 7079

Aumont, O., Maier-Reimer, E., Blain, S., and Monfray, P.: An ecosystem model of the global ocean including Fe, Si, P colimitations, Global Biogeochem. Cy., 17, 1–23, doi:10.1029/2001GB001745, 2003. 7064, 7103

GMDD
8, 7063–7187, 2015

Barange, M., Merino, G., Blanchard, J. L., Scholtens, J., Harle, J., Allison, E. H., Allen, J. I., Holt, J., and Jennings, S.: Impacts of climate change on marine ecosystem production in societies dependent on fisheries, Nature Climate Change, 4, 211–216, doi:10.1038/nclimate2119, 2014. 7064, 7065, 7066

Baretta, J., Ruardij, P., Billings, W. D., Golley, F., Lange, O. L., Olson, J. S., and Remmert, H. (Eds.): Tidal Flat Estuaries, vol. 71 of Ecological Studies, Springer Berlin Heidelberg, Berlin, Heidelberg, Germany, available at: http://link.springer.com/10.1007/978-3-642-73753-4 (last access: 14 August 2015), 1988. 7065

Baretta, J. W.: Preface, J. Sea Res., 38, 169–171, doi:10.1016/S1385-1101(97)00054-3, 1997. 7065, 7066

Baretta, J. W., Ebenhöh, W., and Ruardij, P.: The European regional seas ecosystem model, a complex marine ecosystem model, Neth. J. Sea Res., 33, 233–246, doi:10.1016/0077-7579(95)90047-0, 1995. 7065, 7067

Baretta-Bekker, H., Bot, P., Prins, T., and Zevenboom, W.: Report on the second application of the OSPAR Comprehensive Procedure to the Dutch marine waters, Tech. rep., OSPAR Comission, London, 2008. 7150

Baretta-Bekker, J. G.: Note of the editor, Neth. J. Sea Res., 33, 230–231, doi:10.1016/0077-7579(95)90046-2, 1995. 7066

Baretta-Bekker, J. G., Baretta, J. W., and Rasmussen, E. K.: The microbial food web in the European Regional Seas Ecosystem Model, Neth. J. Sea Res., 33, 363–379, 1995. 7080

Baretta-Bekker, J. G., Baretta, J. W., and Ebenhöh, W.: Microbial dynamics in the marine ecosystem model ERSEM II with decoupled carbon assimilation and nutrient uptake, J. Sea Res., 38, 195–211, doi:10.1016/S1385-1101(97)00052-X, 1997. 7085, 7148

Bellerby, R. G. J., Olsen, A., Furevik, T., and Anderson, L. G.: Response of the surface ocean CO_2 system in the Nordic Seas and northern North Atlantic to climate change, in: The Nordic Seas: An Integrated Perspective, edited by: Drange, H., Dokken, T., Furevik, T., Gerdes, R., and Berger, W., 189–197, American Geophysical Union, Washington, DC, USA, doi:10.1029/158GM13, 2005. 7107

Blackford, J., Artioli, Y., Kelly-Gerreyn, B., Martin, A., Tyrrell, T., and Somavilla, R.: Sub-model acidification-sensitive calcification rate, including user guide, Project Report, Plymouth Marine Laboratory, Plymouth, UK, D2.2, EC FP7 MEECE – 212085, 2010. 7145

Blackford, J. C.: An analysis of benthic biological dynamics in a North Sea ecosystem model, J. Sea Res., 38, 213–230, doi:10.1016/S1385-1101(97)00044-0, 1997. 7111

GMDD
8, 7063–7187, 2015

Blackford, J. C. and Burkill, P. H.: Planktonic community structure and carbon cycling in the Arabian Sea as a result of monsoonal forcing: the application of a generic model, J. Marine Syst., 36, 239–267, doi:10.1016/S0924-7963(02)00182-3, 2002. 7065, 7105

Blackford, J. C. and Gilbert, F. J.: pH variability and CO(2) induced acidification in the North Sea, Symposium on Advances in Marine Ecosystem Modelling Research, Plymouth, England, 27–29 June 2005, J. Marine Syst., 64, 229–241, doi:10.1016/j.jmarsys.2006.03.016, 2007. 7066, 7105

Blackford, J. C., Allen, J. I., and Gilbert, F. J.: Ecosystem dynamics at six contrasting sites: a generic modelling study, J. Marine Syst., 52, 191–215, 2004. 7065, 7066, 7074, 7076, 7085, 7108, 7138, 7148

Bopp, L., Resplandy, L., Orr, J. C., Doney, S. C., Dunne, J. P., Gehlen, M., Halloran, P., Heinze, C., Ilyina, T., Séférian, R., Tjiputra, J., and Vichi, M.: Multiple stressors of ocean ecosystems in the 21st century: projections with CMIP5 models, Biogeosciences, 10, 6225–6245, doi:10.5194/bg-10-6225-2013, 2013. 7064

Borges, A. V. and Frankignoulle, M.: Daily and seasonal variations of the partial pressure of CO_2 in surface seawater along Belgian and southern Dutch coastal areas, J. Marine Syst., 19, 251–266, doi:10.1016/S0924-7963(98)00093-1, 1999. 7107

Broekhuizen, N., Heath, M. R., Hay, S. J., and Gurney, W. S. C.: Modelling the dynamics of the North Sea's Mesozooplankton, Neth. J. Sea Res., 33, 381–406, doi:10.1016/0077-7579(95)90054-3, 1995. 7080

Burchard, H., Bolding, K., Kühn, K., Meister, A., Neumann, T., and Umlauf, L.: Description of a flexible and extendable physical-biogeochemical model system for the water column, J. Marine Syst., 61, 180–211, 2006. 7147, 7149

Butenschön, M., Zavatarelli, M., and Vichi, M.: Sensitivity of a marine coupled physical biogeochemical model to time resolution, integration scheme and time splitting method, Ocean Model., 52–53, 36–53, doi:10.1016/j.ocemod.2012.04.008, 2012. 7069

Chisholm, S.: Phytoplankton size, in: Primary Productivity and Biogeochemical Cycles in the Sea, edited by: Falkowski, P. and Woodhead, A., 213–237, Plenum Press, New York, 1992. 7157

Chust, G., Allen, J. I., Bopp, L., Schrum, C., Holt, J., Tsiaras, K., Zavatarelli, M., Chifflet, M., Cannaby, H., Dadou, I., Daewel, U., Wakelin, S. L., Machu, E., Pushpadas, D., Butenschon, M., Artioli, Y., Petihakis, G., Smith, C., Garaçon, V., Goubanova, K., Le Vu, B., Fach, B. A., Salihoglu, B., Clementi, E., and Irigoien, X.: Biomass changes and trophic

GMDD
8, 7063–7187, 2015

amplification of plankton in a warmer ocean, Glob. Change Biol., 20, 2124–2139, doi:10.1111/gcb.12562, 2014. 7064

Daszykowski, M., Kaczmarek, K., Heyden, Y. V., and Walczak, B.: Robust statistics in data analysis – a review: basic concepts, Chemometr. Intell. Lab., 85, 203–219, doi:10.1016/j.chemolab.2006.06.016, 2007. 7150

de Mora, L., Butenschön, M., and Allen, J. I.: How should sparse marine in situ measurements be compared to a continuous model: an example, Geosci. Model Dev., 6, 533–548, doi:10.5194/gmd-6-533-2013, 2013. 7066, 7159

Dee, D. P., Uppala, S. M., Simmons, A. J., Berrisford, P., Poli, P., Kobayashi, S., Andrae, U., Balmaseda, M. A., Balsamo, G., Bauer, P., Bechtold, P., Beljaars, A. C. M., van de Berg, L., Bidlot, J., Bormann, N., Delsol, C., Dragani, R., Fuentes, M., Geer, A. J., Haimberger, L., Healy, S. B., Hersbach, H., Hólm, E. V., Isaksen, L., Kållberg, P., Köhler, M., Matricardi, M., McNally, A. P., Monge-Sanz, B. M., Morcrette, J.-J., Park, B.-K., Peubey, C., de Rosnay, P., Tavolato, C., Thépaut, J.-N., and Vitart, F.: The ERA-Interim reanalysis: configuration and performance of the data assimilation system, Q. J. Roy. Meteor. Soc., 137, 553–597, doi:10.1002/qj.828, 2011. 7150

Dickson, A., Sabine, C., and Christian, G.: Guide to Best Practices for Ocean CO_2 Measurements, PICES Special Publication 3, PICES, Sidney, British Columbia, available at: http://cdiac.ornl.gov/ftp/oceans/Handbook_2007/Guide_all_in_one.pdf (last access: 14 August 2015), 2007. 7105

Dickson, A. G.: Thermodynamics of the dissociation of boric acid in synthetic seawater from 273.15 to 318.15 K, Deep-Sea Res., 37, 755–766, doi:10.1016/0198-0149(90)90004-F, 1990. 7106

Doney, S. C., Ruckelshaus, M., Emmett Duffy, J., Barry, J. P., Chan, F., English, C. A., Galindo, H. M., Grebmeier, J. M., Hollowed, A. B., Knowlton, N., Polovina, J., Rabalais, N. N., Sydeman, W. J., and Talley, L. D.: Climate change impacts on marine ecosystems, Annual Review of Marine Science, 4, 11–37, doi:10.1146/annurev-marine-041911-111611, 2012. 7064

Ebenhöh, W., Kohlmeier, C., and Radford, P. J.: The benthic biological submodel in the European regional seas ecosystem model, Neth. J. Sea Res., 33, 423–452, doi:10.1016/0077-7579(95)90056-X, 1995. 7111

GMDD
8, 7063–7187, 2015

Edwards, K. P., Barciela, R., and Butenschön, M.: Validation of the NEMO-ERSEM operational ecosystem model for the North West European Continental Shelf, Ocean Sci., 8, 983–1000, doi:10.5194/os-8-983-2012, 2012. 7066, 7138

Fasham, M. J. R., Ducklow, H. W., and McKelvie, S. M.: A nitrogen-based model of plankton dynamics in the oceanic mixed layer, J. Mar. Res., 48, 591–639, 1990. 7064

Finkel, Z. V., Beardall, J., Flynn, K. J., Quigg, A., Rees, T. A. V., and Raven, J. A.: Phytoplankton in a changing world: cell size and elemental stoichiometry, J. Plankton Res., 32, 119–137, doi:10.1093/plankt/fbp098, 2010. 7157

Flynn, K. J.: Ecological modelling in a sea of variable stoichiometry: dysfunctionality and the legacy of Redfield and Monod, Prog. Oceanogr., 84, 52–65, doi:10.1016/j.pocean.2009.09.006, 2010. 7064

Follows, M. J., Dutkiewicz, S., Grant, S., and Chisholm, S. W.: Emergent biogeography of microbial communities in a model ocean, Science, 315, 1843–1846, doi:10.1126/science.1138544, 2007. 7064

Gehlen, M., Gangstø, R., Schneider, B., Bopp, L., Aumont, O., and Ethe, C.: The fate of pelagic $CaCO_3$ production in a high CO_2 ocean: a model study, Biogeosciences, 4, 505–519, doi:10.5194/bg-4-505-2007, 2007. 7145

Geider, R. J., MacIntyre, H. L., and Kana, T. M.: A dynamic model of phytoplankton growth and acclimation: responses of the balanced growth rate and chlorophyll *a*:carbon ratio to light, nutrient limitation and temperature, Mar. Ecol-Prog. Ser., 148, 187–200, 1997. 7064, 7074, 7076, 7155, 7156, 7186

Gentleman, W., Leising, A., Frost, B., Strom, S., and Murray, J.: Functional responses for zooplankton feeding on multiple resources: a review of assumptions and biological dynamics, Deep-Sea Res. Pt. II, 50, 2847–2875, doi:10.1016/j.dsr2.2003.07.001, 2003. 7080

Glibert, P. M., Icarus Allen, J., Artioli, Y., Beusen, A., Bouwman, L., Harle, J., Holmes, R., and Holt, J.: Vulnerability of coastal ecosystems to changes in harmful algal bloom distribution in response to climate change: projections based on model analysis, Glob. Change Biol., 20, 3845–3858, doi:10.1111/gcb.12662, 2014. 7064

Greenwood, N., Parker, E. R., Fernand, L., Sivyer, D. B., Weston, K., Painting, S. J., Kröger, S., Forster, R. M., Lees, H. E., Mills, D. K., and Laane, R. W. P. M.: Detection of low bottom water oxygen concentrations in the North Sea; implications for monitoring and assessment of ecosystem health, Biogeosciences, 7, 1357–1373, doi:10.5194/bg-7-1357-2010, 2010. 7151, 7181

GMDD
8, 7063–7187, 2015

Hansell, D. A.: Recalcitrant dissolved organic carbon fractions, Annual Review of Marine Science, 5, 421–445, doi:10.1146/annurev-marine-120710-100757, 2013. 7088
Harris, R.: The L4 time-series: the first 20 years, J. Plankton Res., 32, 577–583, doi:10.1093/plankt/fbq021, 2010. 7150
Hirata, T., Hardman-Mountford, N. J., Brewin, R. J. W., Aiken, J., Barlow, R., Suzuki, K., Isada, T., Howell, E., Hashioka, T., Noguchi-Aita, M., and Yamanaka, Y.: Synoptic relationships between surface Chlorophyll-*a* and diagnostic pigments specific to phytoplankton functional types, Biogeosciences, 8, 311–327, doi:10.5194/bg-8-311-2011, 2011. 7153
Holt, J., Butenschön, M., Wakelin, S. L., Artioli, Y., and Allen, J. I.: Oceanic controls on the primary production of the northwest European continental shelf: model experiments under recent past conditions and a potential future scenario, Biogeosciences, 9, 97–117, doi:10.5194/bg-9-97-2012, 2012. 7065, 7066, 7138, 7154
Holt, J. T. and James, I. D.: An s coordinate density evolving model of the northwest European continental shelf: 1. Model description and density structure, J. Geophys. Res.-Oceans, 106, 14015–14034, doi:10.1029/2000JC000304, 2001. 7147, 7154
ICES: ICES Dataset on Ocean Hydrography, The International Council for the Exploration of the SeaCopenhagen, Copenhagen, Denmark, 2009. 7154
Ingri, N., Kakolowicz, W., Sillén, L. G., and Warnqvist, B.: High-speed computers as a supplement to graphical methods V1: Haltafall, a general program for calculating the composition of equilibrium mixtures, Talanta, 14, 1261–1286, doi:10.1016/0039-9140(67)80203-0, 1967. 7106
Jiao, N., Herndl, G. J., Hansell, D. A., Benner, R., Kattner, G., Wilhelm, S. W., Kirchman, D. L., Weinbauer, M. G., Luo, T., Chen, F., and Azam, F.: Microbial production of recalcitrant dissolved organic matter: long-term carbon storage in the global ocean, Nat. Rev. Microbiol., 8, 593–599, doi:10.1038/nrmicro2386, 2010. 7088
Jiao, N., Robinson, C., Azam, F., Thomas, H., Baltar, F., Dang, H., Hardman-Mountford, N. J., Johnson, M., Kirchman, D. L., Koch, B. P., Legendre, L., Li, C., Liu, J., Luo, T., Luo, Y.-W., Mitra, A., Romanou, A., Tang, K., Wang, X., Zhang, C., and Zhang, R.: Mechanisms of microbial carbon sequestration in the ocean – future research directions, Biogeosciences, 11, 5285–5306, doi:10.5194/bg-11-5285-2014, 2014. 7088
Jolliff, J. K., Kindle, J. C., Shulman, I., Penta, B., Friedrichs, M. A. M., Helber, R., and Arnone, R. A.: Summary diagrams for coupled hydrodynamic-ecosystem model skill assessment, J. Marine Syst., 76, 64–82, doi:10.1016/j.jmarsys.2008.05.014, 2009. 7150

GMDD
8, 7063–7187, 2015

Keir, R. S.: The dissolution kinetics of biogenic calcium carbonates in seawater, Geochim. Cosmochim. Ac., 44, 241–252, doi:10.1016/0016-7037(80)90135-0, 1980. 7144
Kohlmeier, C.: Modellierung des Spiekerooger Rückseitenwatts mit einem gekoppelten Euler-Lagrange-Modell auf der Basis von ERSEM, PhD thesis, Carl von Ossietzky Universität, Oldenburg, 2004. 7111
Kwiatkowski, L., Yool, A., Allen, J. I., Anderson, T. R., Barciela, R., Buitenhuis, E. T., Butenschön, M., Enright, C., Halloran, P. R., Le Quéré, C., de Mora, L., Racault, M.-F., Sinha, B., Totterdell, I. J., and Cox, P. M.: iMarNet: an ocean biogeochemistry model intercomparison project within a common physical ocean modelling framework, Biogeosciences, 11, 7291–7304, doi:10.5194/bg-11-7291-2014, 2014. 7065
Lee, K., Tong, L. T., Millero, F. J., Sabine, C. L., Dickson, A. G., Goyet, C., Park, G.-H., Wanninkhof, R., Feely, R. A., and Key, R. M.: Global relationships of total alkalinity with salinity and temperature in surface waters of the world's oceans, Geophys. Res. Lett., 33, L19605, doi:10.1029/2006GL027207, 2006. 7107
Lee, Z., Du, K., and Arnone, R.: A model for the diffuse attenuation coefficient of downwelling irradiance, J. Geophys. Res., 110, 1–10, doi:10.1029/2004JC002275, 2005. 7108
Leeuwen, S. M. v., Molen, J. v. d., Ruardij, P., Fernand, L., and Jickells, T.: Modelling the contribution of deep chlorophyll maxima to annual primary production in the North Sea, Biogeochemistry, 113, 137–152, doi:10.1007/s10533-012-9704-5, 2012. 7065
Lenhart, H.-J., Mills, D. K., Baretta-Bekker, H., Leeuwen, S. M. v., Molen, J. v. d., Baretta, J. W., Blaas, M., Desmit, X., Kühn, W., Lacroix, G., Los, H. J., Ménesguen, A., Neves, R., Proctor, R., Ruardij, P., Skogen, M. D., Vanhoutte-Brunier, A., Villars, M. T., and Wakelin, S. L.: Predicting the consequences of nutrient reduction on the eutrophication status of the North Sea, J. Marine Syst., 81, 148–170, doi:10.1016/j.jmarsys.2009.12.014, 2010. 7064
Litchman, E., Klausmeier, C. A., Schofield, O. M., and Falkowski, P. G.: The role of functional traits and trade-offs in structuring phytoplankton communities: scaling from cellular to ecosystem level, Ecol. Lett., 10, 1170–1181, doi:10.1111/j.1461-0248.2007.01117.x, 2007. 7157
Litchman, E., Pinto, P. d. T., Klausmeier, C. A., Thomas, M. K., and Yoshiyama, K.: Linking traits to species diversity and community structure in phytoplankton, Hydrobiologia, 653, 15–28, doi:10.1007/s10750-010-0341-5, 2010. 7157
Madec, G.: NEMO Ocean Engine, Note du Pole de modélisation, Institut Pierre-Simon Laplace (IPSL), Paris, France, No 28, 2008. 7147

GMDD
8, 7063–7187, 2015

Mehrbach, C., Culberson, C. H., Hawley, J. E., and Pytkowicx, R. M.: Measurement of the apparent dissociation constants of carbonic acid in seawater at atmospheric pressure, Limnol. Oceanogr., 18, 897–907, doi:10.4319/lo.1973.18.6.0897, 1973. 7106

Millero, F. J.: Thermodynamics of the carbon dioxide system in the oceans, Geochim. Cosmochim. Ac., 59, 661–677, doi:10.1016/0016-7037(94)00354-O, 1995. 7106

Millero, F. J., Lee, K., and Roche, M.: Distribution of alkalinity in the surface waters of the major oceans, Mar. Chem., 60, 111–130, doi:10.1016/S0304-4203(97)00084-4, 1998. 7107

Moore, C. M., Mills, M. M., Arrigo, K. R., Berman-Frank, I., Bopp, L., Boyd, P. W., Galbraith, E. D., Geider, R. J., Guieu, C., Jaccard, S. L., Jickells, T. D., La Roche, J., Lenton, T. M., Mahowald, N. M., Maranon, E., Marinov, I., Moore, J. K., Nakatsuka, T., Oschlies, A., Saito, M. A., Thingstad, T. F., Tsuda, A., and Ulloa, O.: Processes and patterns of oceanic nutrient limitation, Nat. Geosci., 6, 701–710, doi:10.1038/ngeo1765, 2013. 7153, 7184

Nightingale, P. D., Malin, G., Law, C. S., Watson, A. J., Liss, P. S., Liddicoat, M. I., Boutin, J., and Upstill-Goddard, R. C.: In situ evaluation of air-sea gas exchange parameterizations using novel conservative and volatile tracers, Global Biogeochem. Cy., 14, 373–387, doi:10.1029/1999GB900091, 2000. 7138

Paasche, E.: Roles of nitrogen and phosphorus in coccolith formation in *Emiliania huxleyi* (*Prymnesiophyceae*), Eur. J. Phycol., 33, 33–42, 1998. 7145

Platt, T., Harrison, W. G., Irwin, B., Horne, E. P., and Gallegos, C. L.: Photosynthesis and photoadaptation of marine phytoplankton in the arctic, Deep-Sea Res., 29, 1159–1170, doi:10.1016/0198-0149(82)90087-5, 1982. 7075

Polimene, L., Allen, J. I., and Zavatarelli, M.: Model of interactions between dissolved organic carbon and bacteria in marine systems, Aquat. Microb. Ecol., 43, 127–138, doi:10.3354/ame043127, 2006. 7088

Polimene, L., Pinardi, N., Zavatarelli, M., Allen, J. I., Giani, M., and Vichi, M.: A numerical simulation study of dissolved organic carbon accumulation in the northern Adriatic Sea, J. Geophys. Res.-Oceans, 112, C03S20, doi:10.1029/2006JC003529, 2007. 7088

Polimene, L., Archer, S. D., Butenschön, M., and Allen, J. I.: A mechanistic explanation of the Sargasso Sea DMS "summer paradox", Biogeochemistry, 110, 243–255, doi:10.1007/s10533-011-9674-z, 2012. 7066

Polimene, L., Brunet, C., Butenschön, M., Martinez-Vicente, V., Widdicombe, C., Torres, R., and Allen, J. I.: Modelling a light-driven phytoplankton succession, J. Plankton Res., 36, 214–229, doi:10.1093/plankt/fbt086, 2014. 7066

GMDD
8, 7063–7187, 2015

Radford, P. and Joint, I.: The application of an ecosystem model to the Bristol Channel and Severn Estuary, Water Pollut. Control, 2, 244–250, 1980. 7065

Ridgwell, A., Zondervan, I., Hargreaves, J. C., Bijma, J., and Lenton, T. M.: Assessing the potential long-term increase of oceanic fossil fuel CO_2 uptake due to CO_2-calcification feedback, Biogeosciences, 4, 481–492, doi:10.5194/bg-4-481-2007, 2007. 7144

Riegman, R., Stolte, W., Noordeloos, A. A. M., and Slezak, D.: Nutrient uptake and alkaline phosphatase (ec 3 : 1 : 3 : 1) activity of *emiliania huxleyi* (*PRYMNESIOPHYCEAE*) during growth under n and p limitation in continuous cultures, J. Phycol., 36, 87–96, doi:10.1046/j.1529-8817.2000.99023.x, 2000. 7145

Ruardij, P. and Van Raaphorst, W.: Benthic nutrient regeneration in the ERSEM ecosystem model of the North Sea, Neth. J. Sea Res., 33, 453–483, doi:10.1016/0077-7579(95)90057-8, 1995. 7111

Saux Picart, S., Butenschön, M., and Shutler, J. D.: Wavelet-based spatial comparison technique for analysing and evaluating two-dimensional geophysical model fields, Geosci. Model Dev., 5, 223–230, doi:10.5194/gmd-5-223-2012, 2012. 7066

Shutler, J. D., Smyth, T. J., Saux-Picart, S., Wakelin, S. L., Hyder, P., Orekhov, P., Grant, M. G., Tilstone, G. H., and Allen, J. I.: Evaluating the ability of a hydrodynamic ecosystem model to capture inter- and intra-annual spatial characteristics of chlorophyll-a in the north east Atlantic, J. Marine Syst., 88, 169–182, doi:10.1016/j.jmarsys.2011.03.013, 2011. 7066

Smyth, T. J., Fishwick, J. R., AL-Moosawi, L., Cummings, D. G., Harris, C., Kitidis, V., Rees, A., Martinez-Vicente, V., and Woodward, E. M. S.: A broad spatio-temporal view of the Western English Channel observatory, J. Plankton Res., 32, 585–601, doi:10.1093/plankt/fbp128, 2010. 7151

Steinberg, D. K., Carlson, C. A., Bates, N. R., Johnson, R. J., Michaels, A. F., and Knap, A. H.: Overview of the US JGOFS Bermuda Atlantic Time-series Study (BATS): a decade-scale look at ocean biology and biogeochemistry, Deep-Sea Res. Pt. II, 48, 1405–1447, doi:10.1016/S0967-0645(00)00148-X, 2001. 7150, 7152

Stock, C. A., Dunne, J. P., and John, J. G.: Global-scale carbon and energy flows through the marine planktonic food web: an analysis with a coupled physical–biological model, Prog. Oceanogr., 120, 1–28, doi:10.1016/j.pocean.2013.07.001, 2014. 7064

Sukenik, A., Bennett, J., and Falkowski, P.: Light-saturated photosynthesis Limitation by electron transport or carbon fixation?, BBA-Bioenergetics, 891, 205–215, doi:10.1016/0005-2728(87)90216-7, 1987. 7156

GMDD
8, 7063–7187, 2015

Takahashi, T., Williams, R. T., and Bos, D. L.: Carbonate chemistry, Chapter 3, in: GEOSECS Pacific Expedition, Hydrographic Data 1973–1974, Vol. 3., U.S. Governemnt Priniting Office, Washington, D.C., USA, 1982. 7105

Talmy, D., Blackford, J., Hardman-Mountford, N. J., Polimene, L., Follows, M. J., and Geider, R. J.: Flexible C : N ratio enhances metabolism of large phytoplankton when resource supply is intermittent, Biogeosciences, 11, 4881–4895, doi:10.5194/bg-11-4881-2014, 2014. 7156

Timmermans, K. R., van der Wagt, B., Veldhuis, M. J. W., Maatman, A., and de Baar, H. J. W.: Physiological responses of three species of marine pico-phytoplankton to ammonium, phosphate, iron and light limitation, J. Sea Res., 53, 109–120, doi:10.1016/j.seares.2004.05.003, 2005. 7153

van der Molen, J., Smith, H. C. M., Lepper, P., Limpenny, S., and Rees, J.: Predicting the large-scale consequences of offshore wind turbine array development on a North Sea ecosystem, Cont. Shelf Res., 85, 60–72, doi:10.1016/j.csr.2014.05.018, 2014. 7064, 7065

Varela, R. A., Cruzado, A., and Gabaldón, J. E.: Modelling primary production in the North Sea using the European Regional Seas Ecosystem Model, Neth. J. Sea Res., 33, 337–361, doi:10.1016/0077-7579(95)90052-7, 1995. 7073

Veldhuis, M. J. W., Timmermans, K. R., Croot, P., and van der Wagt, B.: Picophytoplankton; a comparative study of their biochemical composition and photosynthetic properties, J. Sea Res., 53, 7–24, doi:10.1016/j.seares.2004.01.006, 2005. 7153

Vichi, M., Ruardij, P., and Baretta, J. W.: Link or sink: a modelling interpretation of the open Baltic biogeochemistry, Biogeosciences, 1, 79–100, doi:10.5194/bg-1-79-2004, 2004. 7065

Vichi, M., Pinardi, N., and Masina, S.: A generalized model of pelagic biogeochemistry for the global ocean ecosystem. Part I: Theory, J. Marine Syst., 64, 89–109, 2007. 7065, 7067, 7068, 7073, 7103

Villarino, E., Chust, G., Licandro, P., Butenschön, M., Ibaibarriaga, L., Larrañaga, A., and Irigoien, X.: Modelling the future biogeography of North Atlantic zooplankton communities in response to climate change, Mar. Ecol.-Prog. Ser., 531, 121–142, doi:10.3354/meps11299, 2015. 7066

Wakelin, S. L., Holt, J. T., Blackford, J. C., Allen, J. I., Butenschön, M., and Artioli, Y.: Modeling the carbon fluxes of the northwest European continental shelf: validation and budgets, J. Geophys. Res., 117, C05020 –, doi:10.1029/2011JC007402, 2012. 7066, 7138

GMDD
8, 7063–7187, 2015

Weiss, R. F.: The solubility of nitrogen, oxygen and argon in water and seawater, Deep-Sea Res., 17, 721–735, doi:10.1016/0011-7471(70)90037-9, 1970. 7138, 7141

Weiss, R. F.: Carbon dioxide in water and seawater: the solubility of a non-ideal gas, Mar. Chem., 2, 203–215, doi:10.1016/0304-4203(74)90015-2, 1974. 7106

Wild-Allen, K., Herzfeld, M., Thompson, P. A., Rosebrock, U., Parslow, J., and Volkman, J. K.: Applied coastal biogeochemical modelling to quantify the environmental impact of fish farm nutrients and inform managers, J. Marine Syst., 81, 134–147, doi:10.1016/j.jmarsys.2009.12.013, 2010. 7064

Yool, A., Popova, E. E., and Anderson, T. R.: MEDUSA-2.0: an intermediate complexity biogeochemical model of the marine carbon cycle for climate change and ocean acidification studies, Geosci. Model Dev., 6, 1767–1811, doi:10.5194/gmd-6-1767-2013, 2013. 7064

Zavatarelli, M. and Pinardi, N.: The Adriatic Sea modelling system: a nested approach, Ann. Geophys., 21, 345–364, doi:10.5194/angeo-21-345-2003, 2003. 7064

Zeebe, R. W. and Wolf-Gladrow, D.: CO_2 in Seawater: Equilibrium, Kinetics, Isotopes, no. 65 in Elsevier Oceanography Series, Elsevier, Amsterdam, the Netherlands, 2001. 7105

GMDD
8, 7063–7187, 2015

Table 1. Pelagic functional types and their components, organic part (squared brackets indicate option states) – chemical components: $\mathbb{C}$ carbon, $\mathbb{N}$ nitrogen, $\mathbb{P}$ phosphorus, $\mathbb{F}$ iron, $\mathbb{S}$ silicate, $\mathcal{C}$ chlorophyll *a*.

Symbol	Code	Description
pico $P_{\mathbb{C},\mathbb{N},\mathbb{P}[,\mathbb{F}],\mathcal{C}}$	`P3c,n,p[,f],Chl3`	Picophytoplankton (< 2 µm)
nano $P_{\mathbb{C},\mathbb{N},\mathbb{P}[,\mathbb{F}],\mathcal{C}}$	`P2c,n,p[,f],Chl2`	Nanophytoplankon (2–20 µm)
micro $P_{\mathbb{C},\mathbb{N},\mathbb{P}[,\mathbb{F}],\mathcal{C}}$	`P4c,n,p[,f],Chl4`	Microphytoplankton (> 20 µm)
dia $P_{\mathbb{C},\mathbb{N},\mathbb{P}[,\mathbb{F}],\mathbb{S},\mathcal{C}}$	`P1c,n,P[,f],Chl1`	Diatoms
HET $Z_{\mathbb{C},\mathbb{N},\mathbb{P}}$	`Z6c,n,p`	Heterotrophic Flagellates
MICRO $Z_{\mathbb{C},\mathbb{N},\mathbb{P}}$	`Z5c,n,p`	Microzooplankton
MESO $Z_{\mathbb{C}}$	`Z4c`	Mesozooplankton
$B_{\mathbb{C},\mathbb{N},\mathbb{P}}$	`B1c,n,p`	Heterotrophic Bacteria
lab $R_{\mathbb{C},\mathbb{N},\mathbb{P}}$	`R1c,n,p`	Labile dissolved organic matter
slab $R_{\mathbb{C}}$	`R2c`	Semi-labile organic matter
srefr $R_{\mathbb{C}}$	`R3c`	Semi-refractory organic matter
small $R_{\mathbb{C},\mathbb{N},\mathbb{P}[,\mathbb{F}]}$	`R4c,n,p[,f]`	Small particulate organic matter
med $R_{\mathbb{C},\mathbb{N},\mathbb{P}[,\mathbb{F}],\mathbb{S}}$	`R6c,n,p[,f],s`	Medium size particulate organic matter
large $R_{\mathbb{C},\mathbb{N},\mathbb{P},\mathbb{S}}$	`R8c,n,p,s`	Large particulate organic matter

GMDD
8, 7063–7187, 2015
ERSEM 15.06
M. Butenschön et al.

Table 2. Pelagic functional types and their components, inorganic part (squared brackets indicate optional states) – chemical components: $\mathbb{C}$ carbon, $\mathbb{N}$ nitrogen, $\mathbb{P}$ phosphorus, $\mathbb{F}$ iron, $\mathbb{S}$ silicate.

Symbol	Code	Description
$\left[{}^{\text{calc}}_{}L_{\mathbb{C}}\right]$	`[L2c]`	Calcite
$O_{\mathbb{O}}$	`O2o`	Dissolved oxygen
$O_{\mathbb{C}}$	`O3c`	Disolved inorganic carbon (DIC)
$N_{\mathbb{P}}$	`N1p`	Phosphate
$N^{\text{ox}}_{\mathbb{N}}$	`N3n`	Oxidised nitrogen
$N^{\text{amm}}_{\mathbb{N}}$	`N4n`	Ammonium
$N_{\mathbb{S}}$	`N5s`	Silicate
$[N_{\mathbb{F}}]$	`[N7f]`	Dissolved iron
$[A_{\text{bio}}]$	`[bioAlk]`	Bioalkalinity

GMDD
8, 7063–7187, 2015
ERSEM 15.06
M. Butenschön et al.

Table 3. Pelagic predators and their preys.

Predator type	Prey types
Heterotrophic flagellates ($\overset{HET}{Z}$)	Bacteria, picophytoplankton, nanophytoplankton, heterotrophic flagellates (B, $\overset{pico}{P}$, $\overset{nano}{P}$, $\overset{HET}{Z}$)
Microzooplankton ($\overset{MICRO}{Z}$)	Bacteria, picophytoplankton, nanophytoplankton, microphytoplankton, diatoms, heterotrophic flagellates, microzooplankton (B, $\overset{pico}{P}$, $\overset{nano}{P}$, $\overset{micro}{P}$, $\overset{dia}{P}$, $\overset{HET}{Z}$, $\overset{MICRO}{Z}$)
Mesozooplankton ($\overset{MESO}{Z}$)	Picophytoplankton, nanophytoplankton, microphytoplankton, diatoms, heterotrophic flagellates, microzooplankton, mesozooplankton, medium size particulate matter ($\overset{pico}{P}$, $\overset{nano}{P}$, $\overset{micro}{P}$, $\overset{dia}{P}$, $\overset{HET}{Z}$, $\overset{MICRO}{Z}$, $\overset{MESO}{Z}$, $\overset{med}{R}$)

GMDD
8, 7063–7187, 2015
ERSEM 15.06
M. Butenschön et al.

Table 4. Particualte organic matter and its origin.

POM type	Originating from
Small particulate organic matter ($\overset{small}{R}$)	Nano- and picophytoplankton ($\overset{nano}{P}$, $\overset{pico}{P}$), heterotrophic flagellates ($\overset{HET}{Z}$)
Medium size particulate organic matter ($\overset{med}{R}$)	Microphytoplankton and diatoms ($\overset{micro}{P}$, $\overset{dia}{P}$), microzooplankton ($\overset{MICRO}{Z}$)
Large particulate organic matter ($\overset{large}{R}$)	Mesozooplankton ($\overset{MESO}{Z}$)

GMDD
8, 7063–7187, 2015

Table 5. Benthic functional types and their components, organic part (squared brackets indicate option states) – chemical components: ℂ carbon, ℕ nitrogen, ℙ phosphorus, 𝔽 iron, 𝕊 silicate.

Symbol	Code	Description
$Y_{\mathbb{C}}^{\mathrm{DEPO}}$	`Y2c`	Deposit feeders
$Y_{\mathbb{C}}^{\mathrm{SUSP}}$	`Y3c`	Suspension feeders
$Y_{\mathbb{C}}^{\mathrm{MEIO}}$	`Y4c`	Meiobenthos
$H_{\mathbb{C}}^{\mathrm{aer}}$	`H1c`	Aerobic bacteria
$H_{\mathbb{C}}^{\mathrm{anaer}}$	`H2c`	Anaerobic bacteria
$Q_{\mathbb{C}}^{\mathrm{dis}}$	`Q1c`	Dissolved organic matter
$Q_{\mathbb{C},\mathbb{N},\mathbb{P}[,\mathbb{F}]}^{\mathrm{slow}}$	`Q6c,n,p[,f],s`	Slowly degradable organic matter
$Q_{\mathbb{C},\mathbb{N},\mathbb{P},\mathbb{S}}^{\mathrm{refr}}$	`Q7c,n,p,s`	Refractory organic matter
$Q_{\mathbb{C},\mathbb{N},\mathbb{P}}^{\mathrm{bur}}$	`Q17c,n,p`	Buried organic matter

GMDD
8, 7063–7187, 2015

Table 6. Benthic functional types and their components, inorgnic part and states of vertical distribution (squared brackets indicate option states) - chemical components: ℂ carbon, ℕ nitrogen, ℙ phosphorus, 𝕊 silicate.

Symbol	Code	Description
$\left[{}^{\text{bcalc}}C_{\mathbb{C}}\right]$	[bL2c]	Calcite
$G_{\mathbb{O}}$	G2o	Dissolved oxygen
$G_{\mathbb{C}}$	G3c	Disolved inorganic carbon (DIC)
$G_{\mathbb{N}}$	G4n	Dinitrogen
$K_{\mathbb{P}}$	K1p	Phosphate
$K^{\text{ox}}_{\mathbb{N}}$	K3n	Oxidised nitrogen
$K^{\text{amm}}_{\mathbb{N}}$	K4n	Ammonium
$K_{\mathbb{S}}$	K5s	Silicate
D^{oxy}	D1m	Depth of oxygen horizon
D^{denit}	D2m	Depth of oxidised nitrogen horizon
$D^{\text{refr}_{\mathbb{C}}}$	D3m	Average penetration depth of refractory carbon
$D^{\text{refr}_{\mathbb{N}}}$	D4m	Average penetration depth of refractory nitrogen
$D^{\text{refr}_{\mathbb{P}}}$	D5m	Average penetration depth of refractory phosphorus
$D^{\text{slow}_{\mathbb{C}}}$	D6m	Average penetration depth of slowly degradable carbon
$D^{\text{slow}_{\mathbb{N}}}$	D7m	Average penetration depth of slowly degradable nitrogen
$D^{\text{slow}_{\mathbb{P}}}$	D8m	Average penetration depth of slowly degradable phosphorus
$D^{\text{slow}_{\mathbb{S}}}$	D9m	Average penetration depth of slowly degradable silicate

GMDD
8, 7063–7187, 2015
ERSEM 15.06
M. Butenschön et al.

Table 7. Benthic predators and their preys.

Predator type	Prey types
Deposit feeders ($\overset{\text{DEPO}}{Y}$)	Aerobic and anaerobic bacteria, meiobenthos, available slowly degradable organic matter ($\overset{\text{aer}}{H}$, $\overset{\text{anaer}}{H}$, $\overset{\text{MEIO}}{Y}$, $\overset{\text{slow}}{Q}\Big\vert_{\overset{\text{SUSP}}{d_Z}}^{\overset{\text{DEPO}}{d_Z}}$)
Suspension feeders ($\overset{\text{SUSP}}{Y}$)	Aerobic bacteria, picophytoplankton, nanophytoplankton, diatoms, medium size particulate matter and available slowly degradable organic matter ($\overset{\text{aer}}{H}$, $d_{\text{SUSP}}\overset{\text{pico}}{P}$, $d_{\text{SUSP}}\overset{\text{nano}}{P}$, $d_{\text{SUSP}}\overset{\text{dia}}{P}$, $d_{\text{SUSP}}\overset{\text{med}}{R}$, $\overset{\text{slow}}{Q}\Big\vert_{0}^{\overset{\text{SUSP}}{d_Z}}$)
Meiobenthos ($\overset{\text{MEIO}}{Y}$)	Aerobic bacteria, anaerobic bacteria, meiobenthos, available slowly degradable organic matter ($\overset{\text{aer}}{H}$, $\overset{\text{anaer}}{H}$, $\overset{\text{MEIO}}{Y}$, $\overset{\text{slow}}{Q}\Big\vert_{0}^{\overset{\text{MEIO}}{d_Z}}$)

GMDD
8, 7063–7187, 2015
ERSEM 15.06
M. Butenschön et al.

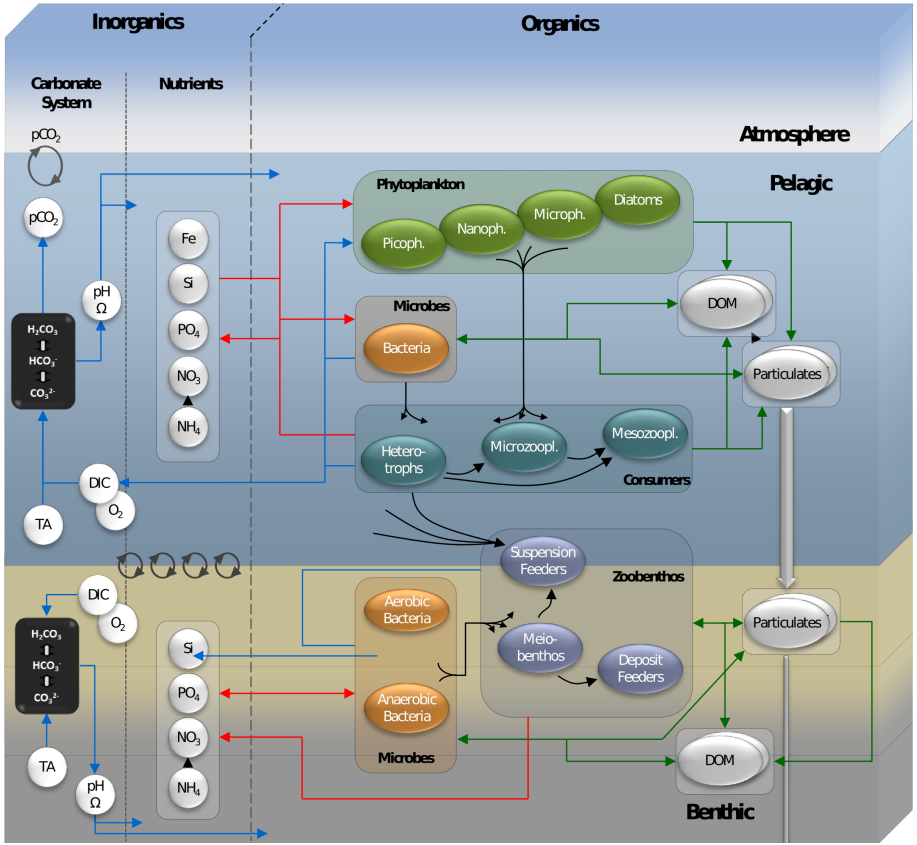

Figure 1. ERSEM schematic. Blue connectors represent inorganic carbon, red represents nutrient fluxes, black represents predator–prey interactions and green represents the non-living organics.

GMDD
8, 7063–7187, 2015
ERSEM 15.06
M. Butenschön et al.

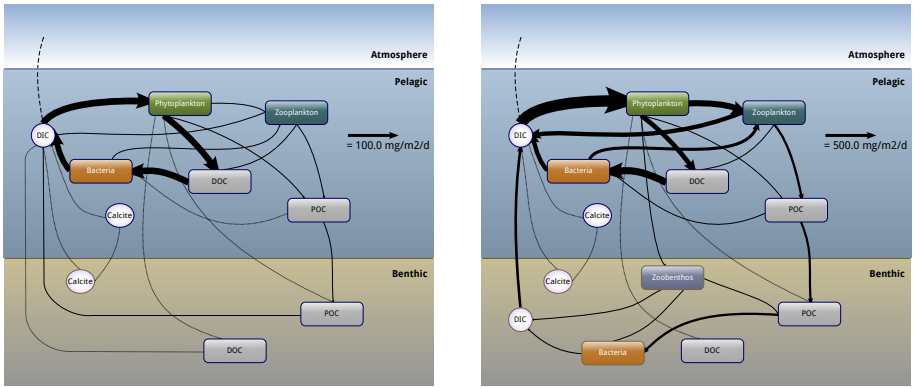

Figure 2. Carbon fluxes in ERSEM under oligotrophic (left) and eutrophic (right) conditions. (Note the different scales of the arrow sizes.)

GMDD
8, 7063–7187, 2015

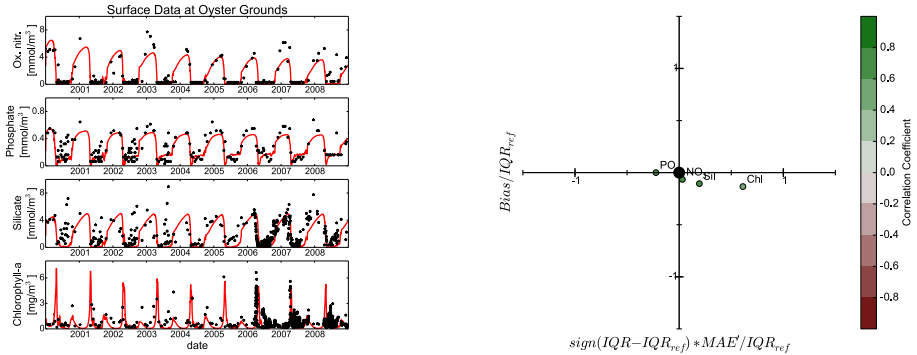

Figure 3. Simulation results vs. in situ data at the Oyster Grounds – left: model time series (red lines) vs. in situ measurements (black dots) for oxidised nitrogen, phosphate, silicate and chlorophyll *a* (top to bottom); right: target diagram with bias (abscissa), MAE' (ordinate) and Spearman correlation (colour code) for oxidised nitrogen (NO3), phosphate (PO4), silicate (Sil) and chlorophyll *a* (Chl). The observations consist of ship-based data collected by Rijkswaterstaat as part of the Dutch national monitoring programme MWTL (see publicwiki.deltares.nl/display/OET/Dataset+documentation+MWTL) and SmartBuoy data collected by Cefas in collaboration with Rijkswaterstaat (Greenwood et al., 2010; http://www.cefas.co.uk/publications-data/smartbuoys).

GMDD
8, 7063–7187, 2015
ERSEM 15.06
M. Butenschön et al.

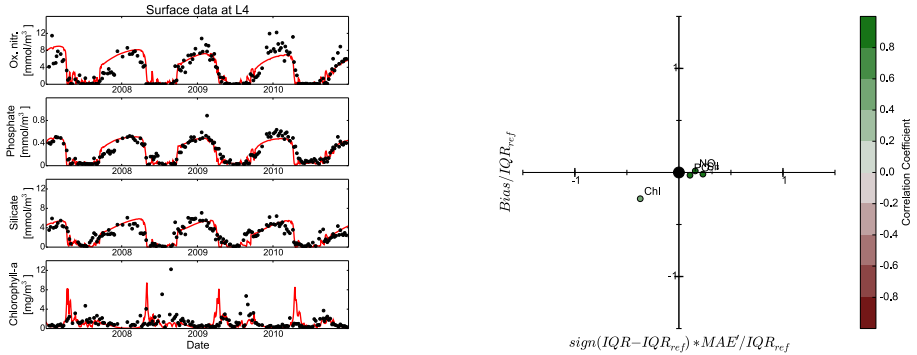

Figure 4. Simulation results vs. in situ data at the L4 site – left: model time series (red lines) vs. in situ measurements (black dots) for oxidised nitrogen, phosphate, silicate and chlorophyll *a* (top to bottom); right: target diagram with bias (abscissa), MAE' (ordinate) and Spearman correlation (colour code) for oxidised nitrogen (NO3), phosphate (PO4), silicate (Sil) and chlorophyll *a* (Chl).

GMDD
8, 7063–7187, 2015
ERSEM 15.06
M. Butenschön et al.

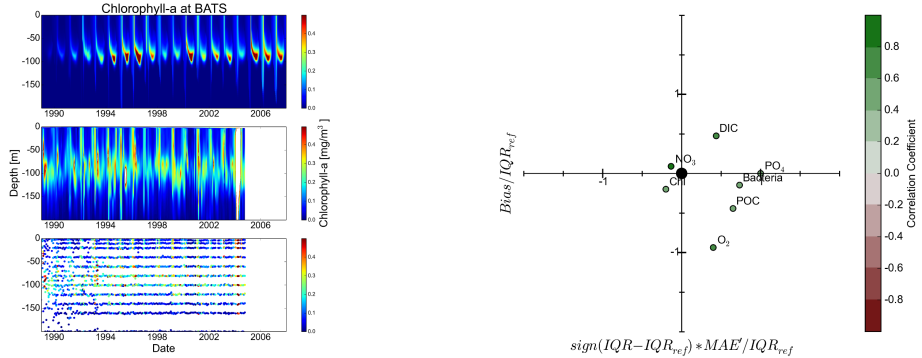

Figure 5. Simulation results vs. in situ data at BATS – left: chlorophyll *a* concentrations (Model, interpolated in situ data, scattered in situ data – top to bottom); right: target diagram with bias (abscissa), MAE' (ordinate) and spearman correlation (colour code) for oxidised nitrogen (NO3), phosphate (PO4), silicate (Sil), dissolved inorganic carbon (DIC), dissolved oxygen (O_2), chlorophyll *a* (Chl) and particulate organic carbon (POC).

GMDD
8, 7063–7187, 2015
ERSEM 15.06
M. Butenschön et al.

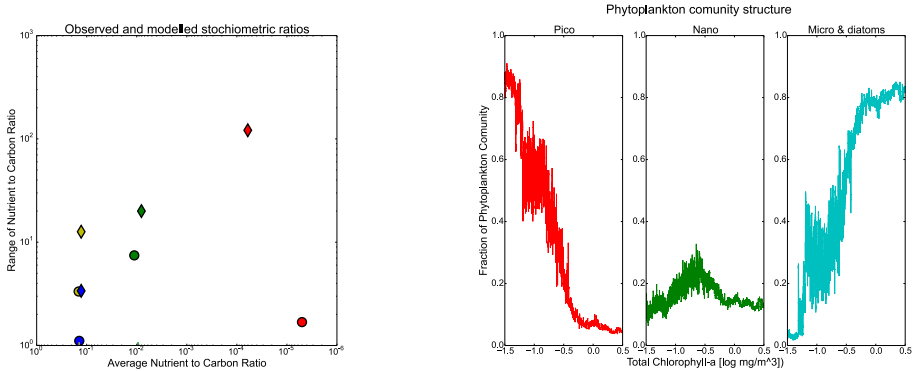

Figure 6. Emergent properties of the simulations across the three 1-D sites. Left: range (ordinate) and mean (abscissa) of internal stoichiometric ratios of phytoplankton – nitrogen (yellow), silicate (blue), phosphorus (green) and iron (red). Data (diamonds, Moore et al., 2013), assembled 1-D model simulations (circles); right: community fraction of total chlorophyll *a* from assembled 1-D model simulations. Picophytoplankton (red), nanophytoplankton (green) and microphytoplankton and diatoms (cyan).

GMDD
8, 7063–7187, 2015
ERSEM 15.06
M. Butenschön et al.

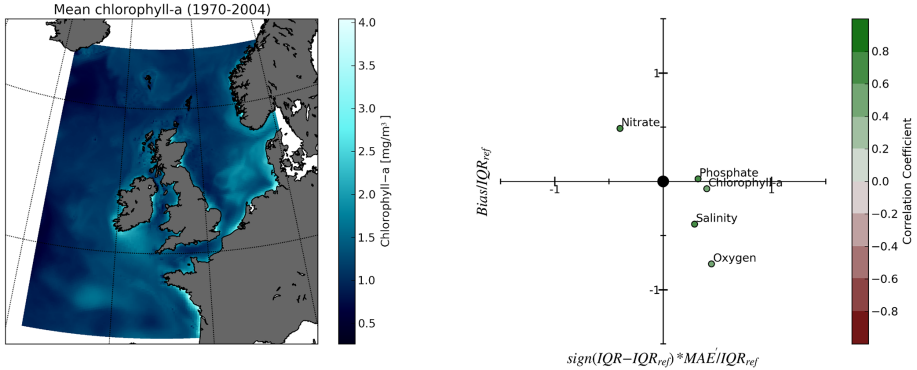

Figure 7. The ERSEM model in a simulation for the North West European Shelf Seas – left: optical-depth-averaged chlorophyll *a*; right: hindcast simulation vs. in situ data.

GMDD
8, 7063–7187, 2015

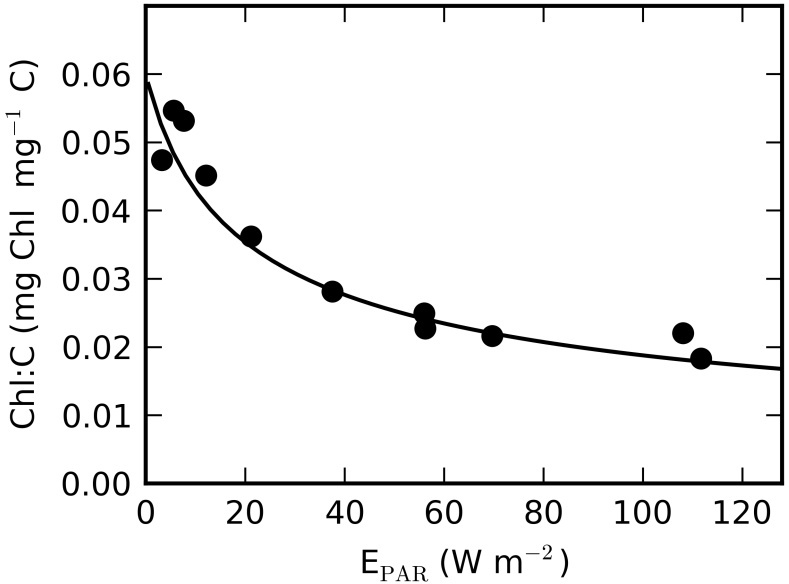

Figure 8. Chlorophyll *a* to carbon ratio of diatoms as a function of PAR under the condition of balanced growth (Eq. 263). The solid line represents output from the model. Black circles show data for nutrient-replete cultures of Thalassiosira pseudonana, digitally extracted from Geider et al. (1997) using Plot Digitizer Version 2.6.6 (see http://plotdigitizer.sourceforge.net).

GMDD
8, 7063–7187, 2015

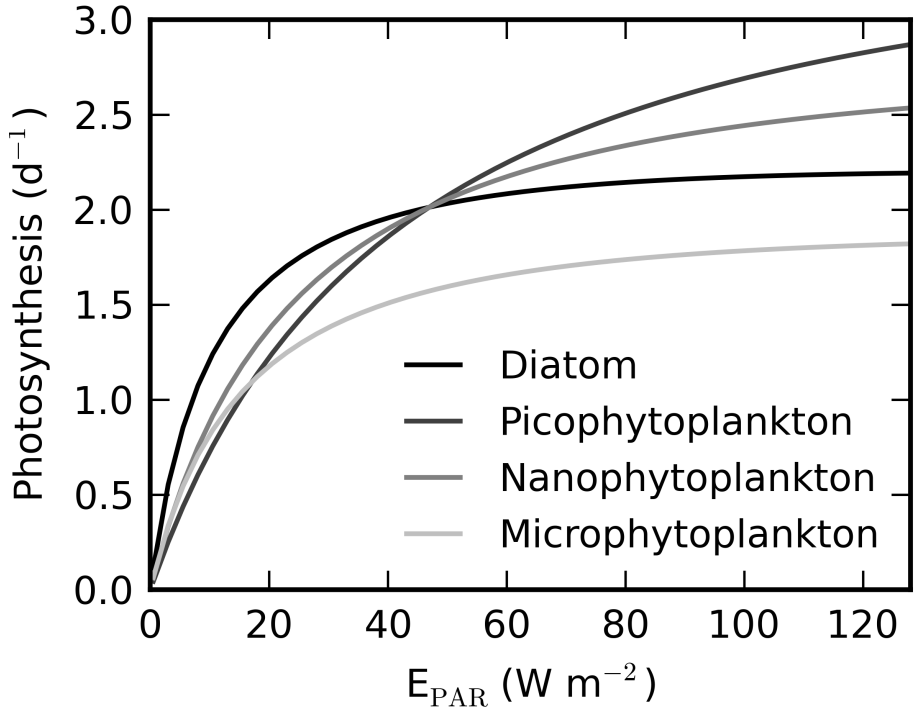

Figure 9. Phytoplankton growth over PAR for the four phytoplankton types.

GMDD
8, 7063–7187, 2015